LIGO Laboratory / LIGO Scientific Collaboration

LIGO-T0900269-v2 *ADVANCED LIGO* 7/8/09

AOS: Stray Light Control (SLC) Preliminary Design

Michael Smith, Riccardo DeSalvo, Niem Nguyen, Mohana Mageswaran, Ken Mailand, Virginio Sannibale, Phil Willems, Luke Williams

Distribution of this document:
LIGO Science Collaboration

This is an internal working note
of the LIGO Project.

California Institute of Technology
LIGO Project – MS 18-34
1200 E. California Blvd.
Pasadena, CA 91125
Phone (626) 395-2129
Fax (626) 304-9834
E-mail: info@ligo.caltech.edu

Massachusetts Institute of Technology
LIGO Project – NW22-295
185 Albany St
Cambridge, MA 02139
Phone (617) 253-4824
Fax (617) 253-7014
E-mail: info@ligo.mit.edu

LIGO Hanford Observatory
P.O. Box 1970
Mail Stop S9-02
Richland, WA 99352
Phone 509-372-8106
Fax 509-372-8137

LIGO Livingston Observatory
P.O. Box 940
Livingston, LA 70754
Phone 225-686-3100
Fax 225-686-7189

http://www.ligo.caltech.edu/

Table of Contents

1 INTRODUCTION 13

1.1 PURPOSE 13
1.2 SCOPE 13
1.3 SCATTERED LIGHT PARAMETERS 13
1.4 WEDGE ANGLES 17
1.5 BEAM PROFILE IN RECYCLING CAVITY 18
1.6 STRAY LIGHT CONTROL BLOCK DIAGRAM 18
1.7 DEFINITIONS 20
1.8 ACRONYMS 20
1.9 APPLICABLE DOCUMENTS 21
1.9.1 *LIGO Documents* *21*
1.9.2 *Non-LIGO Documents* *22*

2 CATALOG OF SLC DESIGN REQUIREMENTS 23

3 STRAY LIGHT CONTROL CONCEPTUAL DESIGN CHARACTERISTICS 24

3.1 PR2 AND SR2 SCRAPER BAFFLE 24
3.1.1 *Stay Clear Diameter* *25*
3.2 PRM AND SRM PLATE BEAM DUMPS 28
3.3 PR2 AND SR2 PLATE BEAM DUMPS 29
3.4 PR3 AND SR3 PLATE BEAM DUMPS 31
3.5 OUTPUT FARADAY ISOLATOR 32
3.5.1 *Stay Clear Diameter* *32*
3.6 ARM CAVITY BAFFLE 33
3.7 COC WIDE ANGLE SCATTER BAFFLE 34
3.8 MANIFOLD/CRYOPUMP BAFFLES 36
3.8.1 *Manifold Baffle* *36*
3.8.2 *Cryopump Baffle* *37*
3.9 ELLIPTICAL BAFFLES 38
3.9.1 *PRM Elliptical Baffle* *38*
3.9.2 *ITM Elliptical Baffles* *39*
3.10 H2 ELLIPTICAL SCRAPER MIRROR/BEAM DUMP 40
3.10.1 *Elliptical Scraper Mirror* *40*
3.10.2 *Scraper Beam Dump* *41*
3.11 H2 FOLD MIRROR BEAM DUMP 42

4 STRAY LIGHT CONTROL PERFORMANCE CHARACTERISTICS 43

4.1 SCATTERED LIGHT SOURCES 43
4.2 SUMMARY OF SCATTERED LIGHT DISPLACEMENT NOISE 45
4.3 SCATTERED LIGHT DISPLACEMENT NOISE SOURCES 47
4.3.1 *Output Faraday Isolator* *47*
4.3.1.1 Faraday Isolator Forward Transmissivity 47
4.3.1.2 Faraday Isolator Reverse Transmissivity 48
4.3.1.3 BRDF of Faraday Surfaces 48
4.3.1.4 Output Faraday Isolator Suspension 48
4.3.1.5 Scattered Light Displacement Noise of Suspended Output Faraday Isolator 49
4.3.1.6 Stay Clear Diameter 49
4.3.2 *Wide Angle COC Scatter Baffle* *50*
4.3.2.1 Arm Cavity Baffle Surface BRDF 50
4.3.2.2 Total Wide Angle COC Scattered Light Displacement Noise 50
4.3.3 *Arm Cavity Baffle* *51*
4.3.3.1 Incident Power on Arm Cavity Baffle 51
4.3.3.2 Arm Cavity Baffle Motion 52
4.3.3.2.1 HEPI Displacement 52

4.3.3.2.2 Arm Cavity Baffle Suspension Transfer Function 53
4.3.3.3 Seismic Motion of the Vacuum Manifold 55
4.3.3.4 Arm Cavity Baffle Surface BRDF 56
4.3.3.5 Arm Cavity Baffle Reflectivity 56
4.3.3.6 Scattered Light Displacement Noise of Suspended Arm Cavity Baffle 56
4.3.3.7 Fringe Wrapping of Arm Cavity Baffle Displacement Noise 57
4.3.3.8 Stay Clear Diameter 58
4.3.4 *Manifold Baffle* *58*
4.3.4.1 Manifold Baffle Surface BRDF 59
4.3.4.2 Seismic Motion of Manifold Baffle 59
4.3.5 *Cryopump Baffle* *59*
4.3.5.1 Cryopump Baffle Suspension 60
4.3.5.2 Cryopump Blocking 60
4.3.5.3 Cryopump Baffle Motion Requirements 60
4.3.5.4 Cryopump Baffle Surface BRDF 60
4.3.5.5 Cryopump Baffle Reflectivity 60
4.3.5.6 Seismic Motion of the Cryopump Scattering Surfaces 61
4.3.5.7 Scattered Light Displacement Noise of Suspended Cryopump Baffle 61
4.3.5.8 Fringe-wrapping of Cryopump Baffle Displacement Noise 61
4.3.5.9 Stay Clear Zone 62
4.3.6 *Elliptical Baffles* *62*
4.3.6.1 ITM Elliptical Baffle 62
4.3.6.1.1 ITM Elliptical Baffle Seismic Attenuation 63
4.3.6.1.2 ITM Elliptical Baffle Surface BRDF 63
4.3.6.1.3 ITM Elliptical Baffle Reflectivity 64
4.3.6.1.4 Seismic Motion of the Vacuum Chamber 64
4.3.6.1.5 Scattered Light Displacement Noise of Suspended ITM Elliptical Baffle 65
4.3.6.1.6 Stay Clear Diameter 65
4.3.6.2 PRM Elliptical Baffle 65
4.3.6.2.1 Motion of PRM Elliptical Baffle 65
4.3.6.2.2 Power Hitting the PRM Elliptical Baffle from IO Side 65
4.3.6.2.3 PRM Elliptical Baffle Surface BRDF 66
4.3.6.2.4 PRM Elliptical Baffle Reflectivity 66
4.3.6.2.5 Scattered Light Displacement Noise of PRM Elliptical Baffle 66
4.3.6.2.6 Stay Clear Diameter 67
4.3.7 *H2 Elliptical Scraper Mirror* *67*
4.3.7.1 H2 Elliptical Scraper Mirror Seismic Attenuation 67
4.3.7.2 H2 Elliptical Scraper Mirror Surface BRDF 67
4.3.7.3 H2 Elliptical Scraper Mirror Reflectivity 67
4.3.7.4 Seismic Motion of the Vacuum Chamber 67
4.3.7.5 Scattered Light Displacement Noise of Suspended H2 Elliptical Scraper Mirror 67
4.3.7.6 Stay Clear Diameter 67
4.3.8 *H2 Elliptical Scraper Beam Dump* *68*
4.3.8.1 H2 Elliptical Scraper Beam Dump Seismic Attenuation 68
4.3.8.2 H2 Elliptical Scraper Beam Dump Surface BRDF 68
4.3.8.3 H2 Elliptical Scraper Beam Dump Reflectivity 68
4.3.8.4 Seismic Motion of the Vacuum Chamber 68
4.3.8.5 Scattered Light Displacement Noise of Suspended H2 Elliptical Scraper Beam Dump 68
4.3.8.6 Stay Clear Diameter 68
4.3.9 *H2 Fold Mirror Beam Dump* *69*
4.3.9.1 H2 Fold Mirror Beam Dump Seismic Attenuation 69
4.3.9.2 H2 Fold Mirror Beam Dump Surface BRDF 69
4.3.9.3 H2 Fold Mirror Beam Dump Reflectivity 69
4.3.9.4 Seismic Motion of the Vacuum Chamber 69
4.3.9.5 Scattered Light Displacement Noise of Suspended H2 Fold Mirror Beam Dump 69
4.3.9.6 Stay Clear Diameter 69
4.3.10 *Output Window* *70*
4.3.10.1 Output Window BRDF 72
4.3.10.2 Seismic Motion of the Output Windows 72
4.3.10.3 Scattered Light Displacement Noise of Output Window 72
4.3.10.4 Reflected Light from AS Output Window 73

4.3.10.5 Output Septum Windows Removal 74
4.3.10.5.1 Stay Clear Diameter 74
4.3.11 *Hartmann Viewports* *74*
4.3.11.1 Hartmann Viewport BRDF 75
4.3.11.2 Reflected Light from Hartmann Viewport 76
4.3.11.2.1 Scattered Light Displacement Noise of Ghost Beams 76
4.3.12 *ITM GBAR1, GBAR3, and GBAR4 Ghost Beams* *76*
4.3.12.1 PR2/SR2 Cavity Beam Dump BRDF 76
4.3.12.2 PR2/SR2Cavity Beam Dump Reflectivity 76
4.3.12.3 Scattered Light Displacement Noise of Ghost Beams 76
4.3.13 *ITM HR, BS AR, AND BS HR Ghost Beams* *77*
4.3.13.1 Beam Tube Baffle BRDF and Reflectivity 77
4.3.13.2 Scattered Light Displacement Noise of Ghost Beams 77
4.3.14 *BS GBHR3P, BS GBHR* *79*
4.3.14.1 Scattered Light Displacement Noise of Ghost Beams 79
4.3.15 *ITMX PO Beam (BS GBAR1)* *80*
4.3.16 *PRM Ghost Beams* *80*
4.3.16.1 PRM GBAR1 80
4.3.16.2 PRM GBAR3 81
4.3.16.3 PRM GBHR3 81
4.3.16.4 PRM Plate Beam Dump Surface BRDF and Reflectivity 81
4.3.16.5 Scattered Light Displacement Noise of Ghost Beams 81
4.3.17 *PR2 Ghost Beams* *81*
4.3.17.1 PR2 GBAR0t 81
4.3.17.2 PR2 GBAR0t Cavity Beam Dump Surface BRDF and Reflectivity 81
4.3.17.3 RC PO Beam (PR2 GBARt) 81
4.3.17.4 PR2 GBAR3 82
4.3.17.5 PR2 GBHR3 82
4.3.17.6 PR2 Plate Beam Dump Surface BRDF and Reflectivity 83
4.3.17.7 Scattered Light Displacement Noise of Ghost Beams 83
4.3.18 *PR3 Ghost Beams* *83*
4.3.18.1 PR3 GBAR0t 83
4.3.18.2 PR3 GBAR3 83
4.3.18.3 PR3 GBHR3 83
4.3.18.4 PR3 Plate Beam Dump Surface BRDF and Reflectivity 83
4.3.18.5 Scattered Light Displacement Noise of PR3 Ghost Beams 84
4.3.19 *SRM Ghost Beams* *84*
4.3.19.1 SRM GBAR3 84
4.3.19.2 SRM GBHR3 84
4.3.19.3 SRM Plate Beam Dump Surface BRDF and Reflectivity 84
4.3.19.4 Scattered Light Displacement Noise of Ghost Beams 84
4.3.20 *SR2 Ghost Beams* *84*
4.3.20.1 SR2 GBAR0t 84
4.3.20.2 SR2 GBAR3 85
4.3.20.3 SR2 GBHR3 85
4.3.20.4 SR2 Plate Beam Dump Surface BRDF and Reflectivity 86
4.3.20.5 Scattered Light Displacement Noise of Ghost Beams 86
4.3.21 *SR3 Ghost Beams* *86*
4.3.21.1 SR3 GBAR0t 86
4.3.21.2 SR3 GBAR3 86
4.3.21.3 SR3 GBHR3 86
4.3.21.4 SR3 Plate Beam Dump Surface BRDF and Reflectivity 86
4.3.21.5 Scattered Light Displacement Noise of SR3 Ghost Beams 87
4.4 STRAY LIGHT CONTROL PHYSICAL CHARACTERISTICS 87
4.4.1 *Faraday Isolator* *87*
4.4.2 *Arm Cavity Baffle* *88*
4.4.3 *Arm Cavity Baffle Cylinder* *89*
4.4.4 *Elliptical Baffle* *90*
4.4.4.1 ITM Elliptical Baffle 90
4.4.4.2 PRM Elliptical Baffle 90

4.4.5 *Manifold Baffle* *90*
4.4.6 *Septum Window* *91*
4.4.7 *PR2/SR2 Cavity Beam Dump* *91*
4.4.8 *Cryopump Baffle* *92*
4.5 STRAY LIGHT CONTROL INTERFACE DEFINITIONS 92
4.5.1 *Interfaces to other LIGO detector subsystems* *92*
4.5.1.1 Mechanical Interfaces 92
4.5.1.2 Electrical Interfaces 93
4.5.1.2.1 Suspended Baffles and Beam Dumps 93
4.5.1.2.2 Faraday Isolator 93
4.5.1.3 Optical Interfaces 93
4.5.1.4 Stay Clear Zone 93
4.5.1.4.1 Arm Cavity Baffle 93
4.5.1.4.2 ITMX, ITMY, and BS Beam Dump 93
4.5.1.4.3 Cryopump Baffle 93
4.5.1.4.4 Elliptical Baffle 93
4.5.2 *Interfaces external to LIGO detector subsystems* *93*
4.6 STRAY LIGHT CONTROL RELIABILITY 93
4.7 STRAY LIGHT CONTROL MAINTAINABILITY 94
4.8 STRAY LIGHT CONTROL ENVIRONMENTAL CONDITIONS 94
4.8.1.1.1.1 Natural Environment 94
4.8.1.1.1.2 Induced Environment 94
4.9 STRAY LIGHT CONTROL TRANSPORTABILITY 95

5 STRAY LIGHT CONTROL DESIGN AND CONSTRUCTION 96

5.1.1.1 Materials and Processes 96
5.1.1.1.1 Materials 96
5.1.1.1.2 Processes 96
5.1.1.1.2.1 Cleaning 96
5.1.1.1.3 Component Naming 96
5.1.1.2 Stray Light Control Workmanship 96
5.1.1.3 Stray Light Control Interchangeability 96
5.1.1.4 Stray Light Control Safety 97
5.1.1.5 Stray Light Control Human Engineering 97
5.1.2 *Stray Light Control Assembly and Maintenance* *97*
5.1.3 *Stray Light Control Documentation* *97*
5.1.3.1 Stray Light Control Specifications 97
5.1.3.2 Stray Light Control Design Documents 97
5.1.3.3 Stray Light Control Engineering Drawings and Associated Lists 97
5.1.3.4 Stray Light Control Technical Manuals and Procedures 98
5.1.3.4.1 Procedures 98
5.1.3.5 Stray Light Control Documentation Numbering 98
5.1.3.6 Stray Light Control Test Plans and Procedures 98
5.1.4 *Stray Light Control Logistics* *98*
5.1.5 *Stray Light Control Precedence* *98*
5.1.6 *Stray Light Control Qualification* *98*

6 QUALITY ASSURANCE PROVISIONS 99

6.1 GENERAL 99
6.1.1 *Responsibility for Tests* *99*
6.1.2 *Special Tests* *99*
6.1.2.1 Engineering Tests 99
6.1.2.1.1 Witness Sample Scattering Tests of Baffle and Beam Dump Material 99
6.1.2.1.2 ETM Telescope Performance Test 99
6.1.2.1.3 ETM Telescope Suspension Damping Test 99
6.1.2.1.4 Faraday Isolator Performance Test 99
6.1.2.1.5 Faraday Isolator Suspension Damping Test 99
6.1.2.1.6 TBD 99
6.1.2.2 Reliability Testing 99

6.1.3 *Configuration Management* *99*
6.2 QUALITY CONFORMANCE INSPECTIONS 99
6.2.1 *Inspections* *99*
6.2.2 *Demonstration* *100*
6.2.3 *Test* *100*

7 PREPARATION FOR DELIVERY 101

7.1 PREPARATION 101
7.2 PACKAGING 101
7.3 MARKING 101

8 APPENDIX A—SCATTERED LIGHT NOISE THEORY 102

8.1 SCATTERED LIGHT REQUIREMENT 102
8.2 SCATTERED POWER INTO THE IFO 103
8.2.1 *Output Faraday Isolator Scatter* *104*
8.2.2 *Arm Cavity Baffle Surface Scatter* *104*
8.2.3 *Arm Cavity Baffle Reflected Light* *105*
8.2.4 *ITM Elliptical Baffle Surface Scatter* *106*
8.2.5 *ITM Elliptical Baffle Reflected Light* *108*
8.2.6 *PRM Elliptical Baffle* *108*
8.2.7 *H2 Elliptical Scraper Mirror* *110*
8.2.8 *H2 Elliptical Scraper Mirror Beam Dump* *110*
8.2.9 *H2 FM Beam Dump Surface Scatter* *111*
8.2.10 *ITM (ETM) Wide-Angle Scatter* *112*
8.2.10.1 Scattering from the Back of Arm Cavity Baffle 112
8.2.10.2 Scattering from the COC Wide Angle Baffle 113
8.2.10.3 Total Scattered Light Displacement Noise from Arm Cavity Baffle and COC Wide Angle Baffle 114
8.2.10.4 Scattering from the Manifold Baffle 114
8.2.10.5 Scatter from ITM Manifold Wall 115
8.2.10.6 Scattering from BSC Chamber Walls 115
8.2.10.7 Total Wide-Angle Scattered Light Displacement Noise from BSC Chamber, Manifold Walls, and Manifold Baffle 116
8.2.11 *Septum Window Scatter* *116*
8.2.11.1 AS Output Window 116
8.2.11.2 AS Output Window Reflection 117
8.2.11.3 ITMX PO Septum Window 117
8.2.11.4 ITMX PO Septum Window Reflection 117
8.2.11.5 RC PO Septum Window 118
8.2.11.6 RC PO Septum Window Reflection 118
8.2.12 *ITMY Hartmann Viewport* *119*
8.2.13 *ITMX Hartmann Viewport* *119*
8.2.14 *Ghost Beams* *120*
8.2.14.1 Ghost Beam Naming Convention 120
8.2.14.2 ITMAR1 121
8.2.14.3 ITMAR1 REFL 121
8.2.14.4 ITMAR3 121
8.2.14.5 ITMAR3 REFL 122
8.2.14.6 ITMHR3 122
8.2.14.7 BSAR3 123
8.2.14.8 BSHR3 123
8.2.14.9 BSAR3P 123
8.2.14.10 BSAR3P REFL 124
8.2.14.11 BSHR3P 124
8.2.14.12 BSHR3P REFL 124
8.2.15 *PRM* *125*
8.2.15.1 PRMAR1 125
8.2.15.2 PRMAR3 125
8.2.15.3 PRMHR3 125
8.2.15.4 Total Displacement Noise from PRM 126

8.2.16 *PRM2* *126*
8.2.16.1 PR2AR0t 126
8.2.16.2 PR2AR3 126
8.2.16.3 PR2HR3 127
8.2.16.4 Total Displacement Noise from PR2 127
8.2.17 *PRM3* *127*
8.2.17.1 PR3AR0t 127
8.2.17.2 PR3AR3 127
8.2.17.3 PR3HR3 128
8.2.17.4 Total Displacement Noise from PR3 128
8.2.18 *SRM* *128*
8.2.18.1 SRMAR3 128
8.2.18.2 SRMHR3 128
8.2.18.3 Total Displacement Noise from SRM 129
8.2.19 *SRM2* *129*
8.2.19.1 SR2AR0t 129
8.2.19.2 SR2AR3 129
8.2.19.3 SR2HR3 130
8.2.19.4 Total Displacement Noise from SR2 130
8.2.20 *SRM3* *130*
8.2.20.1 SR3AR0t 130
8.2.20.2 SR3AR3 130
8.2.20.3 SR3H3 131
8.2.20.4 Total Displacement Noise from SR3AR 131
8.2.21 *Cryopump Baffle Scatter* *131*
8.2.22 *Cryopump Baffle Reflected Scatter* *132*
8.2.23 *Fringe-Wrapping* *132*
8.2.23.1.1.1 Damped Pendulum Example 134

Table of Tables

Table 1: IFO parameter values used for scattered light calculation *13*
Table 2: COC Wedge Angles *17*
Table 3: Scattered Light Source, Incident Power and Scattered Power *43*
Table 4: Faraday Isolator Characteristics *88*
Table 5 : Faraday Isolator Suspension Characteristics *88*
Table 6: Arm Cavity Baffle Characteristics *88*
Table 7: Arm Cavity Baffle Suspension *89*
Table 8: Arm Cavity Baffle Cylinder Characteristics *89*
Table 9: Arm Cavity Baffle Suspension *89*
Table 10: ITM Elliptical Baffle Characteristics *90*
Table 11: PRM Elliptical Baffle Characteristics *90*
Table 12: Manifold Baffle *91*
Table 13: Septum Window Characteristics *91*
Table 14: Cavity Beam Dump Characteristics *91*
Table 15: Cryopump Baffle Characteristics *92*
Table 16 Environmental Performance Characteristics *94*

Table of Figures

Figure 1: AOS System Block Diagram *19*
Figure 2: Scraper Baffle in front of SR2 on HAM4 ..... *24*
Figure 3: Scraper Baffle in front of PR2 on HAM3 ..... *25*

Figure 4: PR2 Scraper Baffle, Beam Clearance *26*
Figure 5: SR2 Scraper Baffle, Beam Clearance *27*
Figure 6: PRM beam dumps, elevation view *28*
Figure 7: SRM beam dumps, elevation view *29*
Figure 8: PR2 Plate Beam Dumps, elevation view *30*
Figure 9: SR2 Plate Beam Dumps, elevation view *30*
Figure 10: PR3 AR beam dump *31*
Figure 11: SR3 AR beam dump *31*
Figure 12: Suspended Faraday Isolator *33*
Figure 13: Suspended Arm Cavity Baffle and COC Wide Angle Baffle in front of H2 ITM *35*
Figure 14: Manifold Baffle *36*
Figure 15: Cryopump Baffle *37*
Figure 16: PRM Elliptical Baffle on HAM3 ..... *38*
Figure 17: Suspended ITM Elliptical Baffle *39*
Figure 18: Viton Damped Suspension *40*
Figure 19: H2 Scraper Mirror/Beam Dump & FM Beam Dumps *41*
Figure 20: Scattered Light Displacement Noise, Septum Windows in Place *46*
Figure 21: Scattered Light Displacement Noise, Septum Windows Removed *47*
Figure 22: HAM optics table Seismic Motion Requirement *49*
Figure 23: Output Faraday Isolator SUS Amplitude Response *50*
Figure 24: Scattered Light Displacement Noise from Suspended Output Faraday Isolator *51*
Figure 25: BSC HEPI Motion Spectrum *53*
Figure 26: Arm Cavity Baffle SUS Amplitude Response *54*
Figure 27: BSC HEPI Motion Spectrum *55*
Figure 28: Seismic motion of vacuum manifold *56*
Figure 29: Arm Cavity Baffle and Cryopump Baffle Scattered Light Displacement Noise *57*
Figure 30: Arm Cavity Baffle Scattered Light Displacement Noise Caused by Fringe-wrapping *58*
Figure 31: Cryopump Baffle and Manifold Baffle SUS transfer function *59*
Figure 32: Cryopump Baffle Scattered Light Displacement Noise *62*
Figure 33: Elliptical Baffle SUS Amplitude Response *63*
Figure 34: Seismic motion of BSC chamber *64*
Figure 35: Elliptical Baffle Scattered Light Displacement Noise *66*
Figure 36: H2 Elliptical Scraper Mirror and Beam Dump Scattered Light Displacement Noise *70*
Figure 37: Output Septum Plate *71*
Figure 38: Output Septum Windows *72*
Figure 39: Displacement Spectrum of HAM 6 Flange *73*
Figure 40: Output Window Scattered Light Displacement noise *74*
Figure 41: Hartmann Viewports *75*
Figure 42: ITM GBAR1, GBAR3, and GBAR4 Beam Dump Scattered Light Displacement Noise *77*
Figure 43: ITM GBHR Beam Dump Scattered Light Displacement Noise *78*
Figure 44: BS GBARX and GBHRX Scattered Light Displacement Noise *79*
Figure 45: BS GBAR3P and BS GBHR3P Beam Dump Scattered Light Displacement Noise *80*
Figure 46: PR2 GBAR0t beam dump *82*
Figure 47: SR2 AR0t beam dump *85*
Figure 48: PRM, PR2, PR3, SRM, SR2, SR3, Scattered Light Displacement Noise *87*
Figure 49: Scattered Light Noise Transfer Functions *103*

Figure 50: ARM CAVITY BAFFLE SCATTER *104*
Figure 51: ITM ELLIPTICAL BAFFLE SCATTER AND REFLECTION *106*
Figure 52: Wide-angle Scatter from ITM (ETM) *112*
Figure 53: PRM, SRM, ITM, and ETM ghost beam naming convention *120*
Figure 54: BS ghost beam naming convention *120*
Figure 55: Noise Waveform at the Onset of Fringe-Wrapping, λ/8 ..... *133*
Figure 56: Displacement Noise waveform with Fringe-wrapping, λ/4 ..... *134*
Figure 57: Scattered Light Displacement Noise Caused by Fringe-wrapping *135*

Abstract

This document will present the preliminary design for the AOS Stray Light Control subsystem for ADLIGO.

1 Introduction

1.1 Purpose

The purpose of this document is to present a preliminary design that meets the SLC Design requirements.

1.2 Scope

This document is based on the conceptual design document T080210-00. Some of the parameters, such as the wedge angles and orientations of the optical elements in the power recycling cavities may have changed.

AOS is responsible for controlling and reducing to acceptable levels the displacement noise due to scattered light injected into the IFO mode.

AOS is not responsible for scattering that occurs in the IO section, which is defined as everything prior to PRM on HAM2 and HAM8; and everything in the ISC section on HAM6, HAM1, HAM12, and HAM7.

1.3 Scattered Light Parameters

The IFO parameters that were used for the design of the SLC elements are listed in Table 1.

Table 1: IFO parameter values used for scattered light calculation

PARAMETER	VALUE
IFO_length;	4.00E+03
IFO_beamwaist;	1.15E-02
IFO_beam_waist_RC;	2.10E-03
beam_radius_ITM;	5.50E-02
beam_waist_photodetector;	5.00E-03
beam_radius_Faraday;	2.10E-03
lambda;	1.06E-06
IFO_diffraction_angle;	2.95E-05
IFO_solid_angle;	2.72E-09
laser_power;	1.25E+02
recycling_cavity_power_gain;	1.69E+01
reflected_port_power_ratio;	1.00E-03
dark_port_signal_ratio;	1.08E-03
recycling_cavity_power;	2.11E+03

PARAMETER	VALUE
arm_cavity_power;	8.34E+05
ETM_transmitted_power;	1.25E+01
reflected_port_power;	1.25E-01
dark_port_power;	1.35E-01
ITM_transmissivity;	5.00E-03
ITM_HR;	9.95E-01
ETM_transmissivity;	1.50E-05
ETM_Reflectivity;	1.00E+00
PRM_AR_reflectivity;	5.00E-05
PRM_HR_transmissivity;	2.12E-01
SRM_AR_reflectivity;	5.00E-05
SRM_HR_reflectivity;	9.60E-01
SRM_HR_transmissivity;	4.00E-02
diameter_ETM;	3.40E-01
diameter_ITM;	3.40E-01
diameter_PRM;	2.65E-01
diameter_SRM;	2.65E-01
diameter_MMT3;	2.65E-01
Radius_Inner_Cryo;	3.85E-01
Radius_Beam_Tube;	5.31E-01
area_arm_cav_baffle;	6.95E-01
length_armcavbaf_wall;	4.40E+00
manifold_wall_length;	1.40E+01
manifold_wall_angle;	6.64E-02
manifold_wide_angle_scattering_efficiency;	2.24E-20
manifold_baffle_wide_angle_scattering_efficiency;	8.84E-24
BSC_wide_angle_scattering_efficiency;	9.74E-22
AC_Baffle_wide_angle_scattering_efficiency;	5.83E-19
AC_Baf_cyl_wide_angle_scattering_efficiency;	1.14E-20
Area_Arm_Cav_Baf_Hole;	9.08E-02
Length_Arm_Cav_Baf;	1.00E+00
Solid_Angle_COC_Wide_Angle;	1.82E-01
AP2_lens_focal_length;	1.00E-01
lens_AR_reflectivity;	2.50E-03

PARAMETER	VALUE
scatter_loss_Brewster_window;	4.00E-05
incident_angle_Faraday_crystal;	1.70E-02
back_transmission_Faraday_Isolator;	1.00E-03
Faraday_Tranmission;	9.00E-01
transmission_ETM_path;	1.00E-02
BRDF_elliptical_baffle_edge;	5.00E-02
BRDF_ETM_Tel_Baffle_Edge;	5.00E-02
BRDF_chamber_walls;	1.00E-01
BRDF_Nozzle;	1.00E-01
BRDF_photodetector;	1.00E-03
BRDF_ITMX_PO_steer_mirror;	1.00E-05
BRDF_COC_30urad;	1.36E+03
BRDF_elliptical_baffle;	5.00E-02
BRDF_arm_cav_baffle;	5.00E-02
BRDF_cryopump_baffle;	5.00E-02
BRDF_Brewster_window;	1.00E-06
BRDF_beam_dump;	5.00E-02
BRDF_ETM_Tel_Baffle;	5.00E-02
BRDF_lens;	1.00E-03
BRDF_Faraday;	4.92E-04
BRDF_manifold_baffle;	5.00E-02
BRDF_OMMT2;	3.00E-03
BRDF_Faraday;	4.92E-04
BRDF_COC_wide_angle;	4.76E-06
a;	1.12E-01
b;	1.30E-01
w;	2.10E-03
h;	1.23E-01
N_Cryopump_Baffles;	4.00E+00
N_Arm_Cavity_Baffle;	4.00E+00
N_Elliptical_Baffle;	0.00E+00
N_ETM_Tel_Baffle;	2.00E+00
N_Manifold;	4.00E+00
N_Surfaces_Faraday;	5.00E+00

PARAMETER	VALUE
N_Surfaces_Brewster;	2.00E+00
Scatter_Efficiency_Cryo_Baffle;	3.32E-06
Scatter_Efficiency_AC_Baffle;	8.79E-06
Scatter_Efficiency_Ellip_Baffle;	3.51E-04
Scatter_Efficiency_ETM_Tel_Baffle;	3.90E-03
Scatter_Efficiency_PRM_Ellip_Baffle;	9.46E-05
Scatter_Efficiency_Wide_Angle;	1.50E-05
cryopump_sus_length;	4.00E-01
cryopump_sus_freq;	7.88E-01
cryopump_sus_Q;	1.00E+03
arm_cavity_baf_sus_length;	8.00E-01
arm_cavity_baf_sus_freq;	2.50E+00
arm_cavity_baf_sus_Q;	1.00E+03
ellip_baf_sus_length;	1.00E+00
ellip_baf_sus_freq;	4.98E-01
ellip_baf_sus_Q;	1.00E+03
cav_bd_sus_length;	1.00E+00
cav_bd_sus_freq;	4.98E-01
cav_bd_sus_Q;	1.00E+02
Faraday_sus_length;	4.00E-01
Faraday_sus_freq;	7.88E-01
Faraday_sus_Q;	1.00E+02
reflectivity_ellip_baffle;	2.40E-05
reflectivity_arm_cav_baffle;	2.40E-05
reflectivity_cryopump_baffle;	2.40E-05
reflectivity_cavity_beam_dump;	2.40E-05
Reflectivity_Brewster;	2.50E-03
reflectivity_ETM_Tel_Baffle;	7.00E-02
reflectivity_manifold_baffle;	7.00E-02
Reflectivity_Faraday_AR;	2.50E-03
PRM_AR_transmissivity;	1.00E+00
PRM_HR_reflectivity;	7.88E-01
SRM_AR_transmissivity;	1.00E+00

1.4 Wedge Angles

The wedge angles were determined by the SYS Group, in cooperation with AOS. The wedge angles for the folded IFO are exactly the same as for the straight IFO.

In addition, the FM wedge angles will be 0.04 deg, the same as the BS, to minimize tooling requirements.

Table 2: COC Wedge Angles

Mirror	Wedge Angle, deg	Orientation	Direction	Symmetry
PRM	1	vertical	thick side down	symmetric
PR2	1	vertical	thick side down	symmetric
PR3	0.6	vertical	thick side up	symmetric
SRM	1	vertical	thick side down	symmetric
SR2	1	vertical	thick side down	symmetric
SR3	0.6	vertical	thick side up	symmetric
BS	0.04	horizontal	thin side +Y	symmetric
CPX	0.04	horizontal	thin side -Y	symmetric
CPY	0.04	horizontal	thin side -X	symmetric
ITMX	0.08	horizontal	thin side -Y	AR face perpendicular to substrate cylindrical axis
ITMY	0.08	horizontal	thin side -X	AR face perpendicular to substrate cylindrical axis
ETMX	0.08	horizontal	thin side -Y	AR face perpendicular to substrate cylindrical axis
ETMY	0.08	horizontal	thin side +X	AR face perpendicular to substrate cylindrical axis
ReMX	0.04	horizontal	thin side +Y	symmetric
ReMY	0.04	horizontal	thin side -X	symmetric
FMX	0.04	horizontal	thin side -Y	symmetric
FMY	0.04	horizontal	thin side -Y	symmetric

1.5 Beam Profile in Recycling Cavity

The Beam cross section within the recycling cavity is non-Gaussian. The beam profile is approximately an ellipse with the horizontal semi-diameter of 107 mm and the vertical semi-diameter of 125 mm (see G070657 LSC-Virgo meeting, 10/24/07, Hiro Yamamoto , RC beam size calculation).

1.6 Stray Light Control Block Diagram

A block diagram showing the principal scattering sources of the AOS System is shown in Figure 1.

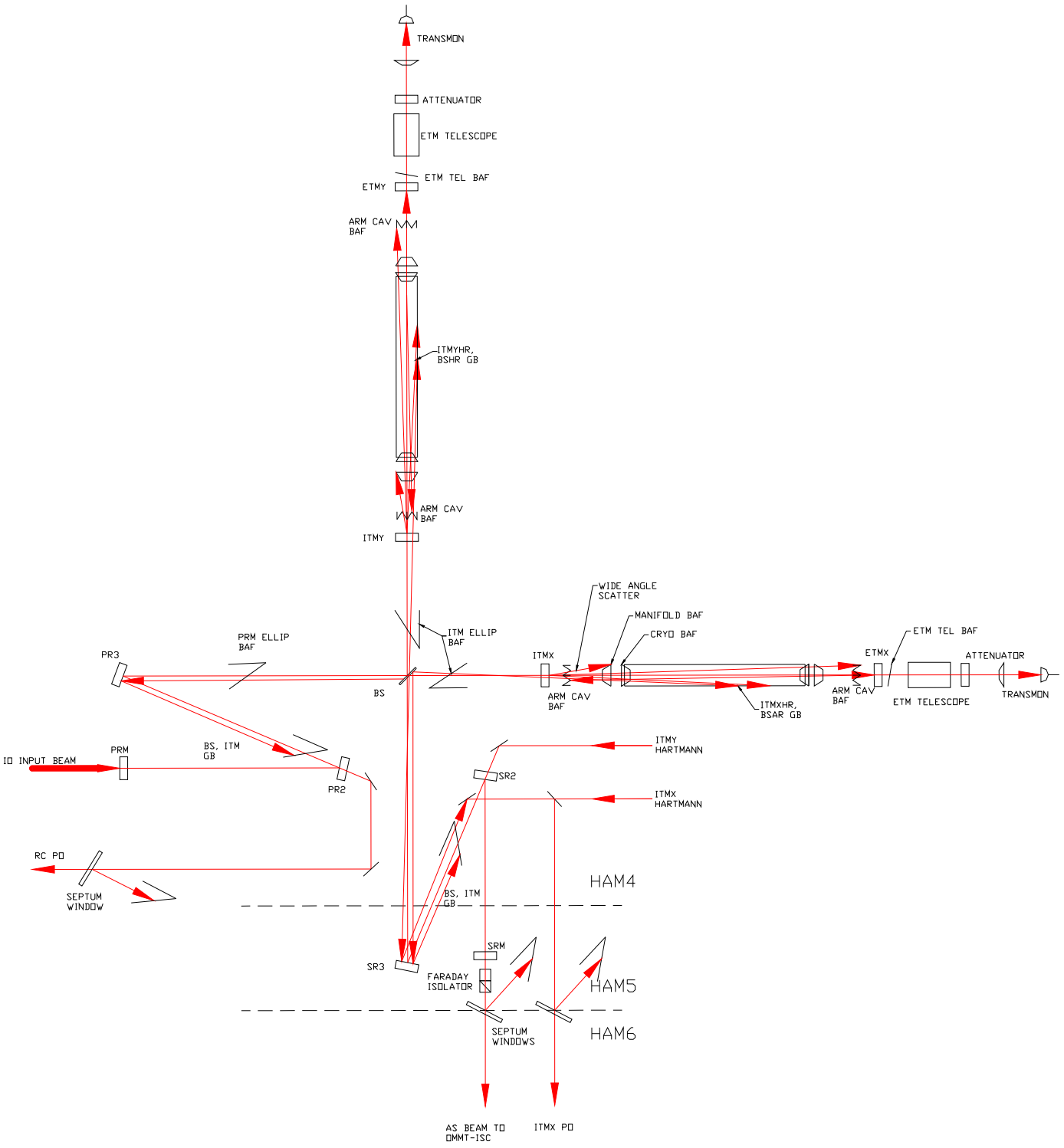

Figure 1: AOS System Block Diagram

1.7 Definitions

1.8 Acronyms

AOS - Auxiliary Optics Support

AR - Antireflection mirror coating

AS - anti-symmetric port signal

ASC - Alignment Sensing and Control

BS - Beam Splitter

BSC - Beam Splitter Chamber

CDS – Computer Data Systems

CP – Compensation plate

ETMx, ETMy - End Test Mass in the interferometer ‘X’ or ‘Y’ arm

HAM - Horizontal Access Module

HR – Hi-reflectance mirror coating

IFO - LIGO interferometer

IO - Input Optics

ISC- Interferometer Sensing and Control

ITMx, ITMy - Input Test Mass in the interferometer ‘X’ or ‘Y’ arm

LIGO - Laser Interferometer Gravity Wave Observatory

LSC - Length Sensing and Control

LVEA-vacuum equipment area

mm – millimeter

MMT – mode matching telescope

mrad – milliradian

MTBF – mean time before failure

NA – not applicable

nm – nanometer

OSEM – sensor/actuator head

PO - Pick-off

p-p, peak to peak

ppm - parts per million

PRM – Power Recycling Mirror

p-v, peak to valley

Q – quality factor

QPD – quadrant photo diode

RH – relative humidity

ReM – Reaction mass

rms - root-mean-square

rtHz – square root Hertz

SLC – Stray Light Control

SOS – Small Optic Suspension

SRD - Science Requirements Document

SRM – Signal Recycling Mirror

SW – Solid Works

TBD - To Be Determined

W - Watt

WFS – wave front sensor

1.9 Applicable Documents

1.9.1 LIGO Documents

1. E950111-A LIGO Naming Convention
2. E960022-B LIGO Vacuum Compatibility, Cleaning Methods and Qualification Procedures
3. L970061-00-D Guidance for Seismic Component Cleaning, Baking, and Shipping Preparation
4. M950046-F LIGO Project System Safety Management Plan
5. T040126-A Baffle Furnace Bake Procedure
6. G070657 LSC-Virgo meeting, 10/24/07, Hiro Yamamoto
7. MIL-C-104B
8. M060056-06 Advanced LIGO Reference Design
9. E990303-03 Seismic Isolation Subsystem Design Requirements Document
10. LIGO-T960065-03 Seismic Isolation Design Requirements Document
11. T060013-02, Inputs to Beam Tube Scattering and Optical Surface Roughness Requirement Analysis for Advanced LIGO (table2)
12. T060360-02 PO Mirror Assembly & Telescope, and OMMT Conceptual Design Requirements
13. T960151-02 Large and Small Optics Suspension Electronics Design Requirements

14. T070089-02 Wide-angle Scatter from LIGO Arm Cavities
15. T010076-01 Optical Layout for Advanced LIGO
16. M060062-00 HAM Single-stage Isolation Baseline Option Review Report
17. T060073-00 Transfer Functions of Injected Noise
18. T920004-00 Estimation of Special Optical Properties of a Triangular Ring Cavity
19. T980104-00 COS Final Design
20. T070003-00 Backscattering from the AS Port: A Comparison of P. Fritschel's Estimate and
21. T070061-00 AOS: Stray Light Control (SLC) Design Requirements
22. T080064-00 Controlling Light Scatter in Advanced LIGO
23. Robert Schofield (11/17/06 LHO ILOG)
24. T980027-00, Baffling Requirements for the 4K and 2K IFO
25. E980131-A, Component Specification, Faraday Isolator, 20 mm

1.9.2 Non-LIGO Documents

2 Catalog of SLC Design Requirements

The requirements for the SLC subsystem are derived in T070061-00 AOS: Stray Light Control (SLC) Design Requirements and are referenced below by paragraph number.

1. 4.2 Noise Requirements
2. 4.2.1 Direct Requirements
3. 4.2.2 Implied Requirement for Scattering Surfaces
4. 4.3 Faraday Isolator Requirements
5. 4.4 IO Baffle Requirement
6. 4.5 Cryopump Baffle Requirement
7. 4.6 BSC Chamber Components
8. 4.7 Clear Aperture Requirements
9. 4.8 Generic Requirements
10. 4.8.1 Mechanical Characteristics & Standards
11. 4.8.2 Electrical Characteristics & Standards
12. 4.8.3 Vacuum Compatibility Requirements
13. 4.8.4 Acoustic Requirements
14. 4.8.5 Earthquake Requirements
15. 4.8.6 Operating Environment
16. 4.8.7 Quality Assurance
17. 4.8.8 Reliability
18. 4.8.9 Maintainability
19. 4.8.10 Documentation
20. 4.8.11 Transportability
21. 4.8.11 Safety

3 Stray Light Control Conceptual Design Characteristics

3.1 PR2 and SR2 Scraper Baffle

The ghost beams from the ITMs and from the internal reflections of the CP enter the power recycling and the signal recycling telescopes and are caught by the "scraper" baffles in front of the PR2 and SR2 mirrors, as shown in Figure 2, and Figure 3.

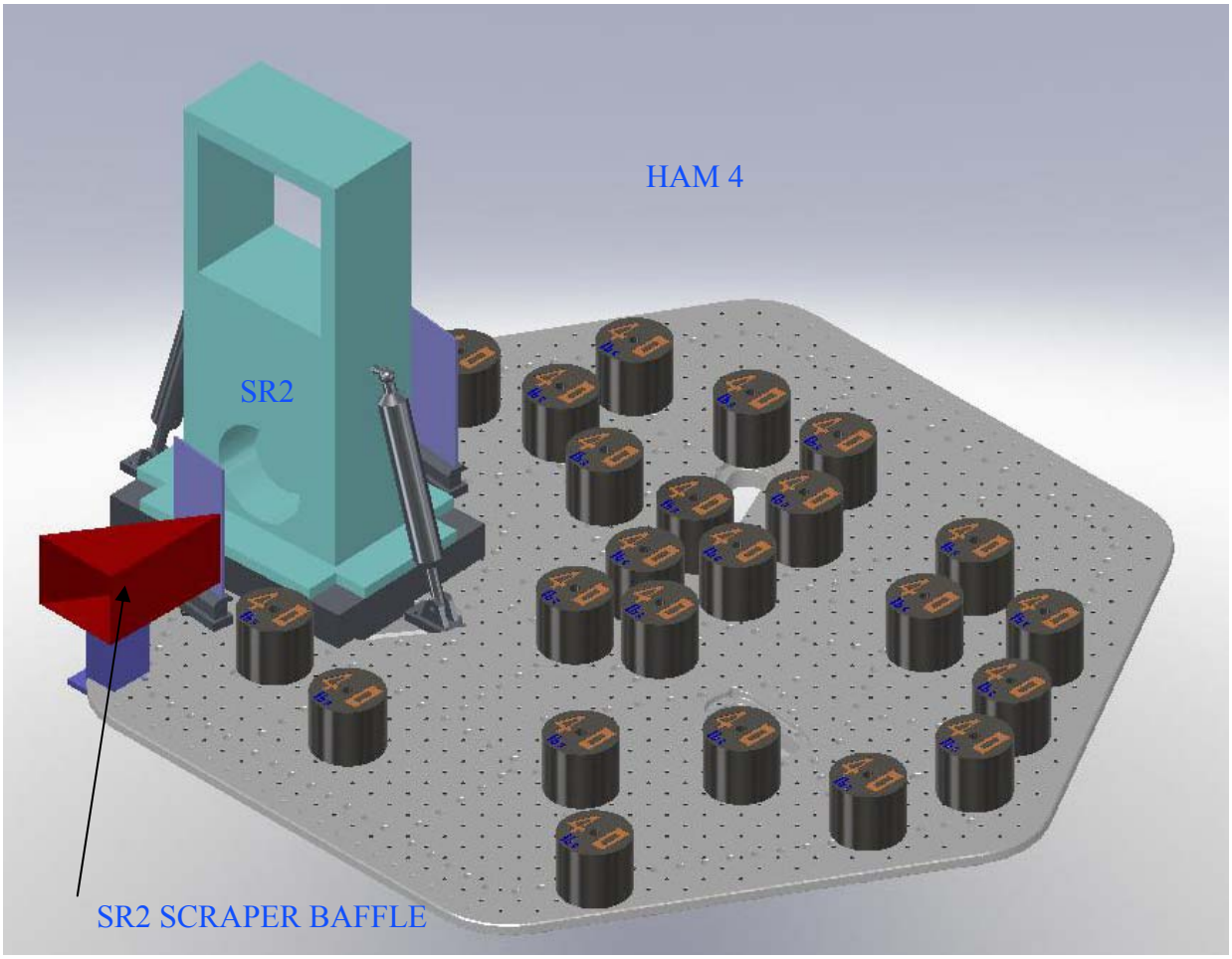

Figure 2: Scraper Baffle in front of SR2 on HAM4

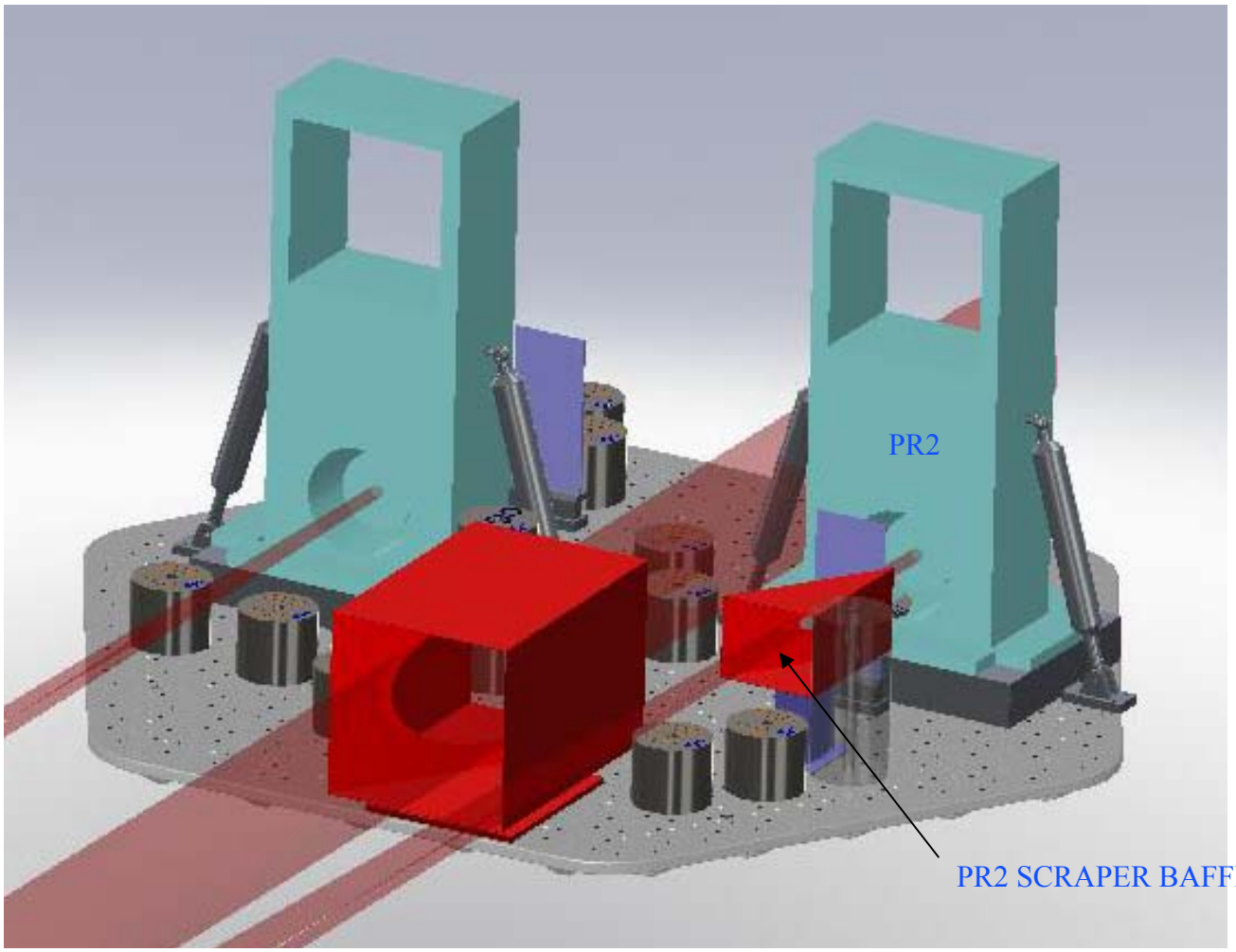

Figure 3: Scraper Baffle in front of PR2 on HAM3

3.1.1 Stay Clear Diameter

The clearance between the main beam and the ITM and BS ghost beams that land on the PR2 scraper cavity beam dump is shown in Figure 4. The minimum spacing between the main beam and the closest ghost beam is approximately 40 mm. The Gaussian beam diameters are less then 4 mm.

The clearance between the main beam and the ITM and BS ghost beams that land on the SR2 scraper baffle is shown in Figure 5. The minimum spacing between the main beam and the closest ghost beam is approximately 25 mm.

The beams are in the vicinity of the telescope's beam waists and the diameters of the beams will be < 2 mm.

This meets the requirement 4.7 Clear Aperture Requirements

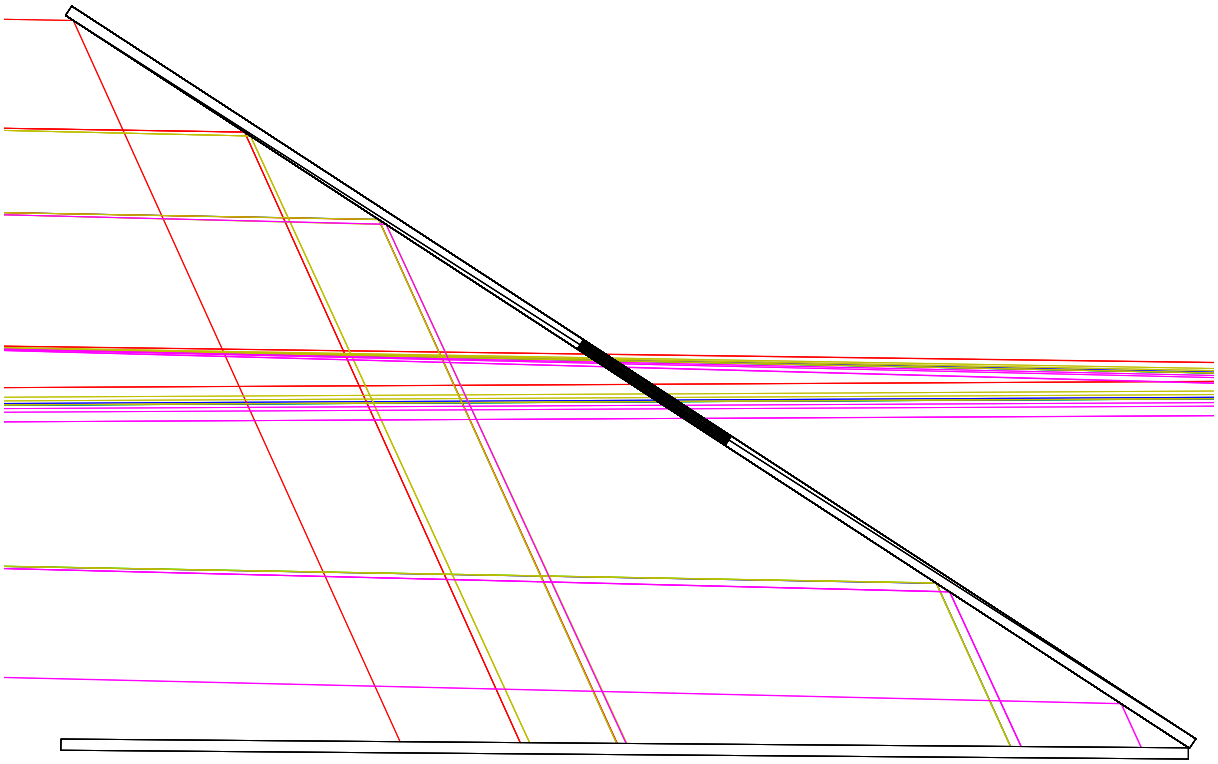

Figure 4: PR2 Scraper Baffle, Beam Clearance

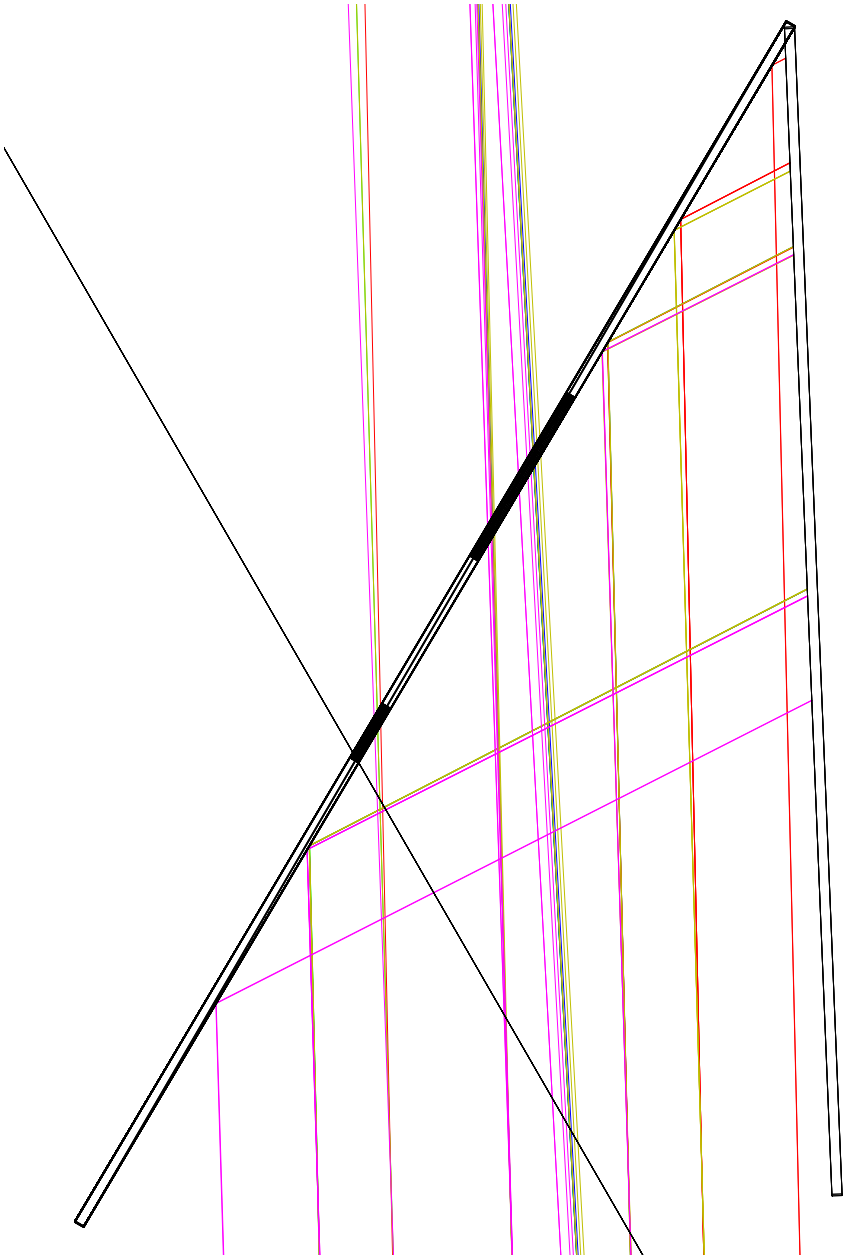

Figure 5: SR2 Scraper Baffle, Beam Clearance

3.2 PRM and SRM Plate Beam Dumps

The PRM and SRM AR and HR ghost beams separate far enough from the main beam to be caught in nearby beam dumps, as shown in Figure 6, and Figure 7.

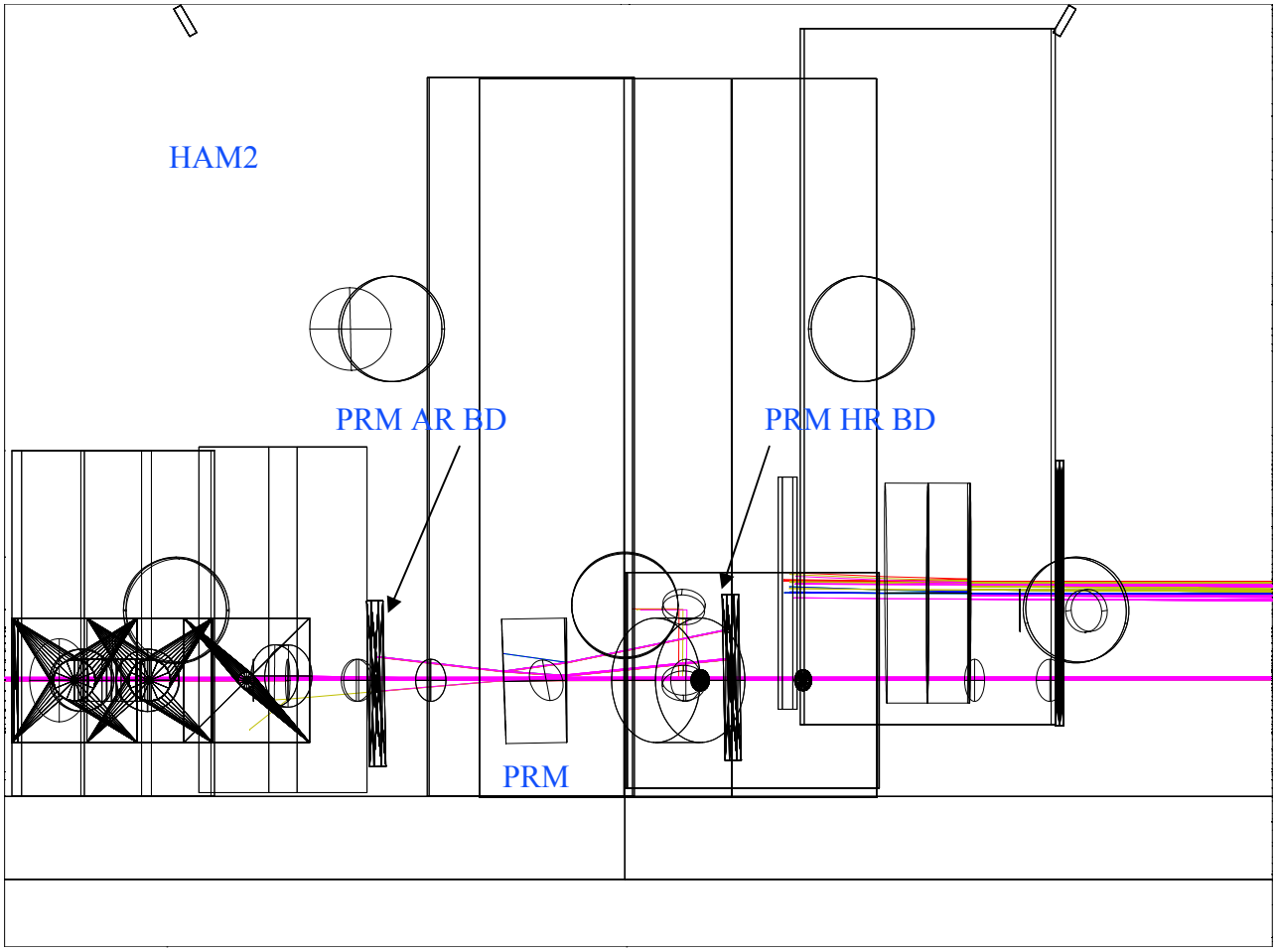

Figure 6: PRM beam dumps, elevation view

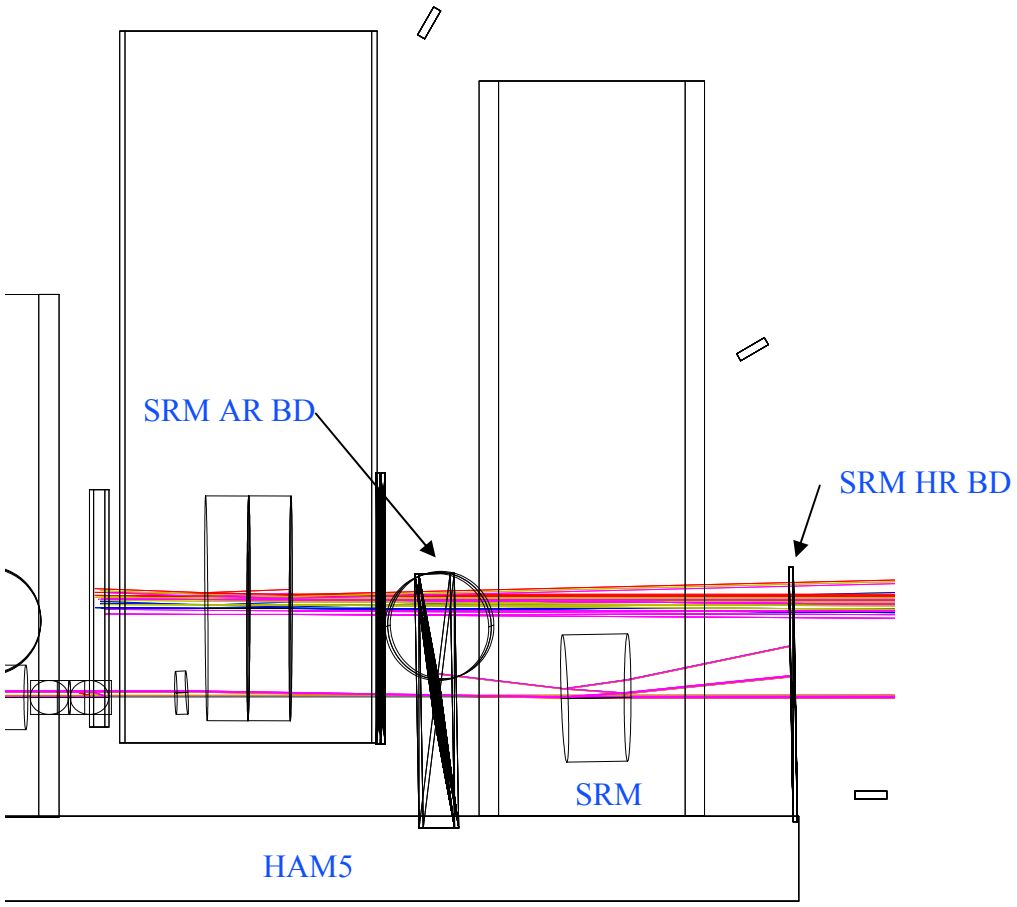

Figure 7: SRM beam dumps, elevation view

3.3 PR2 and SR2 Plate Beam Dumps

The PRM and SRM ghost beams separate far enough from the main beam to be caught in nearby beam dumps, as shown in Figure 8 and Figure 9.

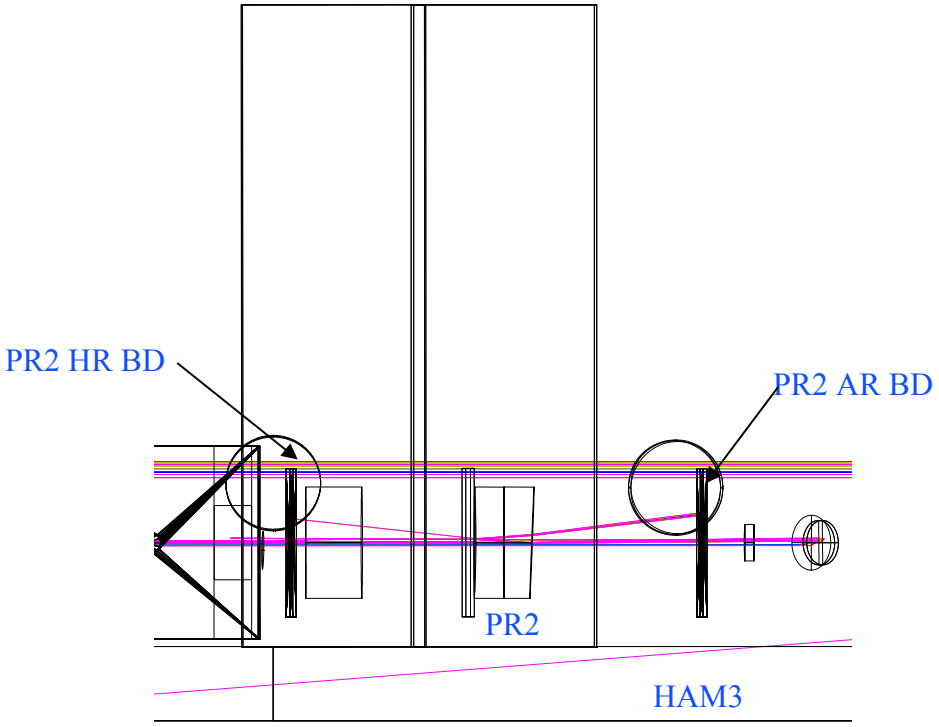

Figure 8: PR2 Plate Beam Dumps, elevation view

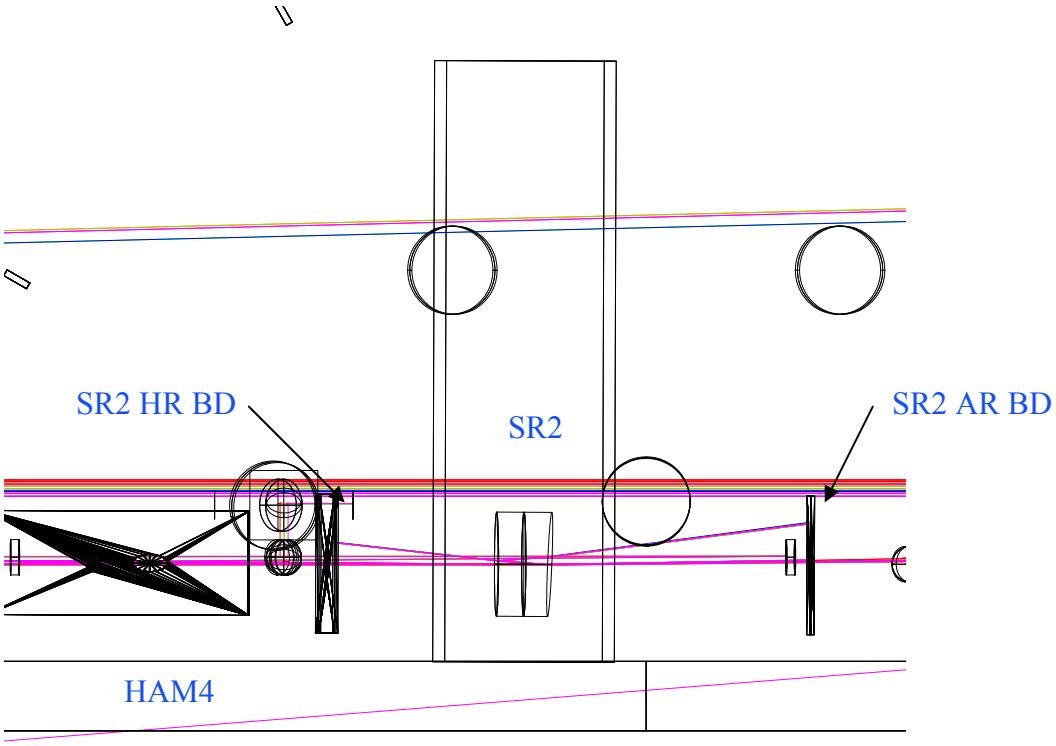

Figure 9: SR2 Plate Beam Dumps, elevation view

3.4 PR3 and SR3 Plate Beam Dumps

The PR3 and SR3 ghost beams from the AR side will be caught in the beam dump adjacent to the AR surface, as shown in Figure 10, and Figure 11.

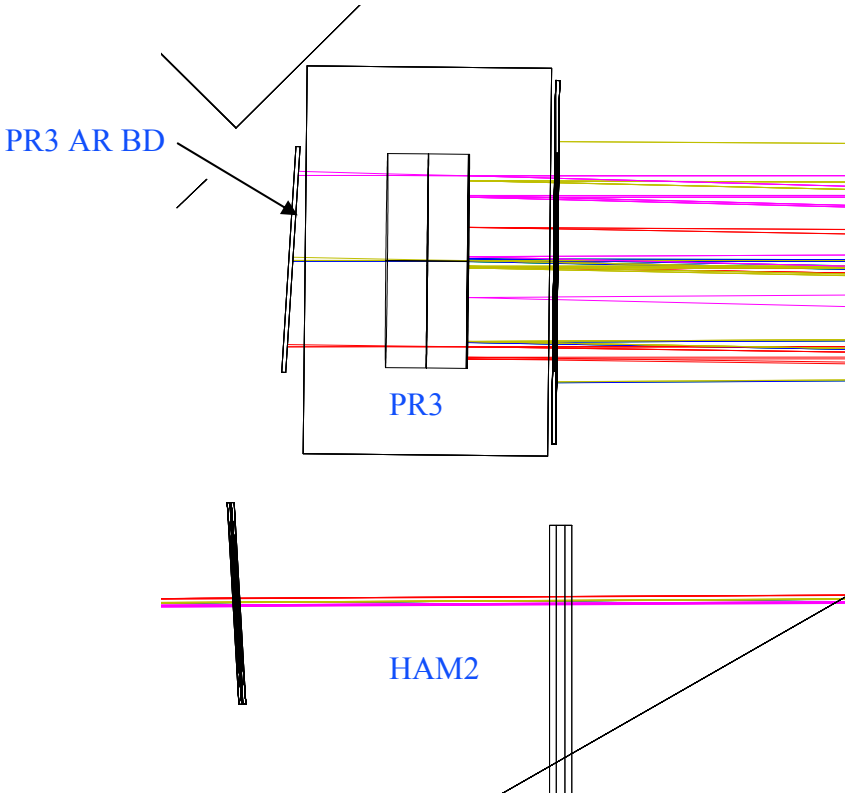

Figure 10: PR3 AR beam dump

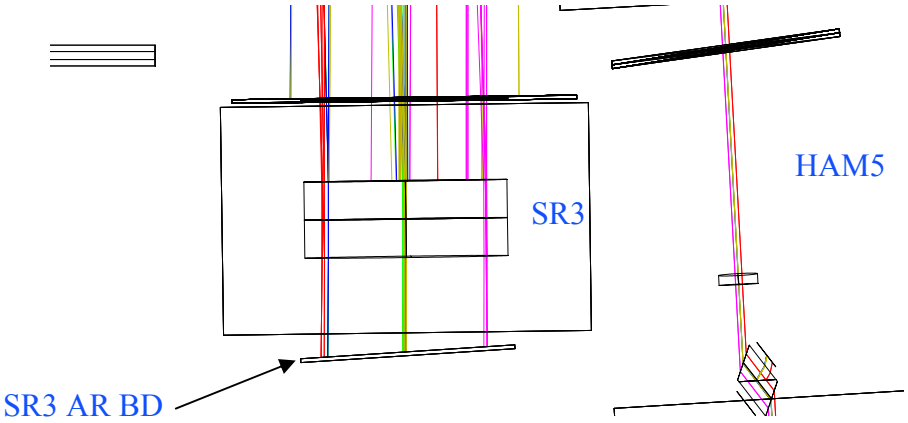

Figure 11: SR3 AR beam dump

The ghost beams from the HR surfaces of PR3 and SR3 will hit the IO and OUT beam tube walls and will not cause excessive scattered light noise.

3.5 Output Faraday Isolator

The components from the Initial LIGO Faraday Isolators will be re-used for ADLIGO with a modification to preserve the in-line beam direction and to allow the provision for injecting an external "squeezing" beam into the AS port of the IFO.

The scattered light model indicates that the Output Faraday Isolator must be suspended in order to reduce the scattered light noise from the 16 optical surfaces. Some of the optical surfaces have vertical wedge angles that cause horizontal to vertical motion coupling, therefore motion isolation is also required in the vertical direction.

A preliminary Solid Works model of the Faraday Isolator suspension is shown in **Figure 12**. The optical components are isolated by a two-wire pendulum and by vertical blade springs. The suspended table is damped by a suspended eddy current damping plate that hangs below the Faraday Isolator optical table.

The pitch and yaw pointing angles of the Output Faraday Isolator will be pre-set during initial alignment. A remotely controlled Picomotor will provide a small amount of pitch motion to avoid a possible glint from the optical surfaces of the Faraday Isolator into the AS port of the IFO.

3.5.1 Stay Clear Diameter

The clear aperture of the Faraday Isolator is 20 mm diameter. The AS Gaussian beam diameter at the output of the SRM is approximately 4 mm. The clear aperture of the Faraday Isolator will be pre-aligned within 2 mm of the beam centerline by referencing its position to the center of the ITM.

This meets the requirement 4.7 Clear Aperture Requirements

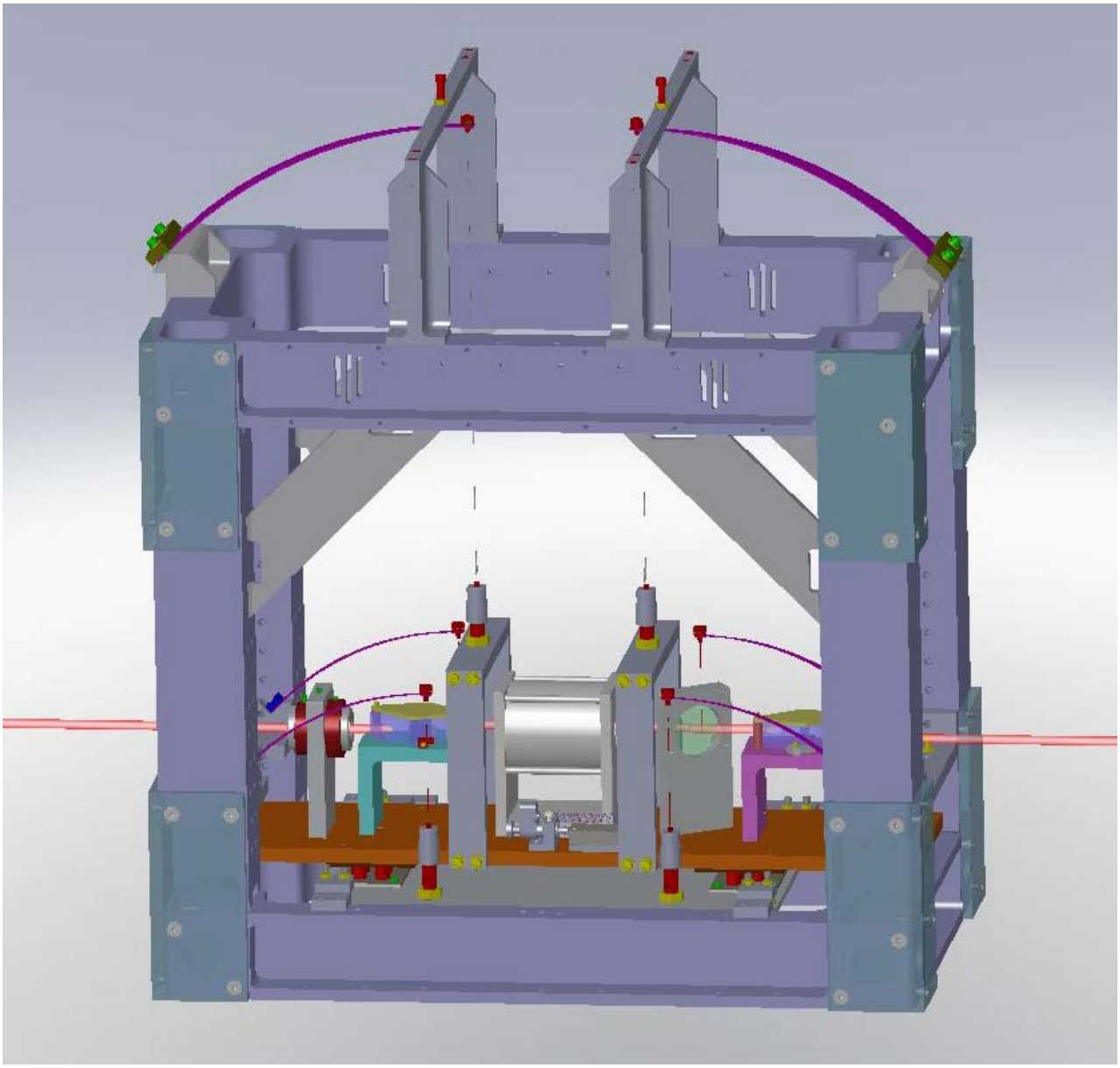

Figure 12: Suspended Faraday Isolator

3.6 Arm Cavity Baffle

The H2 ITM Arm Cavity Baffle is shown in Figure 13. The baffle is suspended with a "viton o-ring-damped" single pendulum suspension from the Stage "0" HEPI support ring of the BSC optical table adjacent to the HR side of the ITM; the details of the Viton damped suspension are shown in **Figure 18**.

The louver structure is made of oxidized, polished stainless steel. The hole diameters in the baffle are slightly larger than the diameter of the ITM and ETM mirrors. The H1 beam passes through the second hole in the baffle.

The same two-hole baffle configuration hangs in front of the H1 ETM. A one-hole version of the baffle will be used in L1 for the ITM and ETM.

Earthquake stops will be mounted to the BSC vacuum enclosure.

3.7 COC Wide Angle Scatter Baffle

The COC Wide Angle Scatter Baffle hangs in front of the COC and intercepts the wide-angle scattered light from point defects on the ITM and ETM mirrors, which is assumed to have a Lambertian distribution with total integrated scattered power equal to 10ppm fraction of the circulating power in the arm cavity. The baffle will either be suspended independently or will be mounted to the Arm Cavity Baffle and suspended as a composite assembly.

Some of the wide angle scattered light will pass through the beam holes in the Arm Cavity Baffle and hit the manifold wall; the rest will be intercepted by the suspended combined Manifold/Cryopump Cryopump Baffle.

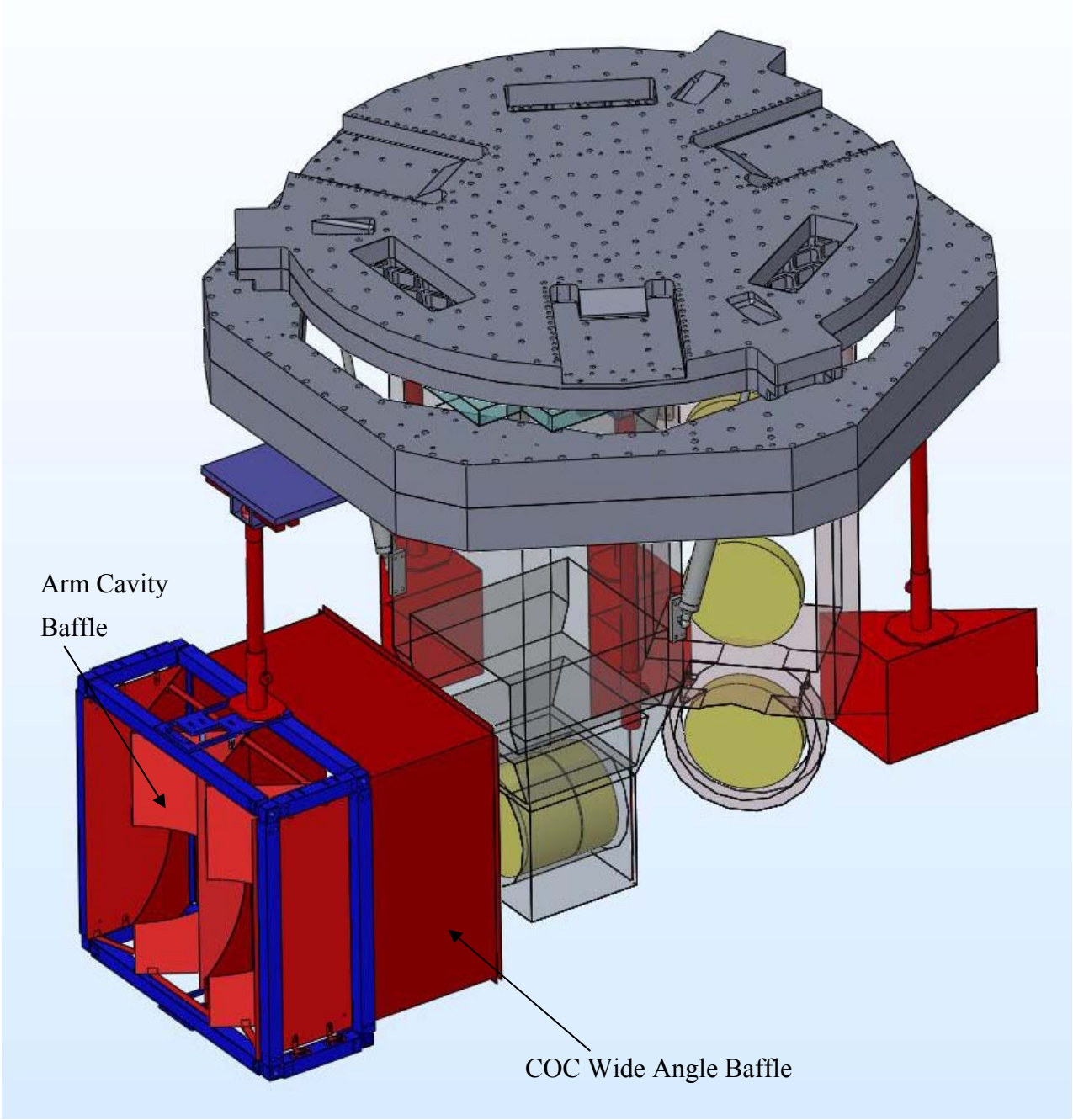

Figure 13: Suspended Arm Cavity Baffle and COC Wide Angle Baffle in front of H2 ITM

.

3.8 Manifold/Cryopump Baffles

The Manifold Baffle and the Cryopump Baffle are integral and are suspended together. The combined baffle, which consists of an inner and outer cylinder, a cone, and an annular baffle plate, is suspended by wires from vertical blade springs that are mounted to a support ring that is compressed against the inside surface of the manifold near the A-1 adapter.

3.8.1 Manifold Baffle

The Manifold Baffle shown in Figure 14, which is a view seen from the direction of the ITM and ETM, hides the corner of the A-1 Adapter flange that seals the end of the manifold leading from the arm to the ITM and ETM mirrors and avoids retro-reflection of the wide angle scattered light from the ITM and ETM.

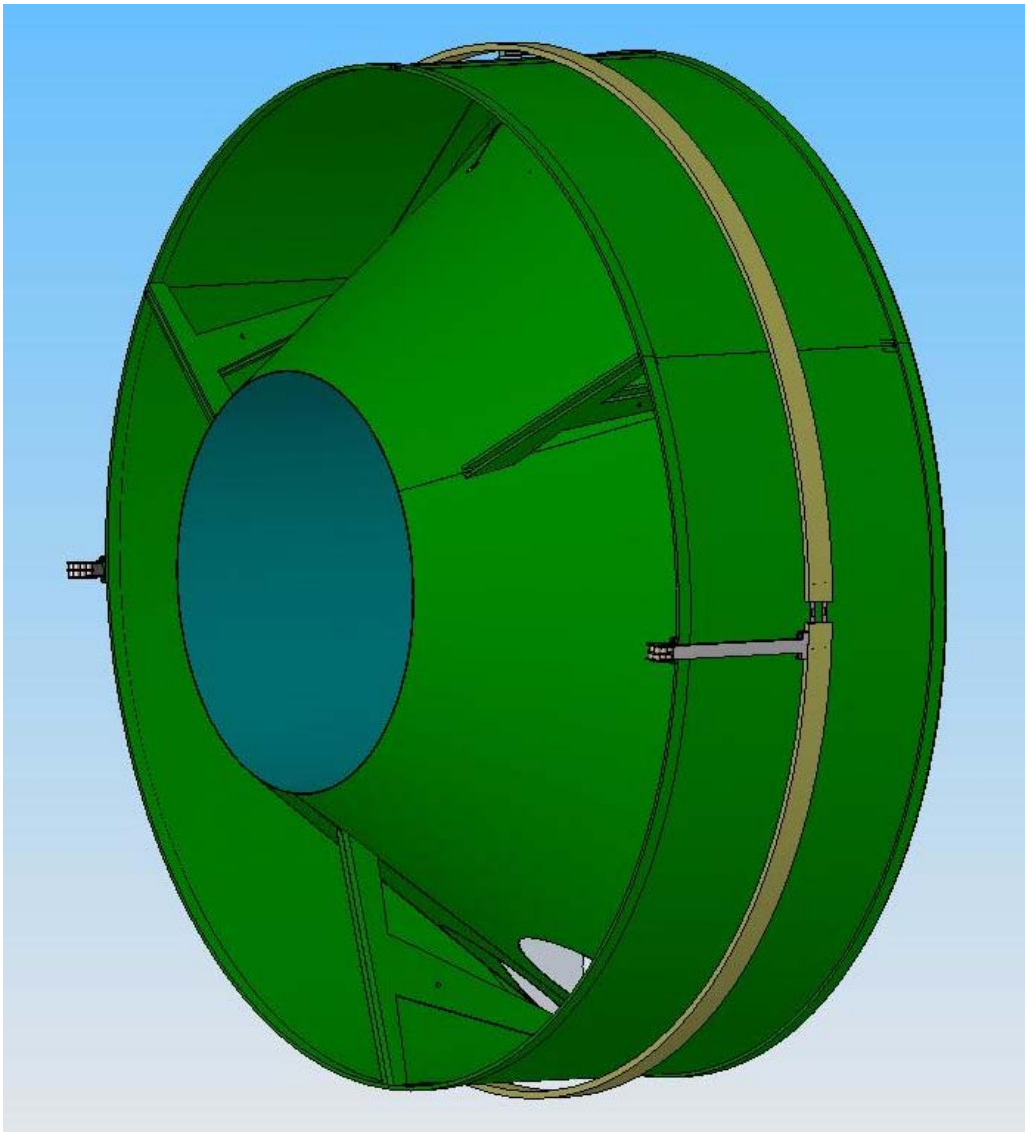

Figure 14: Manifold Baffle

3.8.2 Cryopump Baffle

The Cryopump Baffle is shown in Figure 15, which is a view from the direction of the arm. It consists of a cylinder, a cone, and an annular baffle plate with holes to admit the optical lever beams.

The Cryopump Baffle serves two purposes: 1) It blocks the narrow angle scattered light from the far COC at the opposite end of the beam tube—in the right side in this picture—that floods into the clear annular region between the shark's-tooth beam tube baffles and the cryopump baffle cylinder; this light gets trapped by multiple reflections between the cylinder the cone and the annular plate with the viewport holes. And, 2) it obscures the interior surfaces of the cryopump from the line of sight as viewed from the ITM and ETM HR surfaces and avoids back-scattered light from the

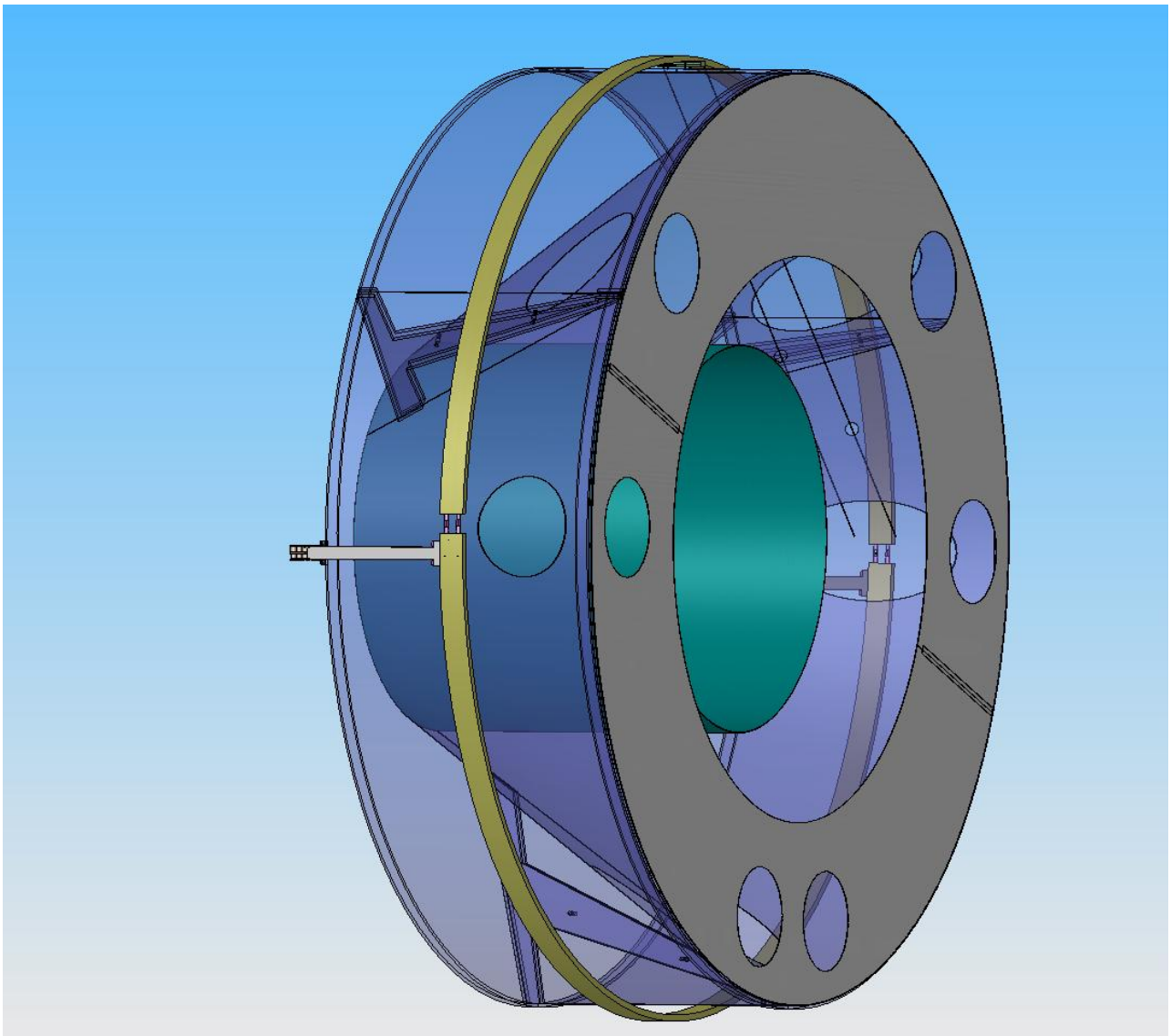

Figure 15: Cryopump Baffle

surfaces of the cryopump impinging on the ITM and ETM HR surfaces.

This meets the requirements: 4.5 Cryopump Baffle Requirement, and 4.7 Clear Aperture Requirements.

3.9 Elliptical Baffles

The PRM Elliptical baffle is placed inside the power recycling cavity between PR3 and the BS. It's purpose is to create an elliptical beam profile at the surface of the BS that matches the clear aperture of the BS, by vignetting the input Gaussian beam with an elliptical shaped aperture.

The ITM Elliptical baffles will be placed on the X and Y arm sides of the BS. The purpose of these baffles is to vignette the Gaussian-shaped beams entering the recycling cavity from the arms so that the wings of the beam do not hit the structure of the BS suspension. The beam shape will match the elliptical beam profile created by the PRM Elliptical Baffle.

3.9.1 PRM Elliptical Baffle

The PRM Elliptical Baffle is shown in Figure 16. The PRM Elliptical Baffle mounts directly to HAM3, and HAM9 optical tables.

The baffle is constructed of oxidized polished stainless steel.

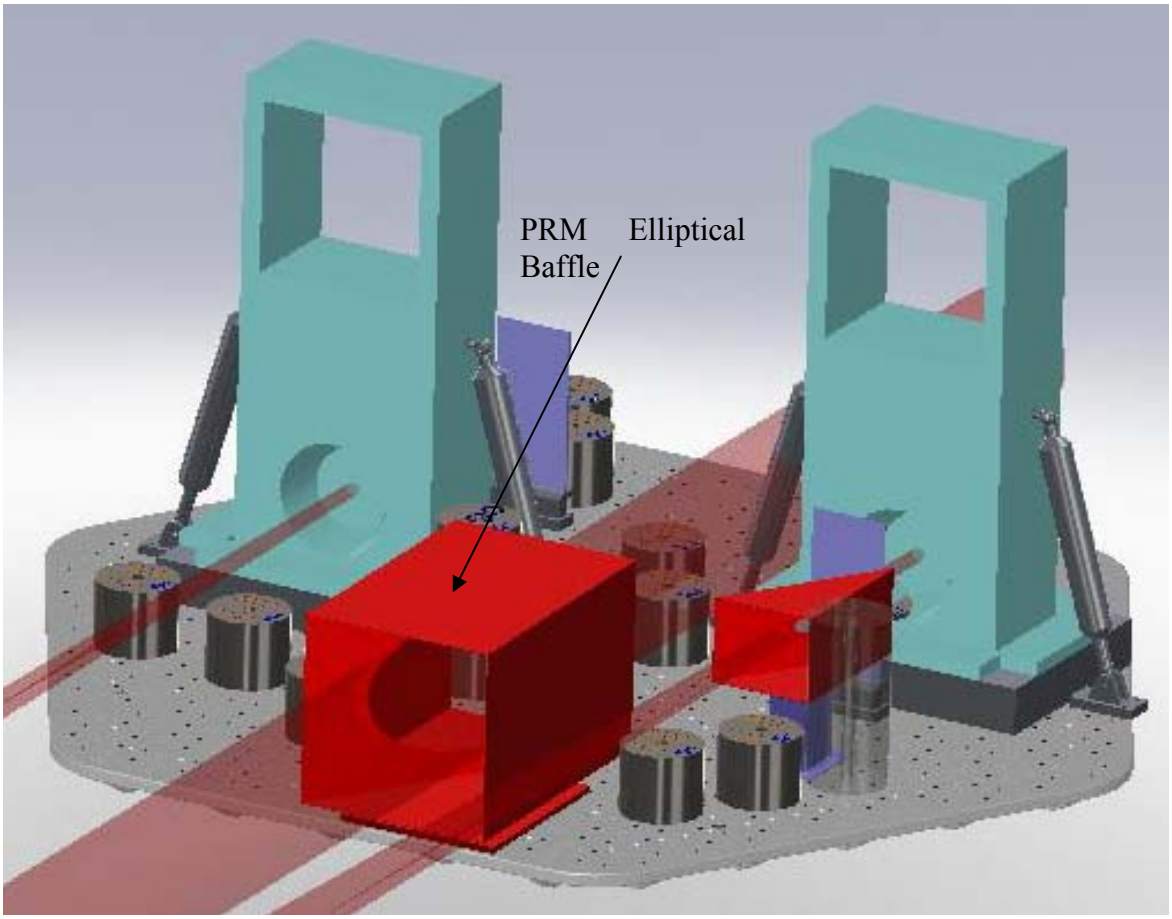

Figure 16: PRM Elliptical Baffle on HAM3

3.9.2 ITM Elliptical Baffles

The ITM elliptical baffle will be suspended with a Viton damped suspension structure shown in Figure 17; the suspension is attached to the HEPI support ring in the BSC2 and BSC4 chambers. Earthquake stops will be mounted to the chamber walls. The open "V" of the baffle points toward the corresponding ITM. The baffle is constructed of oxidized polished stainless steel.

Figure 17: Suspended ITM Elliptical Baffle

The details of the Viton damped suspension shown in Figure 18.

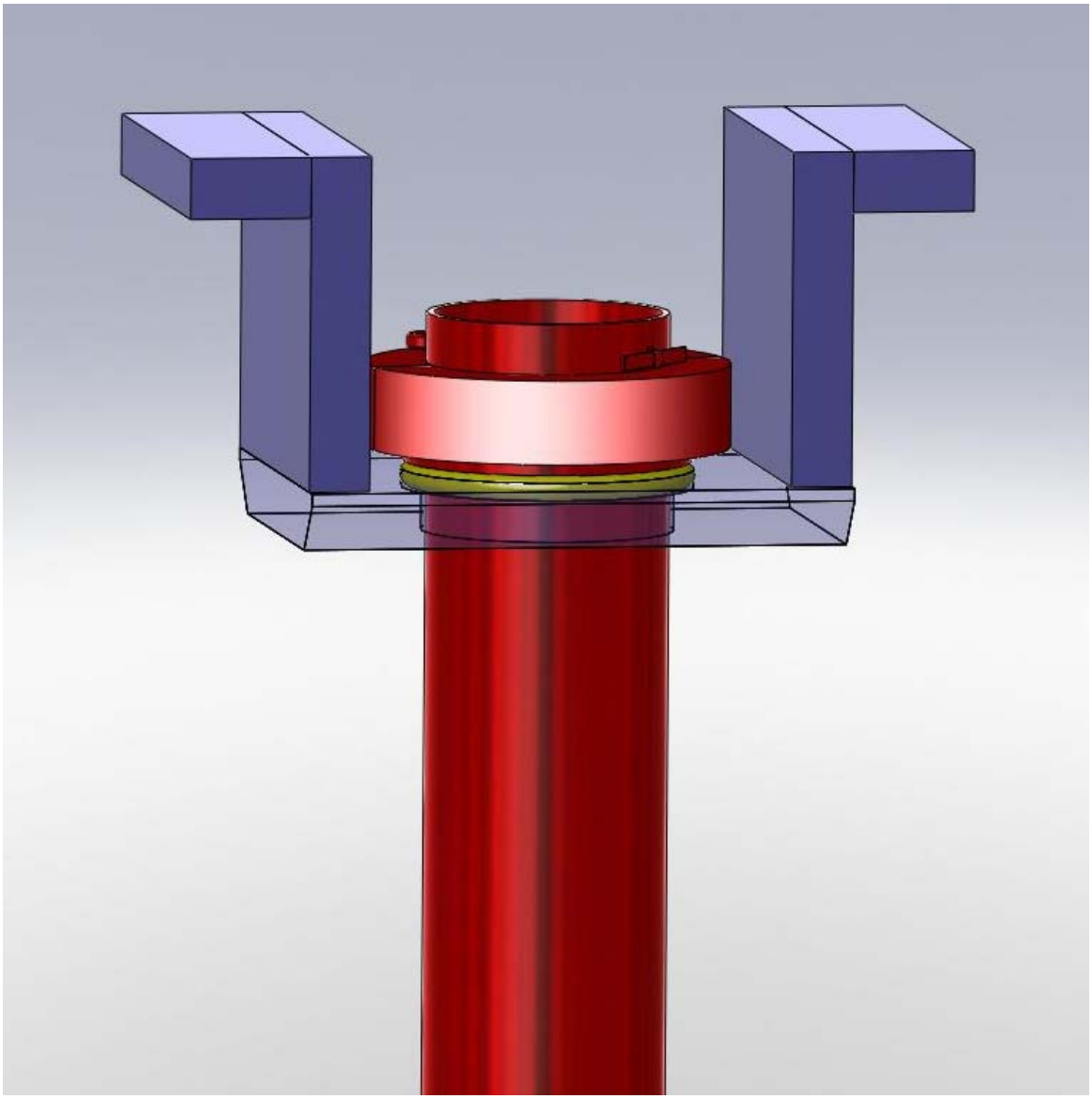

Figure 18: Viton Damped Suspension

3.10 H2 Elliptical Scraper Mirror/Beam Dump

3.10.1 Elliptical Scraper Mirror

The H2 Elliptical Scraper Mirror hangs between the back of the ITM Compensation Plate and the Fold Mirror (FM), as shown in Figure 19. It serves the same purpose as the ITM Elliptical Baffle in H1 and L1 of creating an elliptical beam profile at the surface of the BS that matches the clear aperture of the BS by vignetting the Gaussian beam entering the recycling cavities from the arm direction with an elliptical shaped aperture.

This Scraper Mirror reflects the edges of the Gaussian beam onto the surface of a beam dump and precludes this power from hitting the suspension structures of the FM and BS mirrors.

The Scraper Mirror is made from polished stainless steel and is suspended with a "viton o-ring-damped" single pendulum suspension from the BSC optical table.

3.10.2 Scraper Beam Dump

The Scraper Beam Dump is constructed of oxidized polished stainless steel and is suspended with a "viton o-ring-damped" single pendulum suspension from the Stage "0" HEPI support ring of the BSC optical table, as shown in Figure 19.

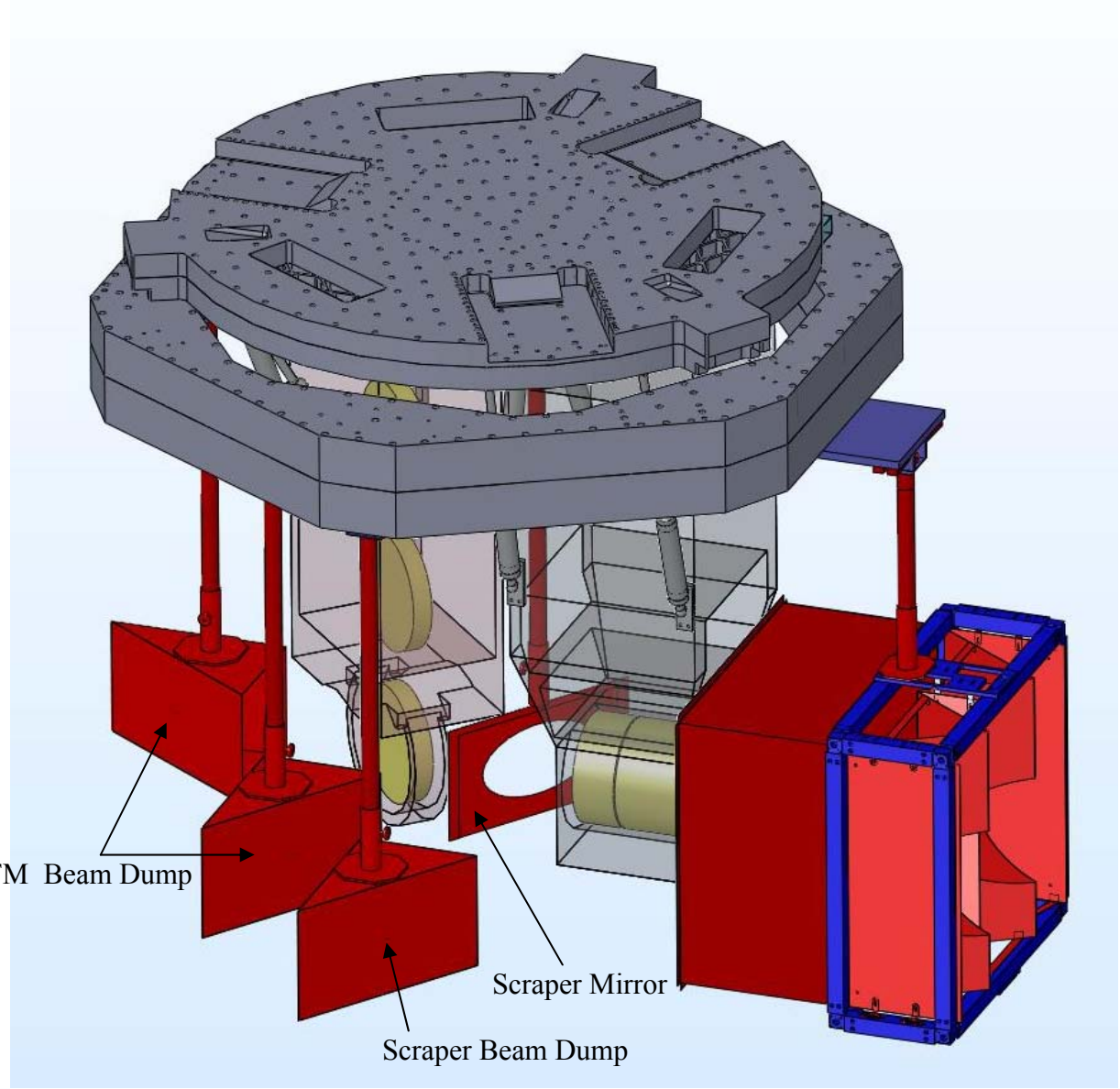

Figure 19: H2 Scraper Mirror/Beam Dump & FM Beam Dumps

3.11 H2 Fold Mirror Beam Dump

One Fold Mirror Beam Dump is placed behind the FM to catch the leakage beam that passes through the HR coating from the arm direction. Another Fold Mirror Beam Dump is placed behind the FM to catch the leakage beam that passes through the HR coating from the recycling cavity direction. The beam dumps are constructed of oxidized polished stainless steel and are suspended with "viton o-ring-damped" single pendulum suspensions from the Stage "0" HEPI support ring of the BSC optical table, shown in Figure 19.

4 Stray Light Control Performance Characteristics

4.1 Scattered Light Sources

The AOS scattered light sources that contribute to the total scattered light displacement noise are listed in Table 3 together with the incident power and the scattered power. The AOS scattered light displacement noise requirement was taken to be < 1/14 of the thermal noise limit, which is one half of the total scattered light power budget.

Table 3: Scattered Light Source, Incident Power and Scattered Power

SCATTERING SOURCE	INCIDENT POWER, W	SCATTERED POWER, W
Faraday	1.35E-01	2.71E-11
AC_Baffle	7.33E+00	7.07E-18
AC_Baffle_Refl	1.76E-04	8.14E-26
AS_Window	1.35E-01	2.20E-17
AS_Window_Refl	3.38E-04	6.88E-19
ITMX_PO_Window	5.27E-02	4.30E-19
RC_PO_Window	1.35E-05	2.20E-22
Cryo_Baffle	2.77E+00	2.67E-18
Cryo_Baffle_Refl	6.64E-05	3.07E-26
ITM_GBAR1_BD	5.27E-02	1.52E-15
ITM_GBAR1_BD_Refl	1.26E-06	1.75E-23
ITM_GBAR3_BD	5.21E-02	1.49E-15
ITM_GBAR3_BD_Refl	1.25E-06	1.71E-23
ITM_GBAR4_BD	2.59E-06	3.68E-24
ITM_GBHR3_BEAM_TUBE_BAF	2.62E-04	1.25E-21
ITM_GBHR4_BEAM_TUBE_BAF	1.30E-08	3.10E-30
BS_GBAR3X_BEAM_TUBE_BAF	1.32E-04	1.12E-22
BS_GBAR4X_BEAM_TUBE_BAF	3.29E-09	6.99E-32
BS_GBHR3X_BEAM_TUBE_BAF	1.32E-04	1.12E-22
BS_GBHR4X_BEAM_TUBE_BAF	3.29E-09	6.99E-32
BS_GBAR3P_BD	2.63E-02	2.68E-16
BS_GBAR3P_Ref	6.32E-07	3.09E-24
BS_GBHR3P_BD	2.63E-02	2.68E-16
BS_GBHR3P_Refl	6.32E-07	3.09E-24

SCATTERING SOURCE	INCIDENT POWER, W	SCATTERED POWER, W
ITM_Ellip_Baffle	3.70E-01	1.26E-21
ITM_Ellip_Baffle	8.88E-06	1.45E-29
BSC_wide_angle	4.25E-04	0.00E+00
manifold_wide_angle	8.93E-01	0.00E+00
Total_BSC_Manifold_Wide_Angle		8.03E-20
AC_Baffle_wide_angle	4.67E+00	
AC_Baf_cyl_wide_angle	2.84E+00	
Total_AC_Baf_cyl_Wide_Angle		9.66E-18
PRM_Ellip_Baffle	2.50E-03	1.19E-17
PRM_Ellip_Baffle_Refl	6.00E-08	5.02E-29
ETM_Tel_Baffle	4.88E-02	3.32E-19
ETM_Tel_Baffle_Refl	3.42E-03	3.26E-21
manifold_wide_angle	8.93E-01	8.03E-20
AS_Window_Refl	3.38E-04	6.88E-19
ITMX_PO_Window_Refl	1.32E-04	1.34E-20
RC_PO_Window_Refl	3.37E-08	6.88E-24
ITMY_HARTMANN_BS_TRANS	1.35E-05	5.51E-19
ITMY_HARTMANN_VIEWPORT	3.37E-08	1.38E-27
ITMX_HARTMANN_VIEWPORT	2.63E-04	2.15E-19
ITMX_HARTMANN_VIEWPORT_REFL	3.29E-07	1.32E-23
PRM_GBAR1	6.25E-03	2.70E-19
PRM_GBAR3	1.76E-02	5.97E-16
PRM_GBHR3	4.71E-03	4.30E-17
PRM_Total		1.28E-15
PR2_GB0t	2.11E-01	8.59E-15
PR2_GBAR3	1.05E-05	2.15E-22
PR2_GBHR3	1.05E-09	2.15E-30
PR2_Total		1.72E-14
PR3_GB0t	2.11E-01	2.86E-15
PR3_GBAR3	1.05E-05	7.16E-24
PR3_GBHR3	1.05E-09	1.43E-31
PR3_GBAR_Total		5.73E-15
PR3_GBHR_Total		2.86E-31
SRM_GBAR3	2.59E-07	2.03E-21

SCATTERING SOURCE	INCIDENT POWER, W	SCATTERED POWER, W
SRM_GBHR3	1.08E-08	3.52E-24
SRM_Total		4.07E-21
SR2_GB0t	1.35E-05	5.51E-19
SR2_GBAR3	6.75E-10	1.38E-26
SR2_GBHR3	6.75E-14	1.38E-34
SR2_GBHR3	6.75E-14	1.38E-34
SR2_Total		1.10E-18
SR3_GB0t	1.35E-05	1.84E-19
SR3_GBAR3	6.75E-10	4.59E-28
SR3_GBHR3	6.75E-14	9.18E-36
SR3_GBAR_Total		3.67E-19
SR3_GBHR_Total		1.84E-35
H2_Elliptical_Scraper_Mirror	0.37	1.134E-21
H2_Elliptical_Scraper_Beam_Dump	0.333	0.782E-20
H2_Foldmirror_Beam_Dump	0.105	3.59E-21

4.2 Summary of Scattered Light Displacement Noise

A summary of the scattered light displacement noise with all the AOS baffles and beam dumps in place, and with the Septum Windows in place is shown in Figure 20. The Scattered Light Noise exceeds the thermal noise requirement at the frequency approximately 26 Hz.

The Septum Windows in the output beam is the main culprit, and removing them meets the AOS Scattered Light Noise Requirement, 4.2.1 Direct Requirements, at most frequencies, as shown in Figure 21.

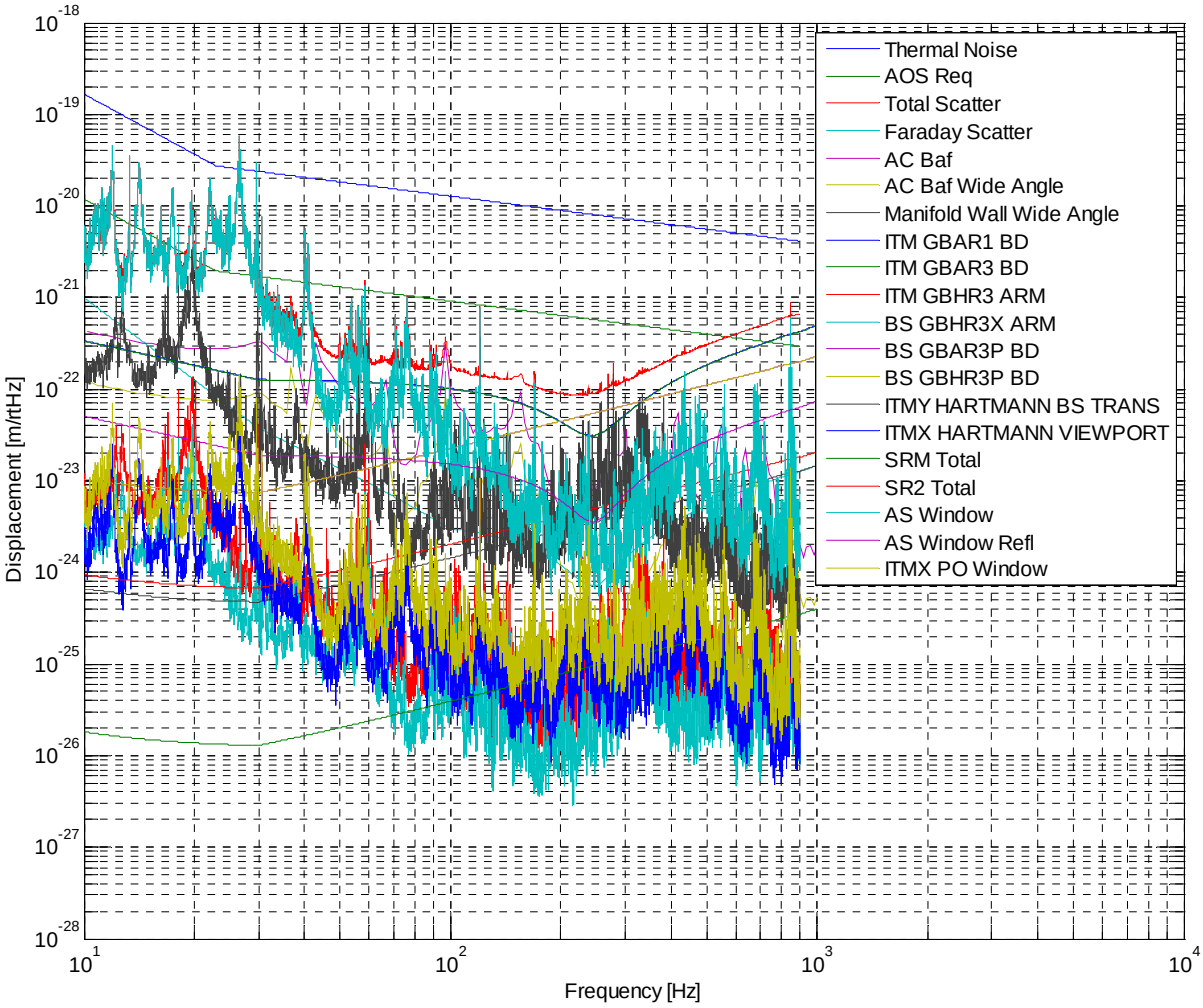

Figure 20: Scattered Light Displacement Noise, Septum Windows in Place

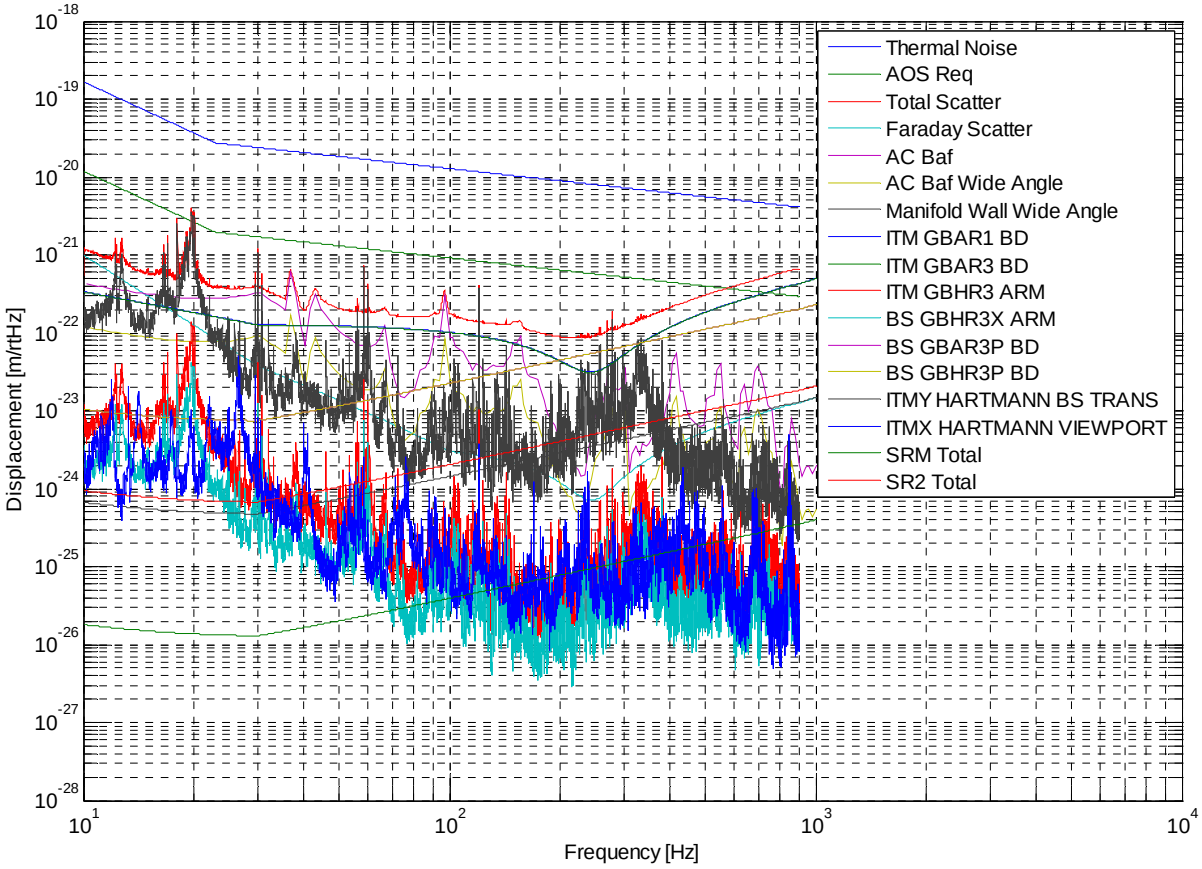

Figure 21: Scattered Light Displacement Noise, Septum Windows Removed

4.3 Scattered Light Displacement Noise Sources

4.3.1 Output Faraday Isolator

The scattered light model indicates that the Output Faraday Isolator must be suspended in order to reduce the scattered light noise from the optical surfaces. The Faraday Isolator crystal has 1 deg wedge angles on the input and output surfaces, which might cause horizontal to vertical motion coupling of the scattering surfaces; therefore motion isolation is provided in the vertical direction by means of blade springs.

A possible glint from the optical surfaces of the Faraday Isolator into the AS port of the IFO will be avoided by pitching the Faraday Isolator table.

4.3.1.1 Faraday Isolator Forward Transmissivity

The measured transmissivity of the Initial LIGO Output Faraday Isolator is 98%.

This meets the requirement 4.3 Faraday Isolator Requirements.

4.3.1.2 Faraday Isolator Reverse Transmissivity

The measured reverse power transmission of the Initial LIGO Output Faraday Isolator is < 0.0001.

This meets the requirement 4.3 Faraday Isolator Requirements.

4.3.1.3 BRDF of Faraday Surfaces

The Output Faraday Isolator has four calcite prism surfaces and one TGG crystal surface on the entrance side. These surfaces will scatter light back toward the antisymmetric port of the IFO. The light scattered by the additional surfaces beyond the Faraday rotator magnet will be attenuated by the reverse transmissivity of the Faraday Isolator and will be ignored.

The BRDF of the TGG surface was estimated using the fractal back-scattering model proposed by R. Weiss; see T920004-00 Estimation of Special Optical Properties of a Triangular Ring Cavity, for incidence angles between 1E-4 and 1E-1 radians.

$$BRDF(\theta) := \frac{\alpha}{\theta^2}$$

where

$$\alpha := 1.5 \cdot 10^{-3} \cdot S$$

and S is the total integrated scattering loss of the surface.

Assuming an incidence angle on the Faraday Isolator surfaces of 1.7E-2 rad (1 deg) and a total scattering loss per surface of 100 ppm, the estimated BRDF is 5E-4 sr^{-1}.

It was assumed that the calcite prisms have a similar BRDF, and that the scattered light noise injected into the IFO will add coherently in phase.

4.3.1.4 Output Faraday Isolator Suspension

The Output Faraday Isolator will be suspended by a two-wire pendulum with vertical blade springs, as shown in **Figure 12**. The vertical bounce frequency of the Output Faraday Isolator is designed to be approximately 1 Hz, and the pendulum frequency is designed to be approximately 0.8 Hz. The suspended eddy current damping plate is expected to provide a Q <15.

The suspension frame will be mounted to the HAM 5 optical table, which has the motion requirement shown in Figure 22.

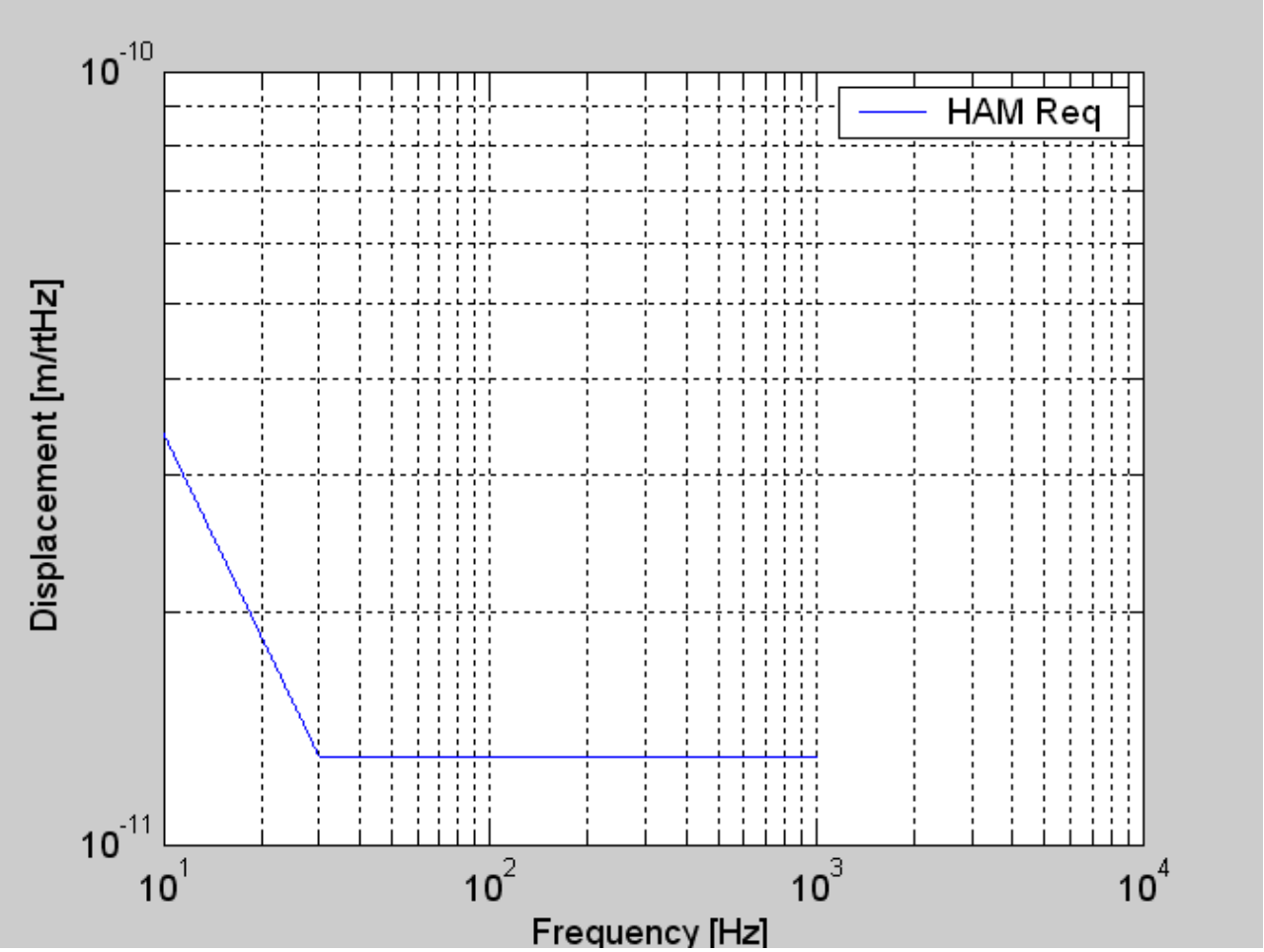

Figure 22: HAM optics table Seismic Motion Requirement

The minimum Output Faraday Isolator motion attenuation requirements were determined using the scattered light model, assuming five surfaces with BRDF of 5E-4 sr^{-1}, and are shown in the blue curve of Figure 23, together with a calculated simple pendulum transfer function, the green curve.

4.3.1.5 Scattered Light Displacement Noise of Suspended Output Faraday Isolator

The scattered light displacement noise caused by the suspended Output Faraday Isolator is shown in **Figure 24**.

4.3.1.6 Stay Clear Diameter

The clear aperture of the Faraday Isolator is 20 mm diameter. The Gaussian beam diameter at the output of the SRM is approximately 4 mm. The clear aperture of the Faraday Isolator will be pre-aligned within 2 mm of the beam centerline by referencing its position to the center of the ITM.

This meets the requirement 4.7 Clear Aperture Requirements

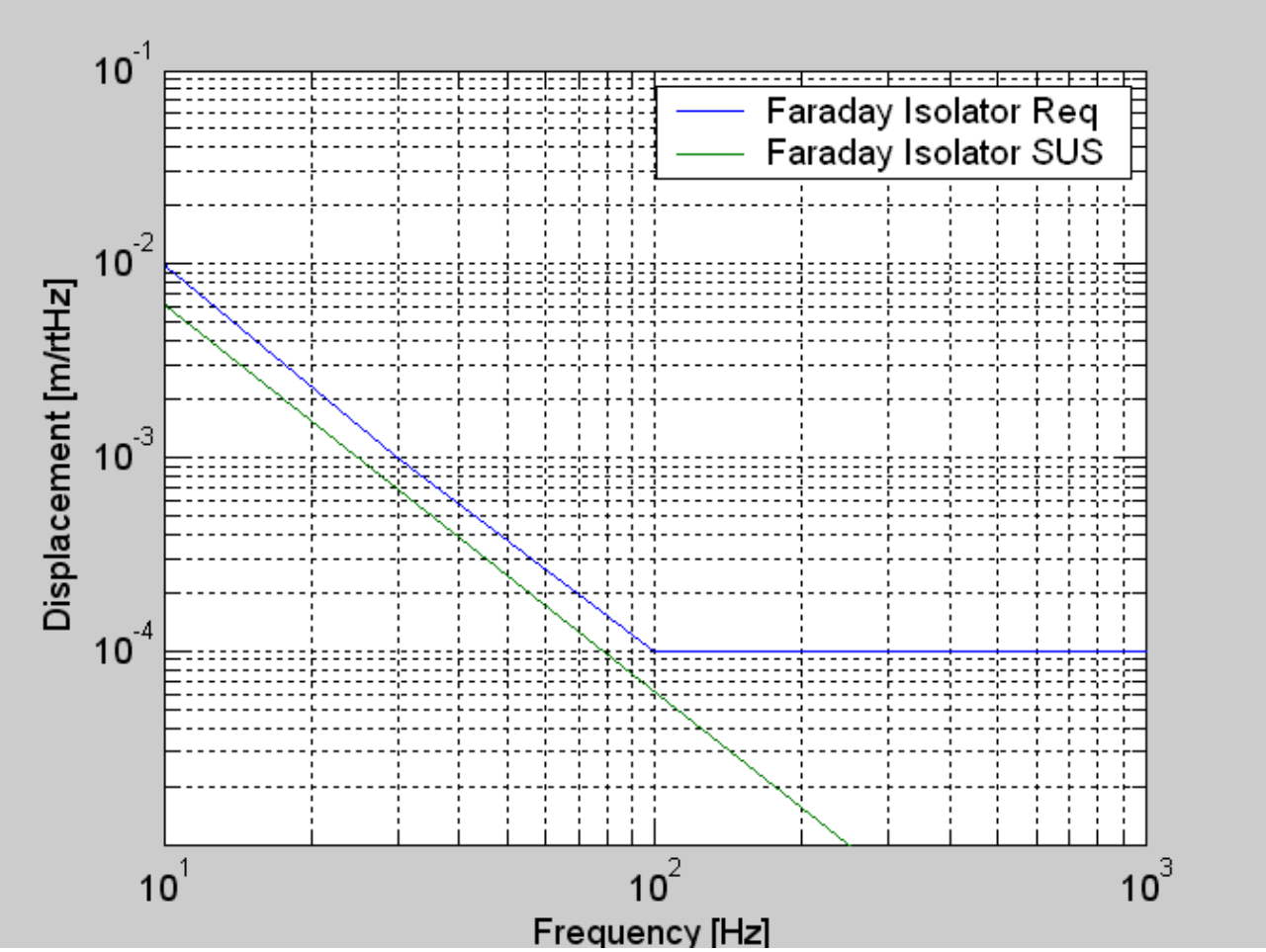

Figure 23: Output Faraday Isolator SUS Amplitude Response

4.3.2 Wide Angle COC Scatter Baffle

4.3.2.1 Arm Cavity Baffle Surface BRDF

The Arm Cavity Baffle will be constructed of oxidized polished stainless steel with the first surface inclined at an incidence angle 56 deg and the measured BRDF < 0.05 sr^{-1}. See T080064-00 Controlling Light Scatter in Advanced LIGO.

4.3.2.2 Total Wide Angle COC Scattered Light Displacement Noise

The wide-angle scatter from point defects on the ITM and ETM mirrors is assumed to have a Lambertian distribution with total integrated scattered power equal to 10ppm fraction of the circulating power in the arm cavity. Most of this scattered light will be intercepted by the Wide Angle Scatter Baffle, which is mounted to the BSC HEPI "0" ring close to the COC and behind the arm cavity baffle, and by the back of the arm cavity baffle itself. A lesser amount of the light will

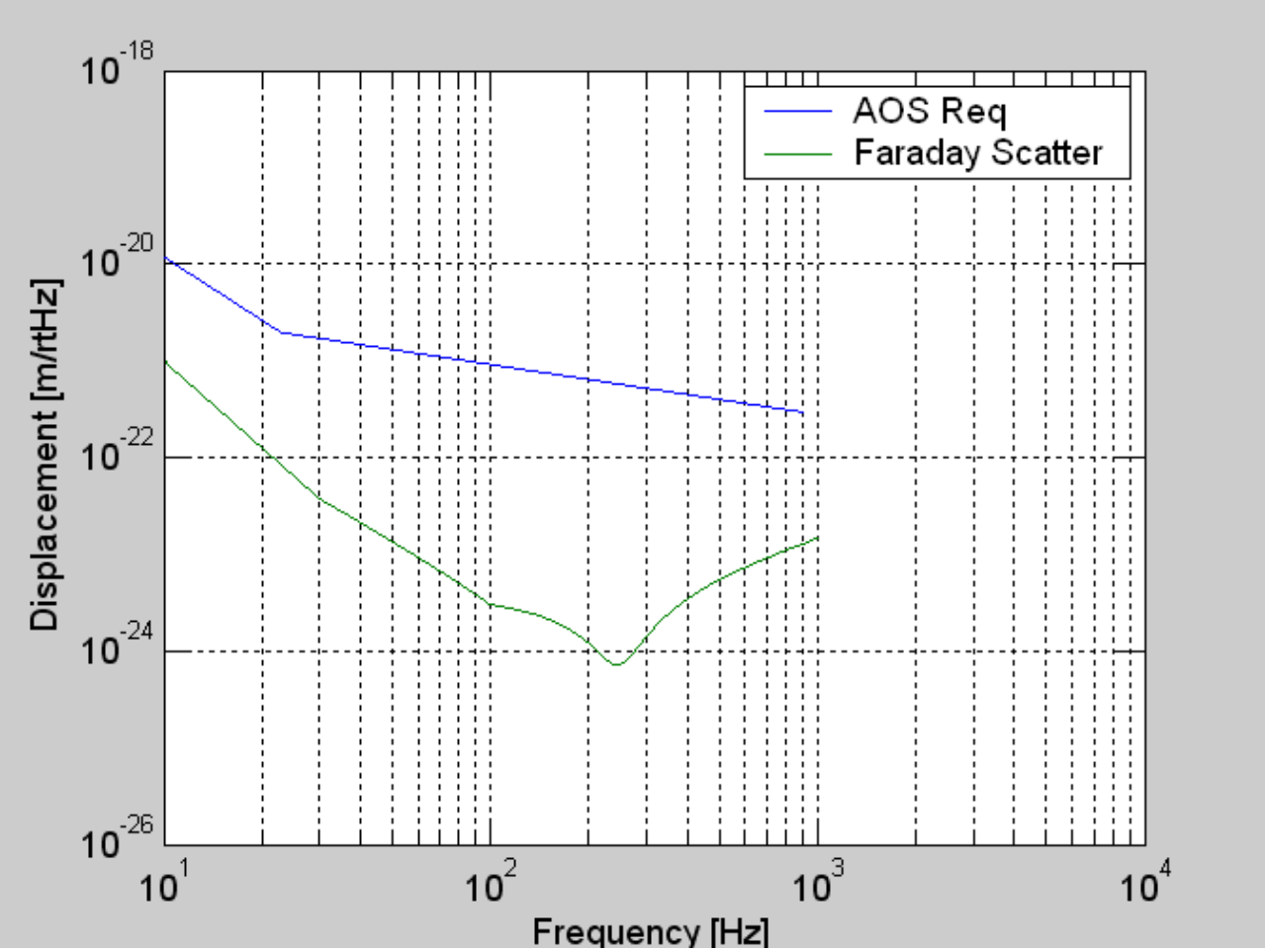

Figure 24: Scattered Light Displacement Noise from Suspended Output Faraday Isolator

pass through the beam holes in the Arm Cavity Baffle and hit the manifold wall and the suspended manifold baffle.

The motion transfer function of the Wide Angle COC Scatter Baffle is identical to that of the Arm Cavity Baffle, shown in Figure 28.

The scattered light noise was calculated using the scattered light model and is shown in Figure 29.

4.3.3 Arm Cavity Baffle

4.3.3.1 Incident Power on Arm Cavity Baffle

The power scattered from the far COC mirror, at the opposite end of the arm cavity, into the annular region bounded by the outer radius of the near COC and the inside radius of the Cryopump Baffle will be incident on the Arm Cavity Baffle. It is given by

$$P_{acb} := P_a \cdot \int_{\theta_{itm}}^{\theta_{cp}} 2 \cdot \pi \cdot \theta \cdot BRDF_1(\theta)\, d\theta$$

The Initial LIGO pathfinder COC CSIRO, surface 2, S/N 2 BRDF measurement was used to estimate the BRDF.

$$BRDF_1(\theta) := \frac{2755.12}{\left(1 + 8.50787 \cdot 10^8 \cdot \theta^2\right)^{1.23597}}$$

Where θ_{itm} is 4.25 E-5 rad

θ_{cp} is 9.612 E-5 rad

and, P_a is the arm power 8.339 E5 W

P_{acb} = 7.3 W

4.3.3.2 Arm Cavity Baffle Motion

4.3.3.2.1 HEPI Displacement

We will assume that the x-displacement spectrum of the BSC HEPI isolation system is described by Brian Lantz in the SEI elog entry ID: 596, 3/14/06, as shown in Figure 25.

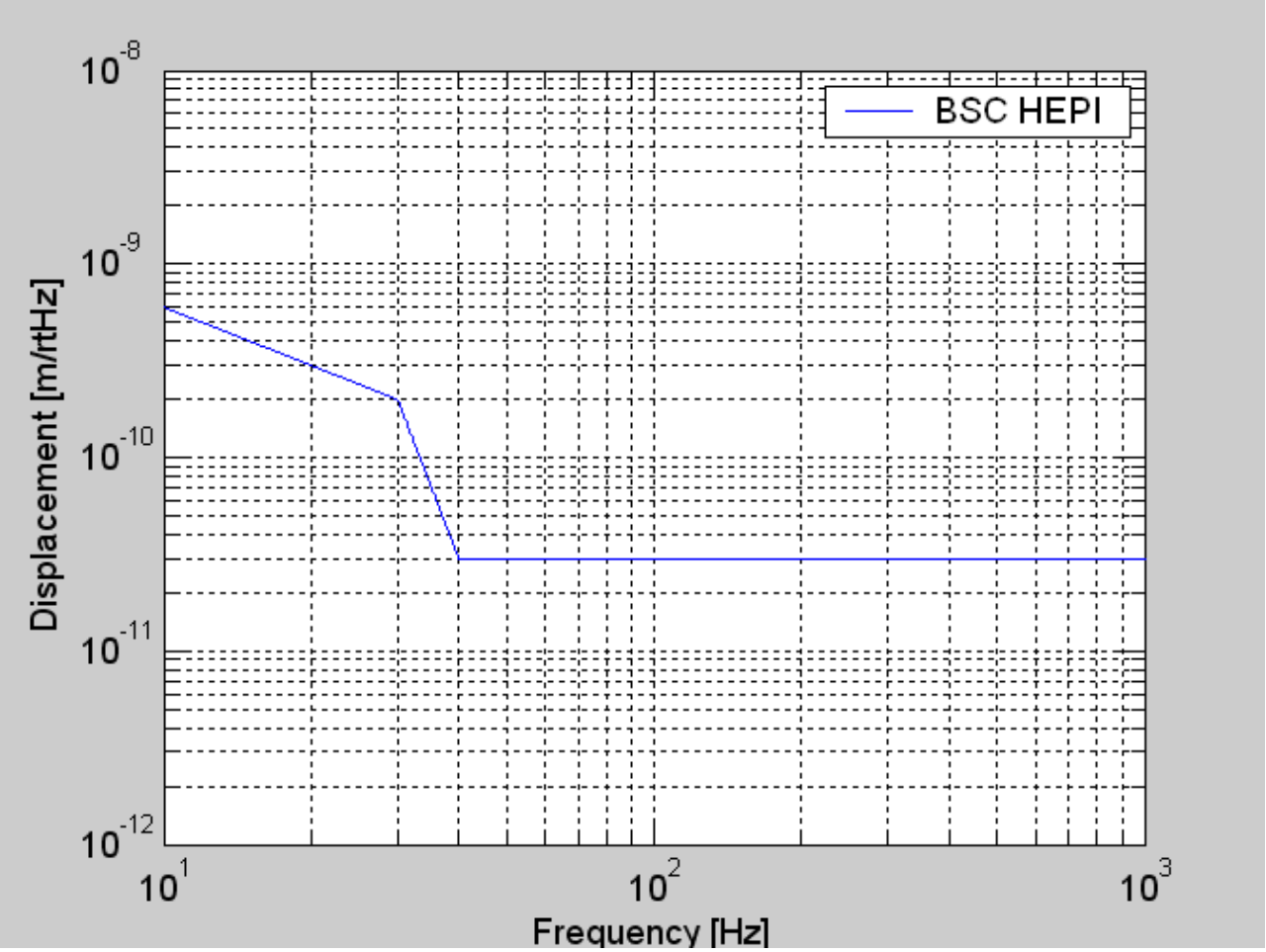

Figure 25: BSC HEPI Motion Spectrum

4.3.3.2.2 Arm Cavity Baffle Suspension Transfer Function

The amplitude motion transfer function of the Arm Cavity Baffle suspension is the same as that of the ITM Elliptical Baffle, and is shown in Figure 26—this is actually a stitching together of the transfer function of the Viton suspension from 10 Hz to 100 Hz and the transfer function of a similar length eddy current damped thick-rod suspension with similar characteristics for f > 100 Hz, because we did not take data for the Viton suspension > 100 Hz.

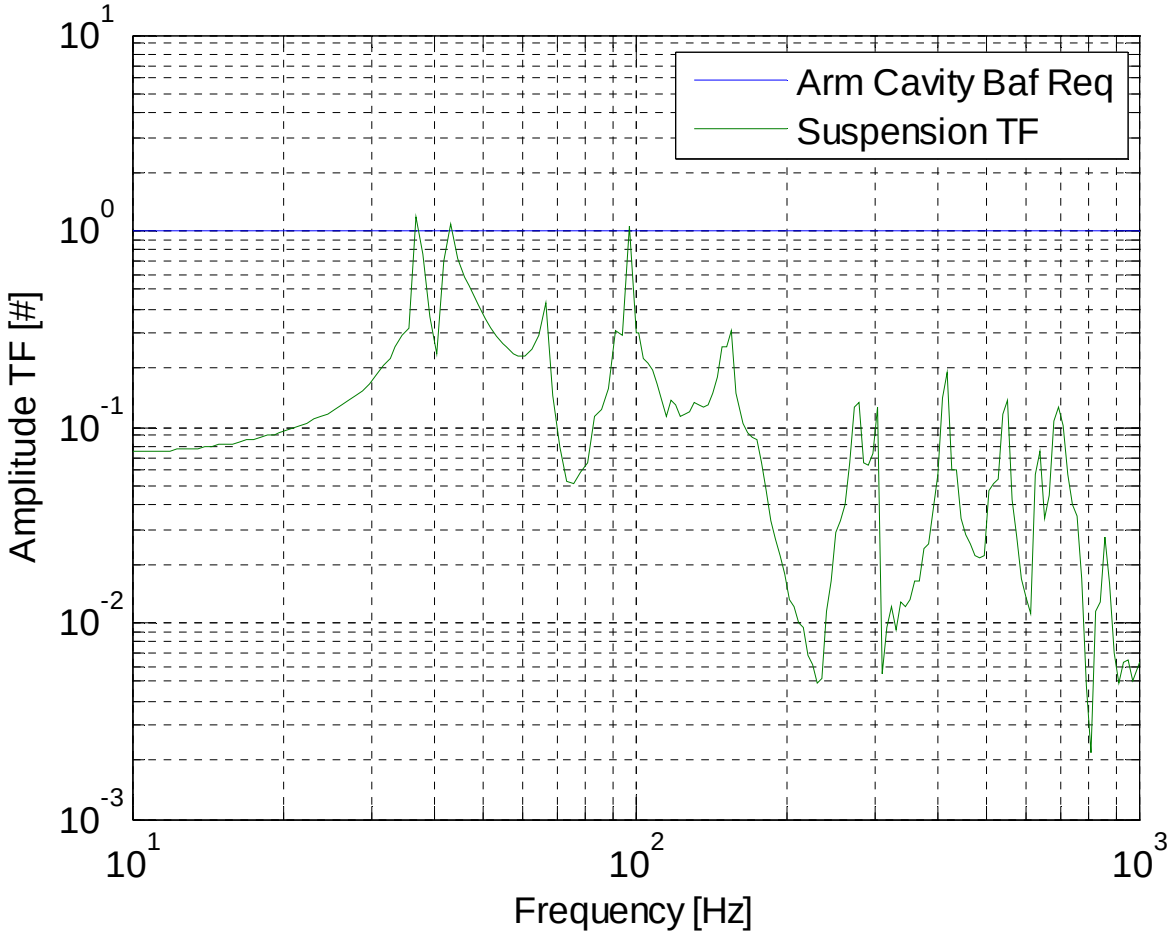

Figure 26: Arm Cavity Baffle SUS Amplitude Response

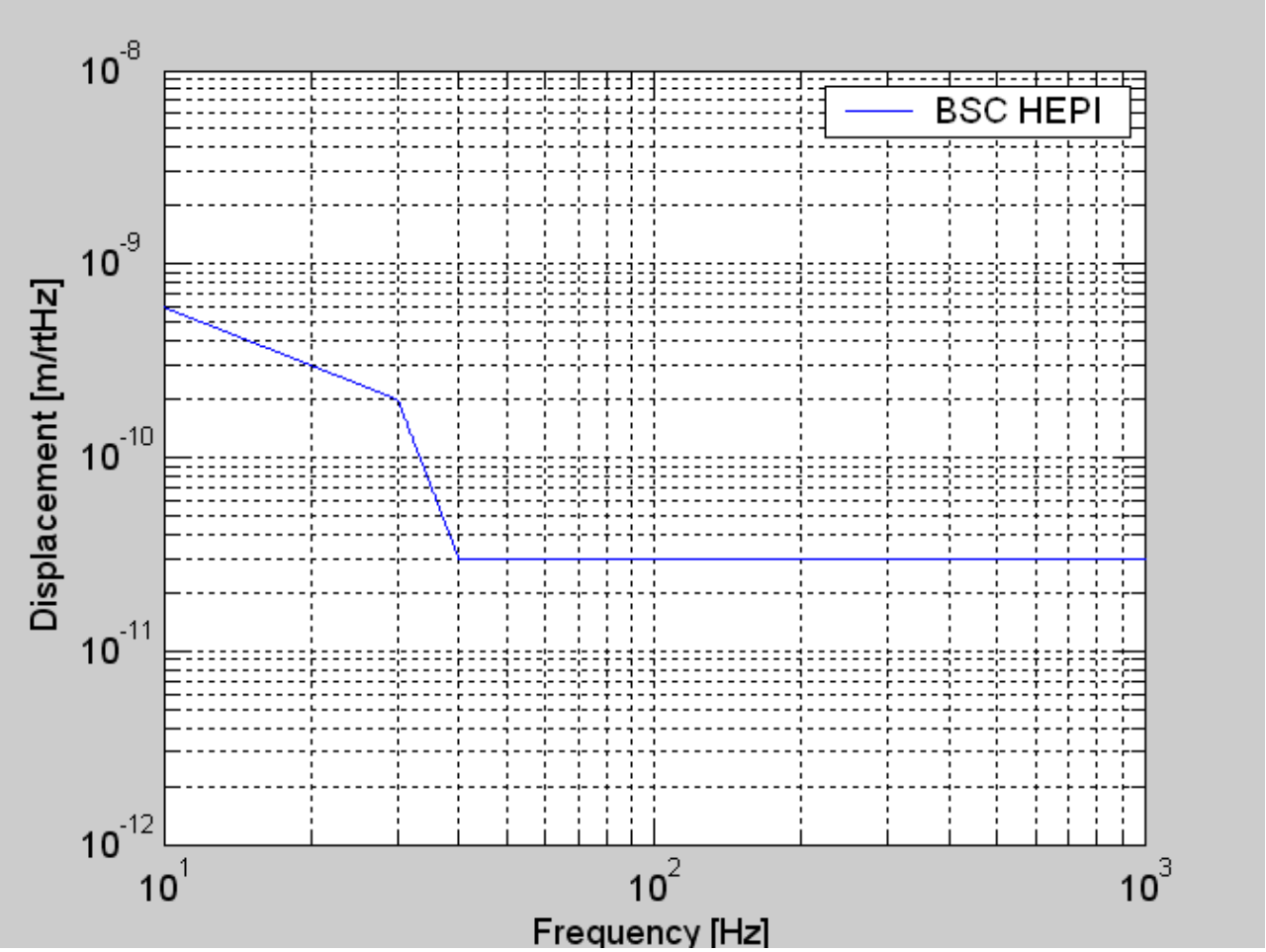

Figure 27: BSC HEPI Motion Spectrum

The hole in the Arm Cavity Baffle for the IFO beam extends in the longitudinal direction because of the tilt angle of the vertical baffle surfaces. The scattering surfaces of the exposed, rough edges of the baffle hole will exhibit a longitudinal motion due to coupling from the vertical motion. The average vertical-to-horizontal coupling factor is estimated to be 0.6.

4.3.3.3 Seismic Motion of the Vacuum Manifold

The light that reflects from the Arm Cavity Baffle will scatter from the vacuum manifold, which has the seismic motion shown in Figure 28. See Robert Schofield (11/17/06 LHO ILOG).

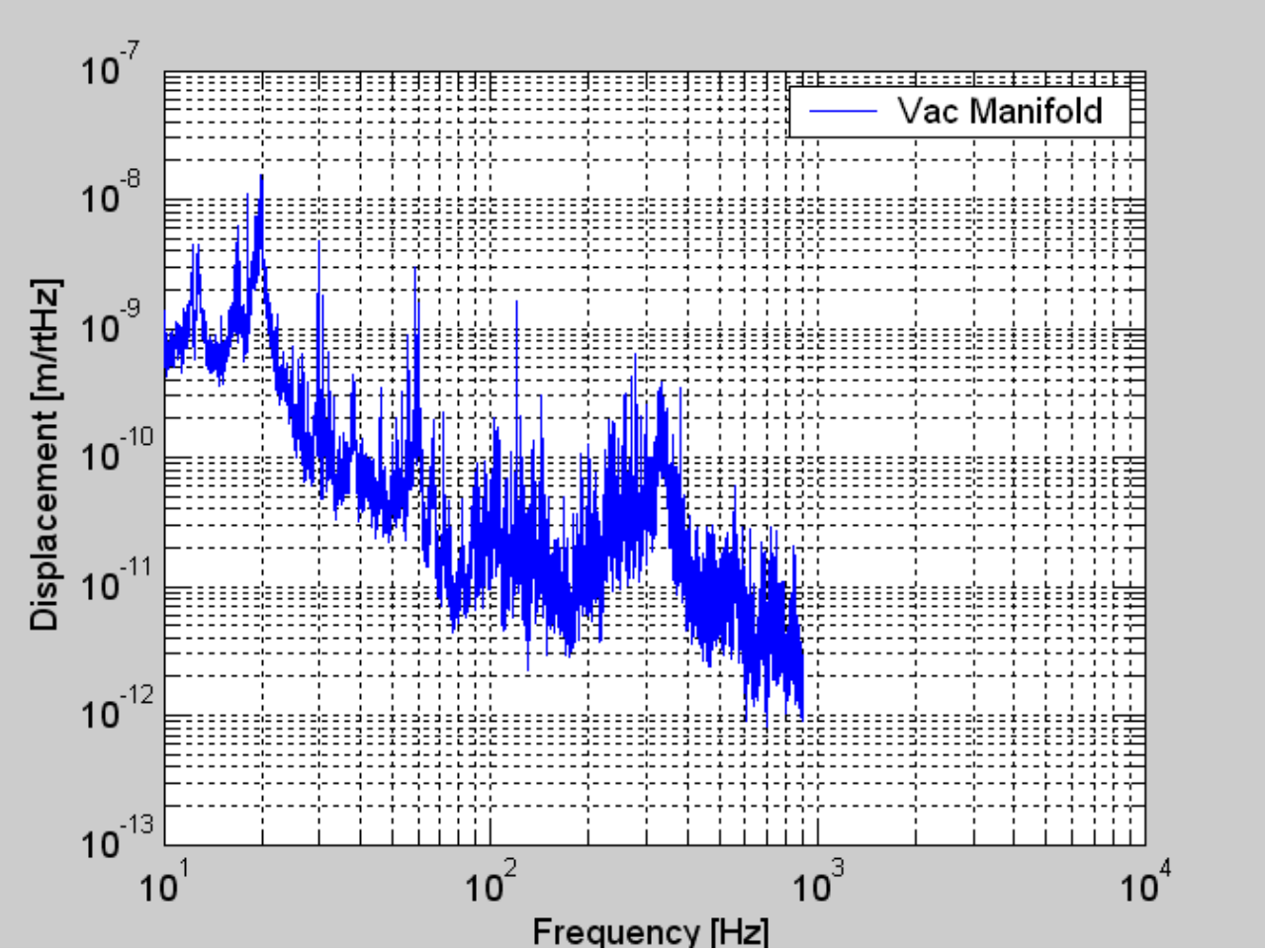

Figure 28: Seismic motion of vacuum manifold

4.3.3.4 Arm Cavity Baffle Surface BRDF

The Arm Cavity Baffle will be constructed of oxidized polished stainless steel with the first surface inclined at an incidence angle 56 deg and was measured to have a BRDF < 0.05 sr^{-1}. See T080064-00 Controlling Light Scatter in Advanced LIGO.

4.3.3.5 Arm Cavity Baffle Reflectivity

The reflectivity of oxidized stainless steel was measured to be 0.007. See T080064-00 Controlling Light Scatter in Advanced LIGO.

The reflectivity of the Arm Cavity Baffle with four internal bounces is estimated to be 2.4 E-5.

4.3.3.6 Scattered Light Displacement Noise of Suspended Arm Cavity Baffle

The light that scatters directly from the surface of the suspended Arm Cavity Baffle has a phase noise caused by the seismic motion of the HEPI support structure attenuated by the transfer function of the Arm Cavity Baffle suspension.

The light that reflects from the baffle and subsequently scatters from the vacuum manifold walls will have a phase noise caused by the seismic motion of the walls. The vacuum manifold is assumed to have a BRDF = 0.1 sr^-1

The scattered light noise was calculated using the scattered light model and is shown in Figure 29.

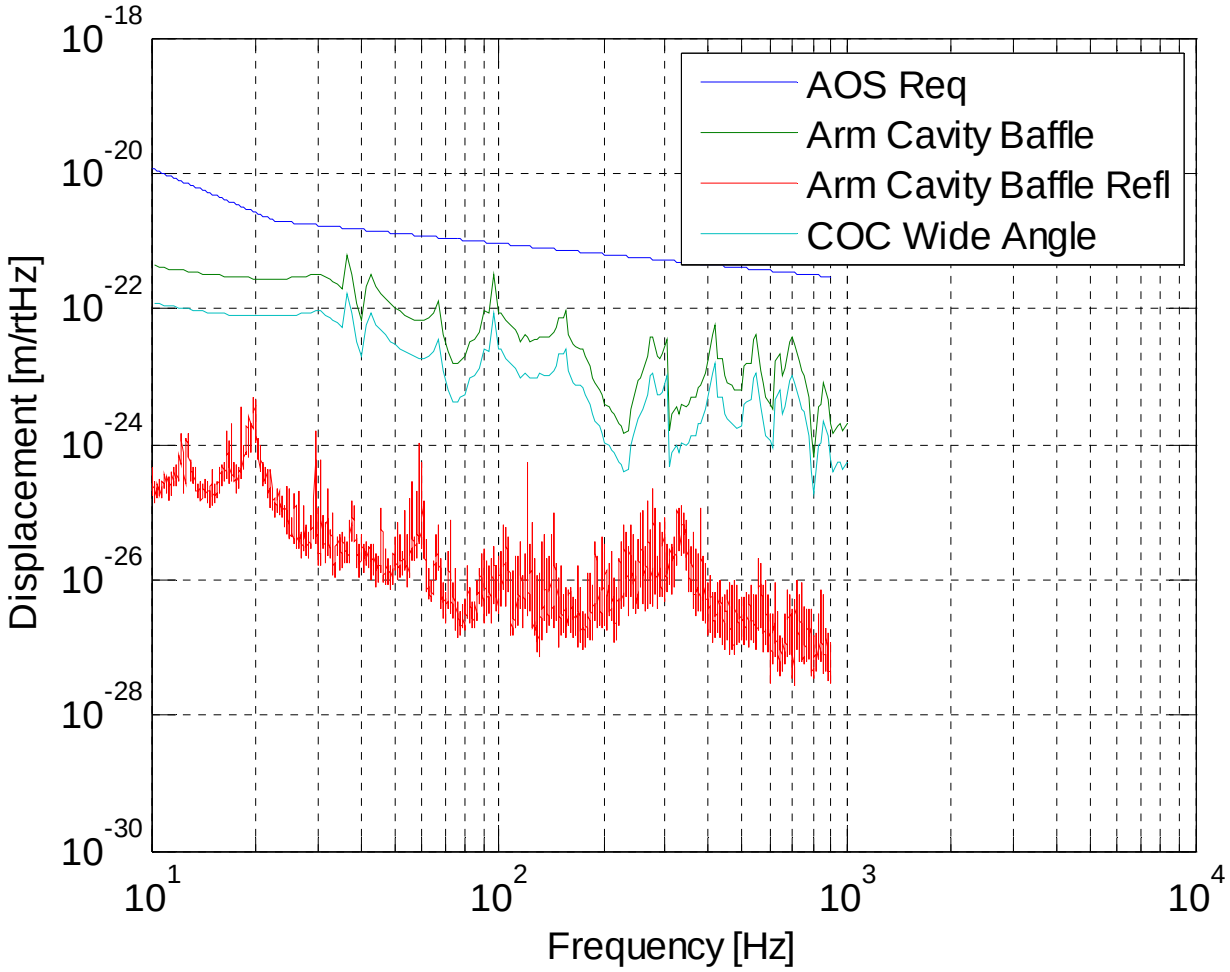

Figure 29: Arm Cavity Baffle and Cryopump Baffle Scattered Light Displacement Noise

4.3.3.7 Fringe Wrapping of Arm Cavity Baffle Displacement Noise

The Arm Cavity Baffle may have a vertical bounce resonance at approximately 2 Hz. The displacement noise at the odd harmonics of the motion due to fringe wrapping was calculated using the fringe wrap model, see Fringe-Wrapping in Appendix A—Scattered Light Noise Theory, assuming a simple pendulum function with a Q = 1000 at the resonant frequency. The fringe wrapping does not cause excessive noise above 10 Hz, as shown in Figure 30.

4.3.3.8 Stay Clear Diameter

The clear aperture of the Arm Cavity Baffle is 346 mm diameter, which is larger than the diameter of the ITM and ETM COC. The clear aperture will be pre-aligned by referencing its position to the center of the HR surface of the COC in the quad suspension frame within 4 mm.

This meets the requirement 4.7 Clear Aperture Requirements.

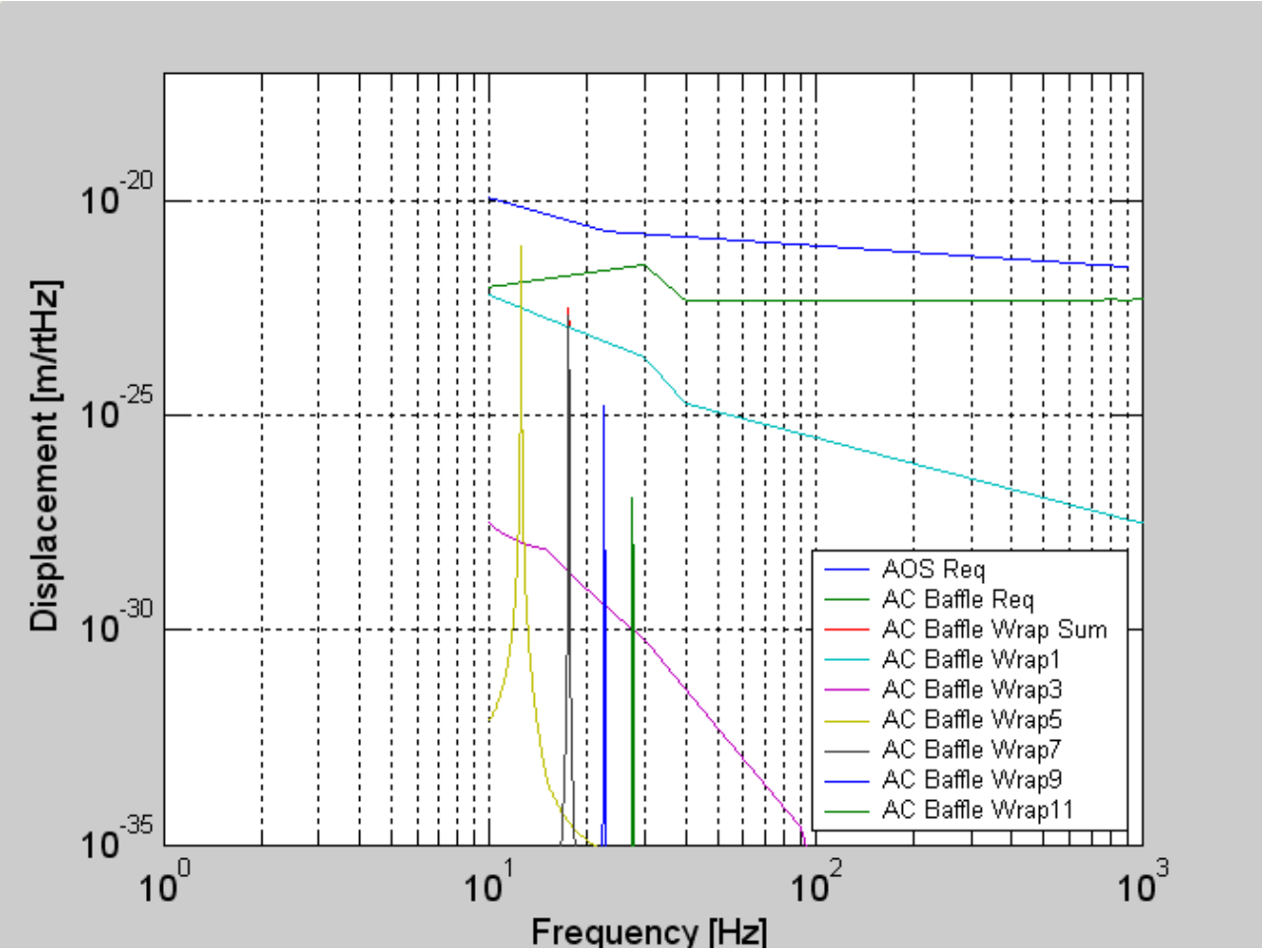

Figure 30: Arm Cavity Baffle Scattered Light Displacement Noise Caused by Fringe-wrapping

4.3.4 Manifold Baffle

The Manifold Baffle will be constructed from oxidized polished stainless steel with the first surface inclined at an incidence angle 56 deg and was measured to have a BRDF < 0.05 sr^{-1}. See T080064-00 Controlling Light Scatter in Advanced LIGO.

4.3.4.1 Manifold Baffle Surface BRDF

The Manifold Baffle will be constructed of oxidized polished stainless steel with the first surface inclined at an incidence angle 56 deg and was measured to have a BRDF < 0.05 sr^{-1}. See T080064-00 Controlling Light Scatter in Advanced LIGO.

4.3.4.2 Seismic Motion of Manifold Baffle

The Manifold Baffle and the Cryopump Baffle are both suspended together from vertical blade springs with a wire pendulum and are damped with eddy current damping magnets attached to the sides of the manifold. The blade springs are mounted to a support ring that is compressed against the inside surface of the manifold near the A-1 adapter. The horizontal motion transfer function of the suspended Manifold Baffle is expected to be similar to that of the Initial LIGO LOS structure with the addition of eddy current damping to the support structure, as shown

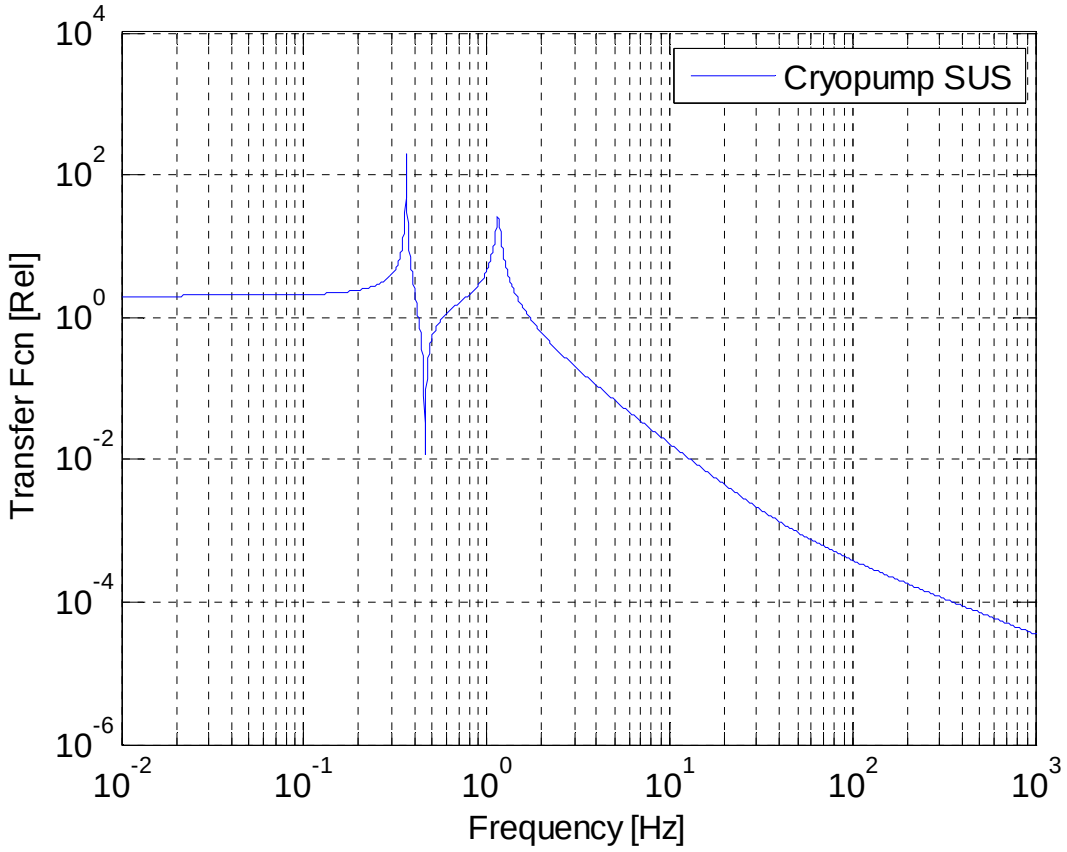

Figure 31: Cryopump Baffle and Manifold Baffle SUS transfer function

4.3.5 Cryopump Baffle

The power scattered from the far COC at the opposite end of the arm cavity into the annular region bounded by the inner radius of the Cryopump Baffle and the beam tube radius is incident on the Cryopump Baffle. The incident power is given by

$$P_{cp} := P_a \cdot \int_{\theta_{cp}}^{\theta_{bt}} 2 \cdot \pi \cdot \theta \cdot BRDF_1(\theta)\, d\theta$$

The Initial LIGO pathfinder COC CSIRO, surface 2, S/N 2 was used to estimate the BRDF.

$$BRDF_1(\theta) := \frac{2755.12}{\left(1 + 8.50787 \cdot 10^{8} \cdot \theta^{2}\right)^{1.23597}}$$

Where θ_{cp} is 9.612 E-5 rad

θ_{bt} is 1.327 E-4 rad

and, P_a is the arm power 8.339 E5 W

P_{cp} = 2.8 W

4.3.5.1 Cryopump Baffle Suspension

The Cryopump Baffle consists of a cylinder, a cone, and an annular baffle plate, which are suspended by springs from the circular, spool piece support ring. Eddy-current or elastomeric damping will be used to damp the pitch, yaw, and vertical motion.

4.3.5.2 Cryopump Blocking

The Cryopump Baffle will be placed inside the spool pieces closest to the cryopumps on the ITM side of the arms and the ETM side of the arms. It obscures the interior surfaces of the cryopump from the line of sight as viewed from the ITM and ETM HR surfaces and avoids backscattered light from the surfaces of the cryopump impinging on the ITM and ETM HR surfaces.

This meets the requirements: 4.5 Cryopump Baffle Requirement, and 4.7 Clear Aperture Requirements.

4.3.5.3 Cryopump Baffle Motion Requirements

The Cryopump Baffle motion transfer function for horizontal motion is shown in Figure 31.

4.3.5.4 Cryopump Baffle Surface BRDF

The Cryopump Baffle will be constructed of oxidized polished stainless steel with the first surface inclined at an incidence angle 56 deg and was measured to have a BRDF < 0.05 sr^{-1}. See T080064-00 Controlling Light Scatter in Advanced LIGO.

4.3.5.5 Cryopump Baffle Reflectivity

The light that is not absorbed by the Cryopump Baffle will reflect from the baffle surface onto the insides of the spool piece. There, it will scatter, reflect again from the Cryopump Baffle, and enter the IFO mode at the far COC.

The scattered light model was used to calculate the requirement for the reflectivity of the Cryopump Baffle. Assuming a BRDF of the spool piece wall of 0.1, the reflectivity of the Cryopump Baffle must is < 0.01.

The reflectivity of the Cryopump Baffle is estimated to be 2.4E-5.

4.3.5.6 Seismic Motion of the Cryopump Scattering Surfaces

The surface of the suspended Cryopump Baffle has the seismic motion of the spool piece attenuated by the transfer function of the Cryopump Baffle suspension.

The light that reflects from the Cryopump Baffle will scatter from the spool piece wall, which has the seismic motion shown in Figure 28.

4.3.5.7 Scattered Light Displacement Noise of Suspended Cryopump Baffle

The scattered light displacement noise from the Cryopump Baffle is shown in Figure 29.

4.3.5.8 Fringe-wrapping of Cryopump Baffle Displacement Noise

The Cryopump Baffle has a pendulum resonance at approximately 0.8 Hz. The displacement noise at the odd harmonics of the motion due to fringe wrapping was calculated using the fringe wrap model, assuming a simple pendulum function with a Q = 1000 at the resonant frequency. The fringe wrapping does not cause excessive noise above 10 Hz.

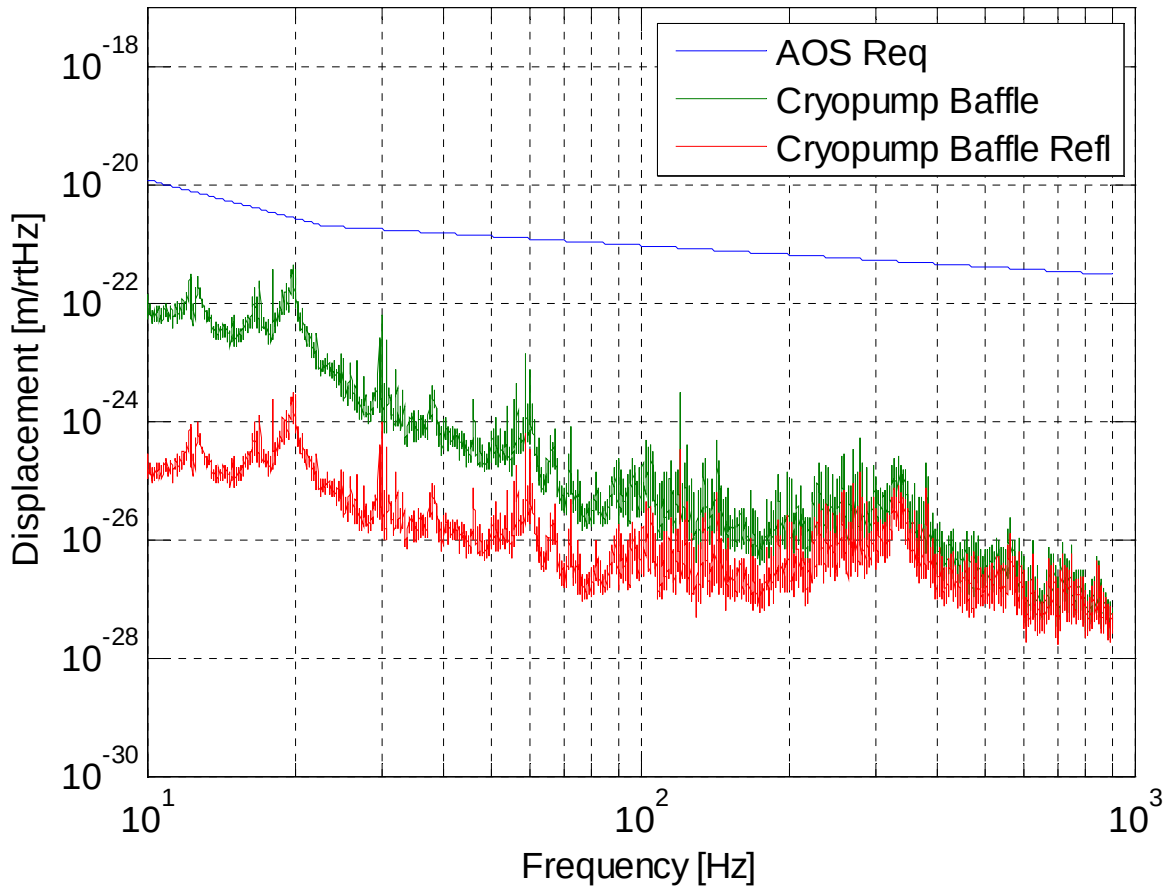

Figure 32: Cryopump Baffle Scattered Light Displacement Noise

4.3.5.9 Stay Clear Zone

The clear aperture diameter of the Cryopump Baffle, 769 mm, is large enough to allow the folded and non-folded IFO beams of 315.4 mm diameter at the 1 ppm diameter to pass through without vignetting. The fractional geometric power loss of the IFO beam with a w = 60 mm passing once through the Cryopump Baffle is 1.4E-8. With a 4 mm decentering of the baffle, the loss increases to 4E-8. This is negligible compared to the transmission loss through the ETM mirror.

This meets the requirement 4.7 Clear Aperture Requirements.

4.3.6 Elliptical Baffles

4.3.6.1 ITM Elliptical Baffle

The baffle ITM Elliptical Baffle will be constructed of oxidized polished stainless steel with the first surface inclined at an incidence angle 56 deg and was measured to have a BRDF < 0.05 sr^{-1}. See T080064-00 Controlling Light Scatter in Advanced LIGO.

4.3.6.1.1 ITM Elliptical Baffle Seismic Attenuation

The amplitude motion transfer function the ITM Elliptical Baffle suspension is shown in Figure 33—this is actually a stitching together of the transfer function of the Viton suspension from 10 Hz to 100 Hz and the transfer function of a similar length eddy current damped thick rod suspension with similar characteristics for f > 100 Hz, because we did not take data for the Viton suspension > 100 Hz.

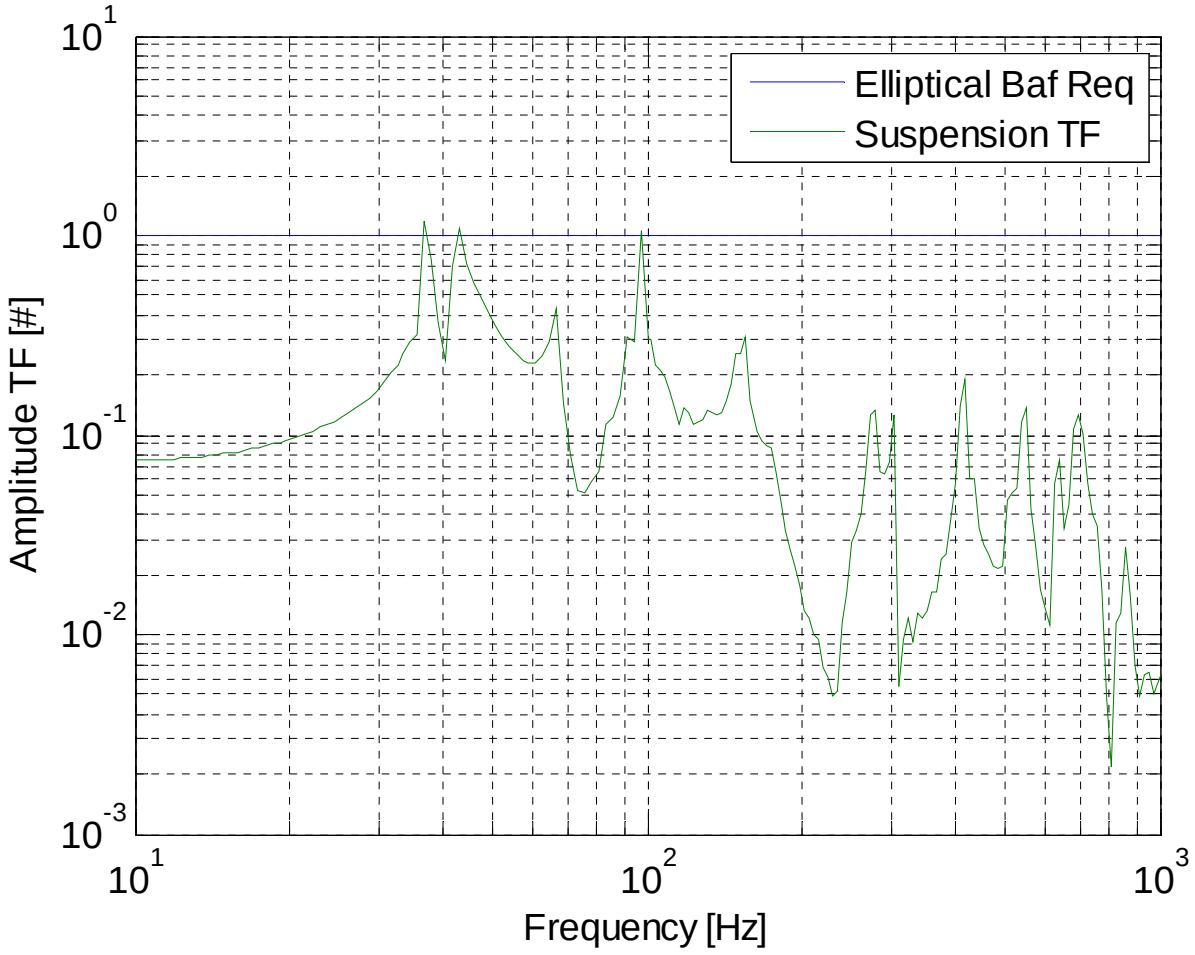

Figure 33: Elliptical Baffle SUS Amplitude Response

4.3.6.1.2 ITM Elliptical Baffle Surface BRDF

The ITM Elliptical Baffle will be constructed of oxidized polished stainless steel with the first surface inclined at an incidence angle 56 deg and was measured to have a BRDF < 0.05 sr^{-1}. See T080064-00 Controlling Light Scatter in Advanced LIGO.

4.3.6.1.3 ITM Elliptical Baffle Reflectivity

The light that is not absorbed by the ITM Elliptical Baffle will reflect from the baffle surface onto the insides of the vacuum chamber. There, it will scatter from the wall, reflect again from the ITM Elliptical Baffle, and enter the IFO mode at the far COC.

The reflectivity of oxidized stainless steel was measured to be 0.007. See T080064-00 Controlling Light Scatter in Advanced LIGO.

The multi-bounce reflectivity of the ITM Elliptical Baffle is estimated to be 2.4E-5.

4.3.6.1.4 Seismic Motion of the Vacuum Chamber

The seismic motion of the vacuum chamber is shown in Figure 34. See Robert Schofield (11/17/06 LHO ILOG).

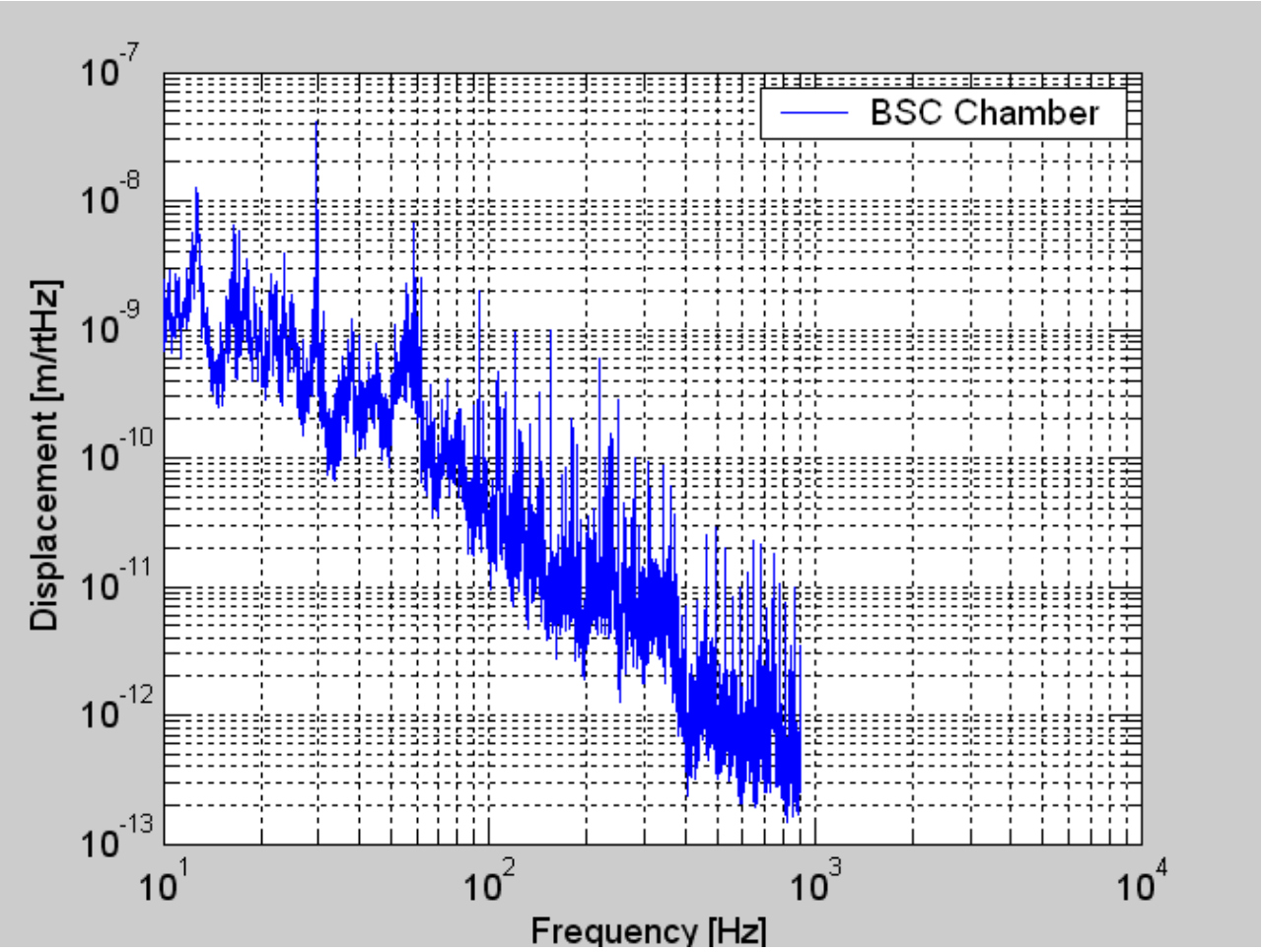

Figure 34: Seismic motion of BSC chamber

4.3.6.1.5 Scattered Light Displacement Noise of Suspended ITM Elliptical Baffle

The light that scatters directly from the surface of the suspended ITM Elliptical Baffle has a phase noise caused by the seismic motion of the HEPI support ring attenuated by the transfer function of the Elliptical Baffle suspension, which is shown in Figure 33.

The light that reflects from the baffle and subsequently scatters will have a phase noise caused by the seismic motion of the chamber walls.

The vacuum chamber walls are assumed to have a BRDF = 0.1 sr^-1. The Elliptical Baffle surface BRDF < 0.005 sr^-1.

The scattered light displacement noise from these two sources is shown in Figure 35.

4.3.6.1.6 Stay Clear Diameter

The clear aperture of the ITM Elliptical Baffle is 224 mm horizontal diameter and 259 mm vertical diameter. This is approximately the optimum beam profile in the recycling cavity as defined by Hiro. See G070657 LSC-Virgo meeting, 10/24/07, Hiro Yamamoto.

The PRM Elliptical Baffle will be aligned within 4 mm of the beam center.

This meets the requirement 4.7 Clear Aperture Requirements.

4.3.6.2 PRM Elliptical Baffle

4.3.6.2.1 Motion of PRM Elliptical Baffle

The seismic motion will be the same as the HAM optical table shown in Figure 22.

4.3.6.2.2 Power Hitting the PRM Elliptical Baffle from IO Side

The prompt PSL light that transmits through the PRM and is scraped off by the periphery of the PRM Elliptical Baffle does not build up within the recycling cavity. It is collected by the PR telescope and hits the PRM mirror at an off-axis location where it is re-scattered into the recycling cavity mode.

The irradiance of the IO Gaussian beam incident on the PRM Elliptical Baffle is given by

$$I_{PSL}(x,y) := 2\cdot\frac{P_{0psl}}{\pi\cdot w^2}\cdot e^{-2\cdot\left(\frac{x^2+y^2}{w^2}\right)}$$

where P_{0psl} is the total power in the IO beam, and w= 0.060 m is the Gaussian beam radius.

The power passing through the hole in the elliptical baffle is given by

$$P_{all} := 4\cdot\int_0^b\int_0^{a\cdot\sqrt{1-\frac{y^2}{b^2}}} I_{PSL}(x,y)\,dx\,dy$$

The power that hits the elliptical baffle is given by

$$P_{prmellbaf} := P_{psl} - P_{el}$$

With a total power input = 125 W, the power hitting the elliptical baffle is = 0.0044 W.

4.3.6.2.3 PRM Elliptical Baffle Surface BRDF

The PRM Elliptical Baffle will be constructed of oxidized polished stainless steel with the first surface inclined at an incidence angle 56 deg and was measured to have a BRDF < 0.05 sr^{-1}. See T080064-00 Controlling Light Scatter in Advanced LIGO.

4.3.6.2.4 PRM Elliptical Baffle Reflectivity

The reflectivity of oxidized stainless steel was measured to be 0.007. See T080064-00 Controlling Light Scatter in Advanced LIGO.

The multi-bounce reflectivity of the PRM Elliptical Baffle is estimated to be 2.4E-5.

4.3.6.2.5 Scattered Light Displacement Noise of PRM Elliptical Baffle

The scattered light displacement noise from both these sources is shown in Figure 35.

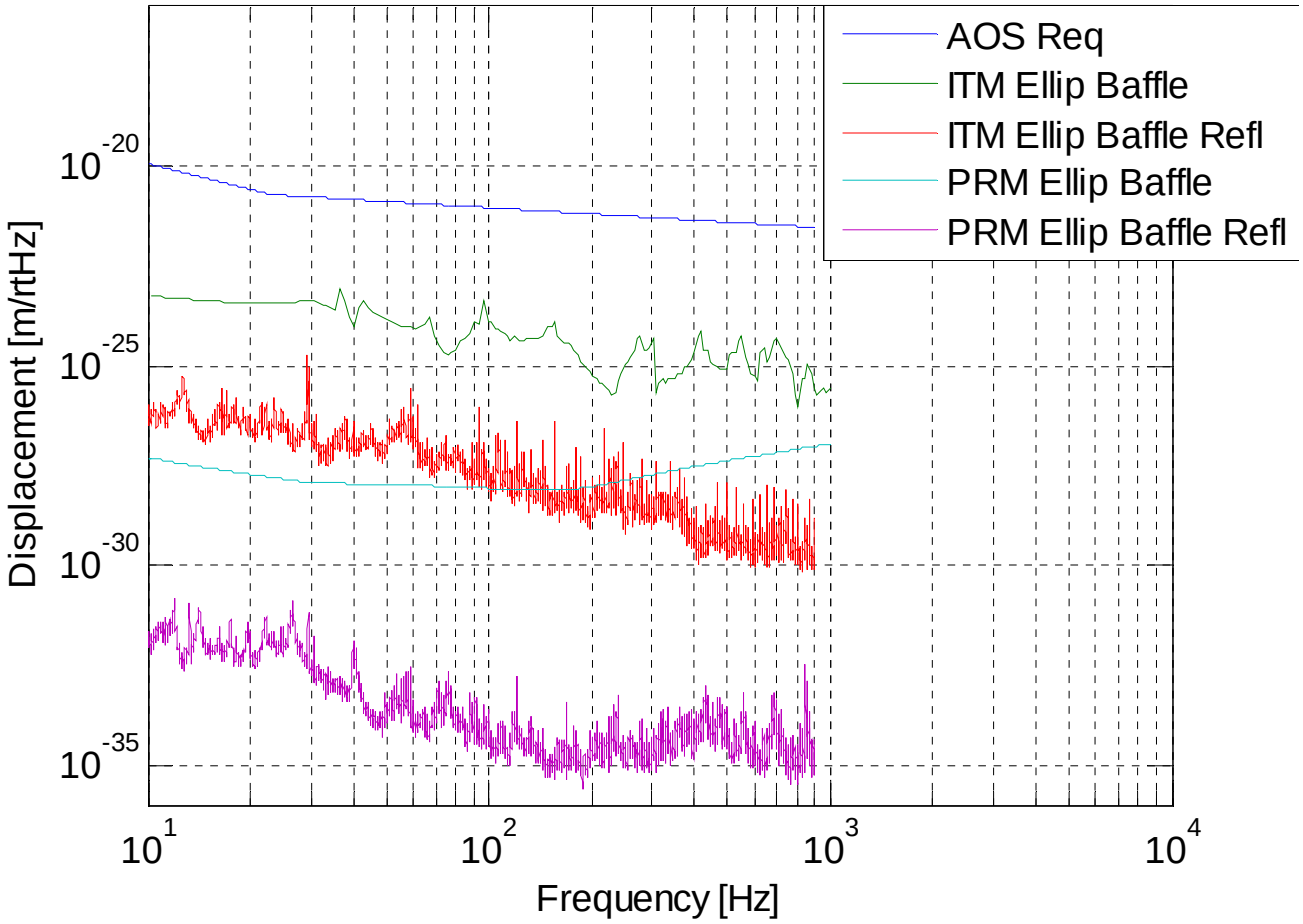

Figure 35: Elliptical Baffle Scattered Light Displacement Noise

4.3.6.2.6 Stay Clear Diameter

The clear aperture of the PRM Elliptical Baffle is 224 mm horizontal diameter and 259 mm vertical diameter. This is approximately the optimum beam profile in the recycling cavity as defined by Hiro. See G070657 LSC-Virgo meeting, 10/24/07, Hiro Yamamoto.

The PRM Elliptical Baffle will be aligned within 4 mm of the beam center.

4.3.7 H2 Elliptical Scraper Mirror

The H2 Elliptical Scraper Mirror will be constructed of polished stainless steel with the first surface inclined at an incidence angle 56 deg.

4.3.7.1 H2 Elliptical Scraper Mirror Seismic Attenuation

The amplitude motion transfer function of the H2 Elliptical Scraper Mirror suspension is shown in Figure 33.

4.3.7.2 H2 Elliptical Scraper Mirror Surface BRDF

The Elliptical Scraper Mirror was measured to have a BRDF < 0.05 sr^{-1}. See T080064-00 Controlling Light Scatter in Advanced LIGO.

4.3.7.3 H2 Elliptical Scraper Mirror Reflectivity

The reflectivity of the Elliptical Scraper Mirror was measured to be approx 0.6; See T080064-00 Controlling Light Scatter in Advanced LIGO.

4.3.7.4 Seismic Motion of the Vacuum Chamber

The seismic motion of the vacuum chamber is shown in Figure 34. See Robert Schofield (11/17/06 LHO ILOG).

4.3.7.5 Scattered Light Displacement Noise of Suspended H2 Elliptical Scraper Mirror

The light that scatters directly from the surface of the suspended Elliptical Scraper Mirror has a phase noise caused by the seismic motion of the BSC optical attenuated by the transfer function of the Elliptical Scraper Mirror suspension, which is shown in Figure 33.

The scattered light displacement is shown in Figure 36.

4.3.7.6 Stay Clear Diameter

The clear aperture of the Elliptical Scraper Mirror is 224 mm horizontal diameter and 259 mm vertical diameter. This is approximately the optimum beam profile in the recycling cavity as defined by Hiro. See G070657 LSC-Virgo meeting, 10/24/07, Hiro Yamamoto.

The Elliptical Scraper Mirror will be aligned within 4 mm of the beam center.

This meets the requirement 4.7 Clear Aperture Requirements.

4.3.8 H2 Elliptical Scraper Beam Dump

The H2 Elliptical Scraper Beam Dump will be constructed of oxidized polished stainless steel with the first surface inclined at an incidence angle 56 deg and was measured to have a BRDF < 0.05 sr^{-1}. See T080064-00 Controlling Light Scatter in Advanced LIGO.

4.3.8.1 H2 Elliptical Scraper Beam Dump Seismic Attenuation

The amplitude motion transfer function the H2 Elliptical Scraper Beam Dump suspension is shown in Figure 33.

4.3.8.2 H2 Elliptical Scraper Beam Dump Surface BRDF

The Elliptical Scraper Beam Dump will be constructed of oxidized polished stainless steel with the first surface inclined at an incidence angle 56 deg and was measured to have a BRDF < 0.05 sr^{-1}. See T080064-00 Controlling Light Scatter in Advanced LIGO.

4.3.8.3 H2 Elliptical Scraper Beam Dump Reflectivity

The light that is not absorbed by the Elliptical Scraper Beam Dump will reflect from the beam dump surface onto the insides of the vacuum chamber. There, it will scatter from the wall, reflect again from the Elliptical Scraper Beam Dump, and enter the IFO mode at the far COC.

The reflectivity of oxidized stainless steel was measured to be 0.007. See T080064-00 Controlling Light Scatter in Advanced LIGO.

The multi-bounce reflectivity of the Elliptical Scraper Beam Dump is estimated to be 2.4E-5.

4.3.8.4 Seismic Motion of the Vacuum Chamber

The seismic motion of the vacuum chamber is shown in Figure 34. See Robert Schofield (11/17/06 LHO ILOG).

4.3.8.5 Scattered Light Displacement Noise of Suspended H2 Elliptical Scraper Beam Dump

The light that scatters directly from the surface of the suspended Elliptical Scraper Mirror has a phase noise caused by the seismic motion of the HEPI support ring attenuated by the transfer function of the Elliptical Scraper Mirror suspension, which is shown in Figure 33.

The scattered light displacement is shown in Figure 36.

4.3.8.6 Stay Clear Diameter

The clear aperture of the Elliptical Scraper Mirror is 224 mm horizontal diameter and 259 mm vertical diameter. This is approximately the optimum beam profile in the recycling cavity as defined by Hiro. See G070657 LSC-Virgo meeting, 10/24/07, Hiro Yamamoto.

The Elliptical Scraper Mirror will be aligned within 4 mm of the beam center.

This meets the requirement 4.7 Clear Aperture Requirements.

4.3.9 H2 Fold Mirror Beam Dump

4.3.9.1 H2 Fold Mirror Beam Dump Seismic Attenuation

The amplitude motion transfer function the H2 Fold Mirror Beam Dump suspension is shown in Figure 33.

4.3.9.2 H2 Fold Mirror Beam Dump Surface BRDF

The Fold Mirror Beam Dump will be constructed of oxidized polished stainless steel with the first surface inclined at an incidence angle 56 deg and was measured to have a BRDF < 0.05 sr^{-1}. See T080064-00 Controlling Light Scatter in Advanced LIGO.

4.3.9.3 H2 Fold Mirror Beam Dump Reflectivity

The light that is not absorbed by the Fold Mirror Beam Dump will reflect from the beam dump surface onto the insides of the vacuum chamber. There, it will scatter from the wall, reflect again from the Fold Mirror Beam Dump, and enter the IFO mode at the far COC.

The reflectivity of oxidized stainless steel was measured to be 0.007. See T080064-00 Controlling Light Scatter in Advanced LIGO.

The multi-bounce reflectivity of the Fold Mirror Beam Dump is estimated to be 2.4E-5.

4.3.9.4 Seismic Motion of the Vacuum Chamber

The seismic motion of the vacuum chamber is shown in Figure 34. See Robert Schofield (11/17/06 LHO ILOG).

4.3.9.5 Scattered Light Displacement Noise of Suspended H2 Fold Mirror Beam Dump

The light that scatters directly from the surface of the suspended Fold Mirror Beam Dump has a phase noise caused by the seismic motion of the HEPI support ring attenuated by the transfer function of the Fold Mirror Beam Dump suspension, which is shown in Figure 33.

The scattered light displacement is shown in Figure 36.

4.3.9.6 Stay Clear Diameter

The clear aperture of the Fold Mirror Beam Dump is 259 mm diameter..

The Fold Mirror Beam Dump will be aligned within 4 mm of the beam center.

This meets the requirement 4.7 Clear Aperture Requirements.

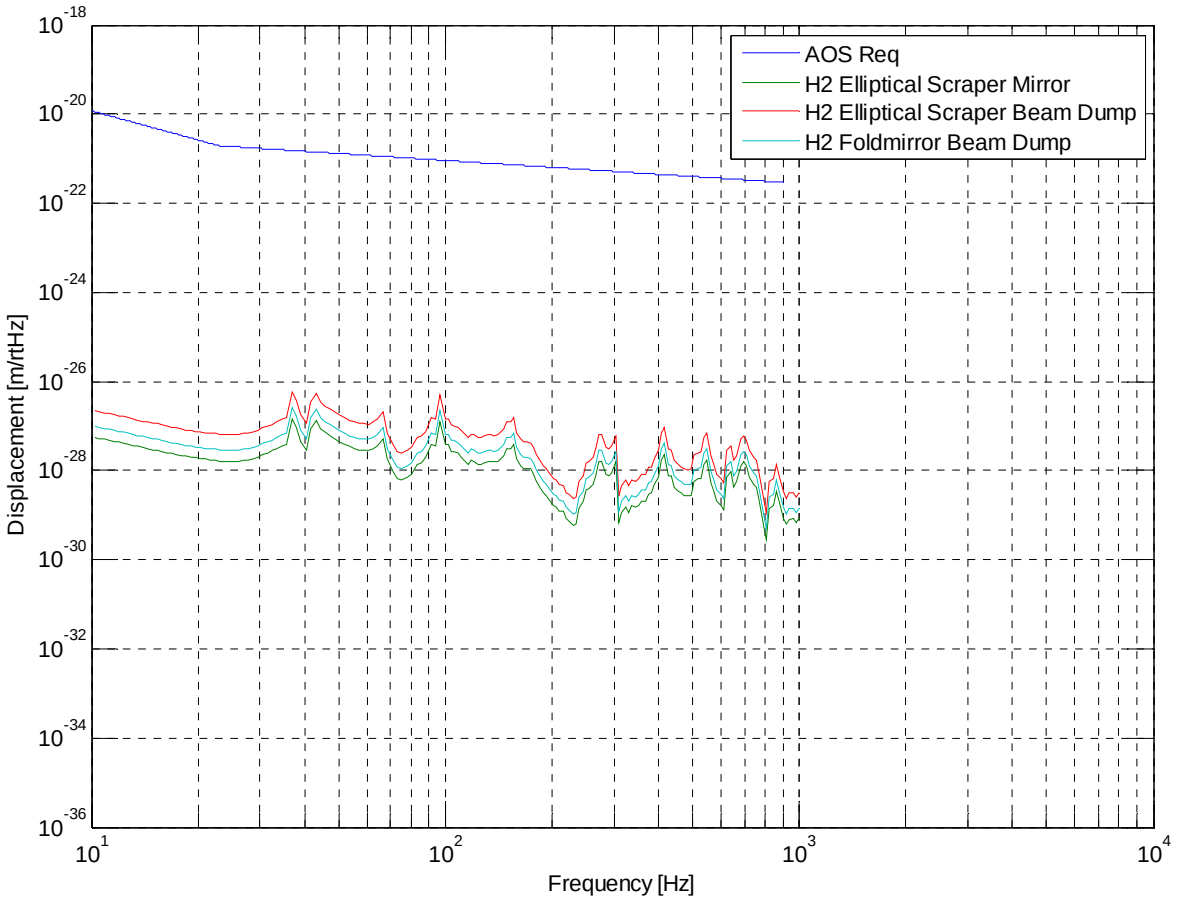

Figure 36: H2 Elliptical Scraper Mirror and Beam Dump Scattered Light Displacement Noise

4.3.10 Output Window

Septum Windows for the AS beam, the ITMX PO beam, and the RC PO beam will be mounted to the HAM1, HAM6, HAM7, and HAM12 septum plates,, which are mounted to the flange of the HAM chamber, as shown in Figure 37 and Figure 38. The compressible bellows between the Septum Plate assembly and the mounting flange of HAM 6 allows the Septum Windows to be removed without moving any other vacuum enclosures.

In addition, the ITMX and ITMY recycling cavity Hartmann beams will enter and exit the vacuum chamber through vacuum viewports located in HAM4 and HAM10. Part of the AS beam that transmits through the SR2 mirror will leak through the ITMY Hartmann coupling dichroic beam splitter, and part of the ITMX PO beam will leak through the ITMX Hartmann coupling dichroic beam splitter and will scatter from the Hartmann output windows.

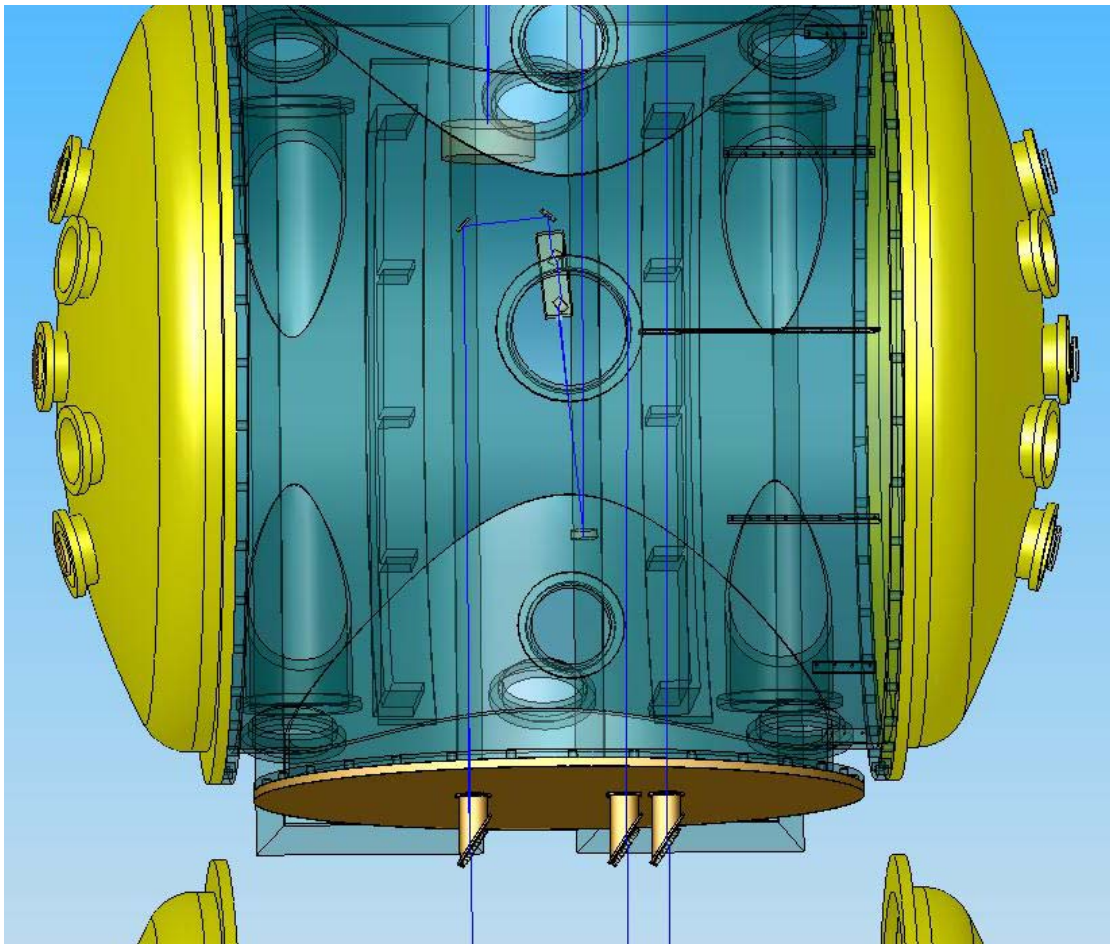

Figure 37: Output Septum Plate

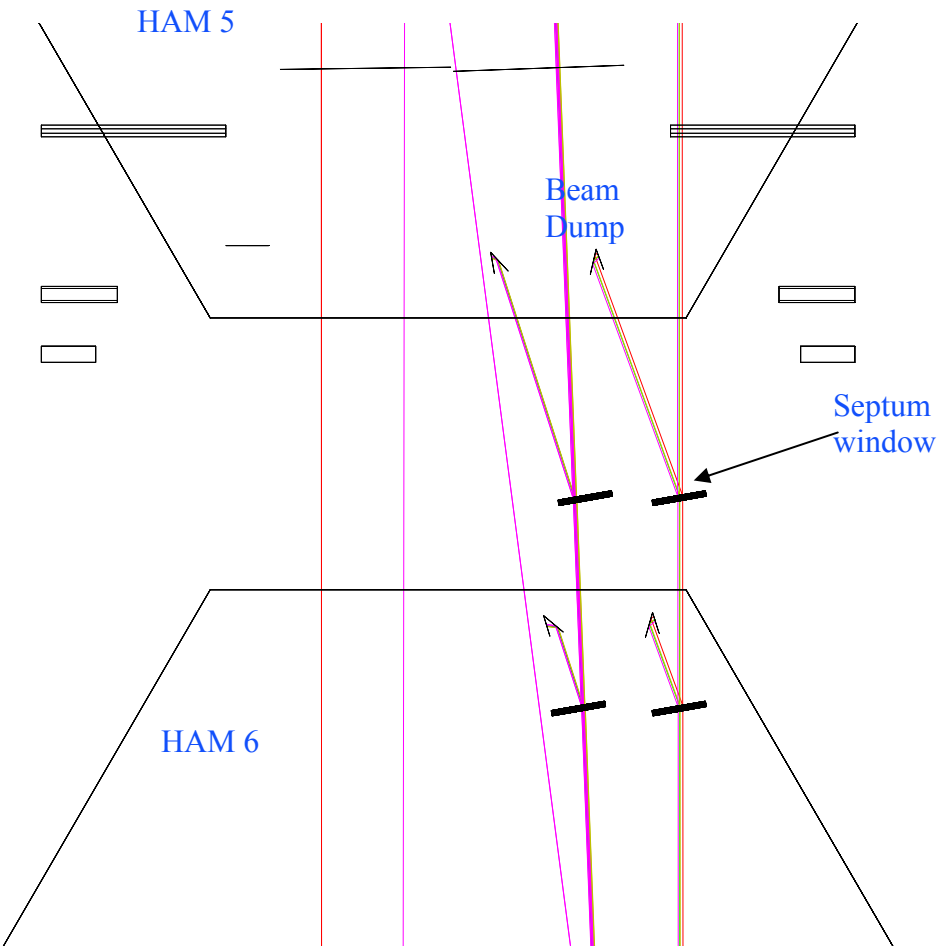

Figure 38: Output Septum Windows

4.3.10.1 Output Window BRDF

The BRDF of the Output Windows were assumed to be the same as the measured BRDF of a super-polished window, 1E-6 sr^-1, see T080064-00 Controlling Light Scatter in Advanced LIGO.

The incidence angle on the Septum Window is 10 degrees.

4.3.10.2 Seismic Motion of the Output Windows

The Output Windows are mounted directly to the HAM1, HAM4, HAM6, HAM7, HAM10, and HAM12 septum plates and doors, and will have a displacement spectrum similar to the HAM6 flange, as shown in Figure 39. See Robert Schofield (11/17/06 LHO ILOG).

4.3.10.3 Scattered Light Displacement Noise of Output Window

The scattered light displacement noise from the Output Windows is shown in Figure 40. The scattered light noise from the AS Window exceeds the AOS requirement and also the ADLIGO Science requirement.

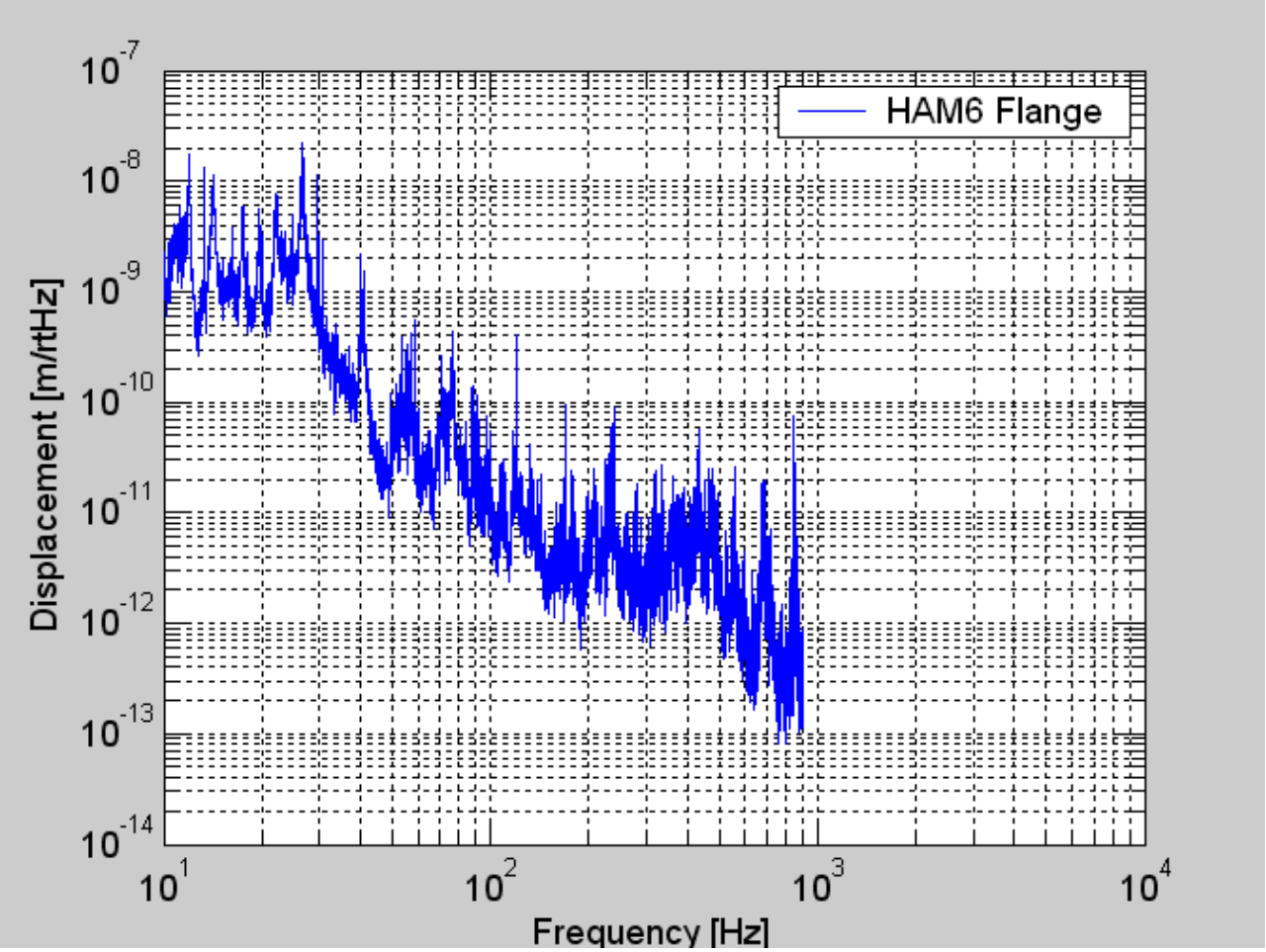

Figure 39: Displacement Spectrum of HAM 6 Flange

4.3.10.4 Reflected Light from AS Output Window

The light that reflects from the two surfaces of the AS Output window will be caught in the cavity beam dumps mounted on HAM chamber optical tables. The cavity beam dump will be made of black glass with the first surface inclined at an incidence angle 56 deg was measured to have a BRDF < 0.05 sr^{-1}. See T080064-00 Controlling Light Scatter in Advanced LIGO.

The multi-bounce reflectivity of the cavity beam dump is estimated to be < 2.4E-5.

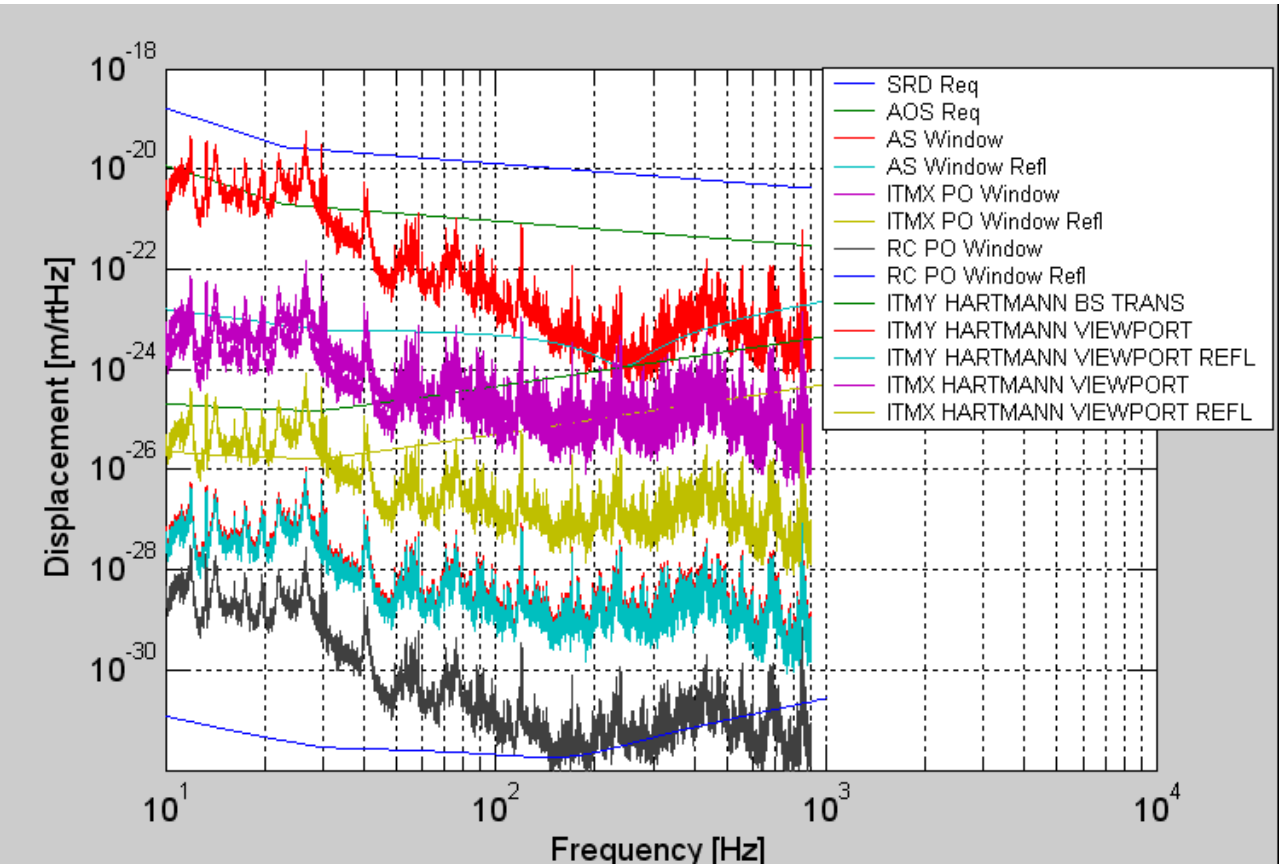

Figure 40: Output Window Scattered Light Displacement noise

4.3.10.5 Output Septum Windows Removal

The Septum Windows are mounted to nozzle pieces with o-rings and a capture flange, and the nozzle piece is mounted independently to the HAM Plenum. Therefore, the nozzle piece can be removed by venting HAM5, with access from the adjoining vented HAM6 chamber, without removing the septum plate.

When the Septum Windows are removed, the total scattered light displacement noise meets the AOS requirement, as shown in Figure 21.

4.3.10.5.1 Stay Clear Diameter

The clear aperture of the Output Window is > 60 mm diameter. The AS beam, the ITMX PO beam, and the RC PO beam have Gaussian diameters approximately 4 mm.

This meets the requirement 4.7 Clear Aperture Requirements.

4.3.11 Hartmann Viewports

The ITMX Hartmann beam is superimposed on the ITMX PO beam with a dichroic beamsplitter that transmits mostly visible light and reflects mostly IR light. However, some of the ITMX PO beam power will transmit through the dichroic beamsplitter and scatter from the ITMX Hartmann Viewport, shown in Figure 41.

Similarly, The ITMY Hartmann beam is superimposed on the beam that leaks through the SR2 HR mirror with a dichroic beamsplitter that reflects mostly visible light and transmits mostly IR light. However, some of the SR2 HR leakage beam power will reflect from the dichroic beamsplitter and scatter from the ITMY Hartmann Viewport

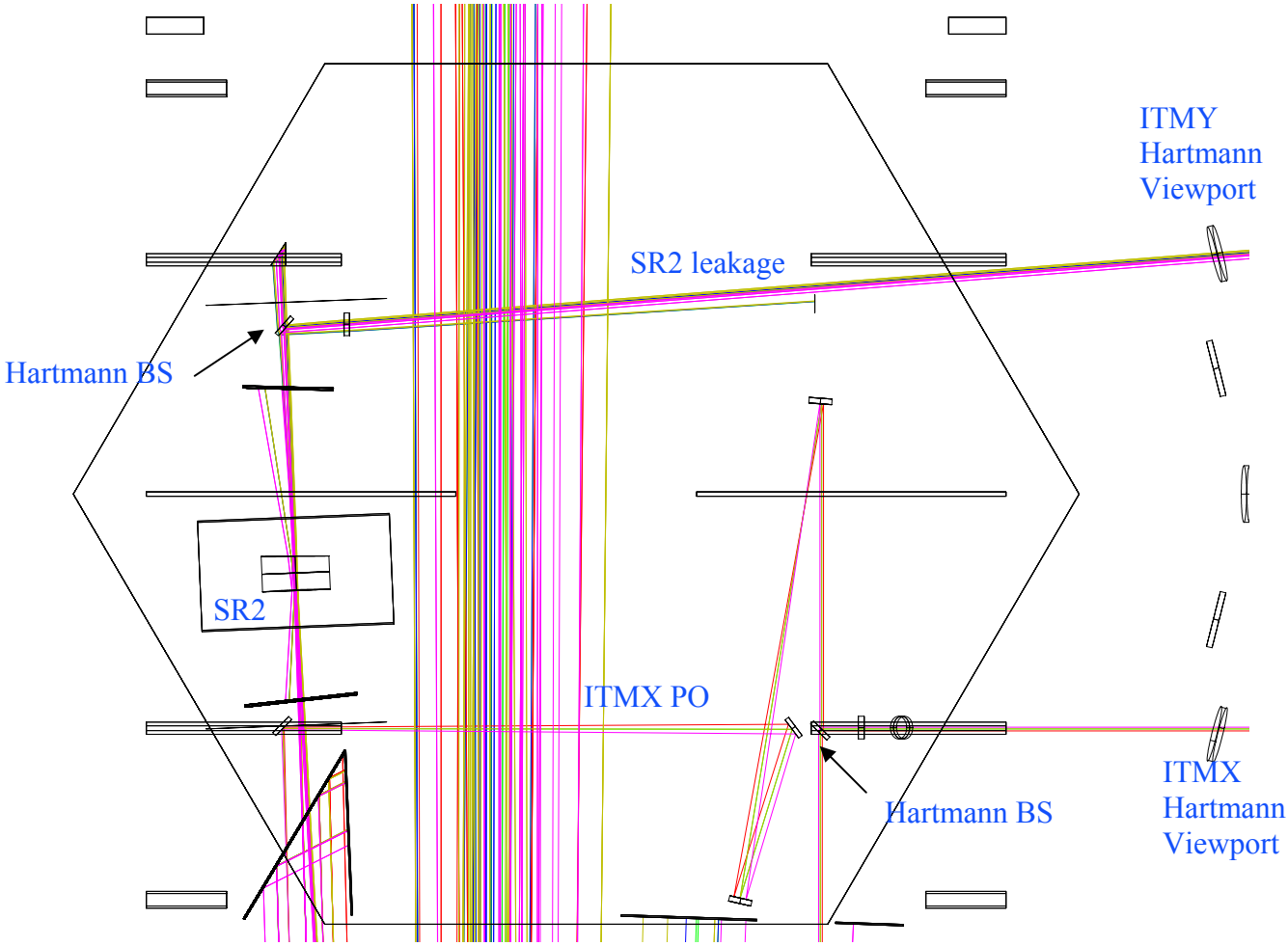

Figure 41: Hartmann Viewports

4.3.11.1 Hartmann Viewport BRDF

The BRDF of the Hartmann Viewport is assumed to be the same as the measured BRDF of a super-polished window, 1E-6 sr^-1, see T080064-00 Controlling Light Scatter in Advanced LIGO.

The incidence angle on the Hartmann Viewport is approximately 10 degrees.

The reflectivity of the Hartmann Viewport is estimated to be<0.025%.

4.3.11.2 Reflected Light from Hartmann Viewport

The light that reflects from the two surfaces of the Hartmann Viewport does not cause excessive displacement noise and will be allowed to hit the walls of the HAM chamber.

4.3.11.2.1 Scattered Light Displacement Noise of Ghost Beams

The scattered light displacement noise from the Hartmann Viewports is shown in Figure 40.

4.3.12 ITM GBAR1, GBAR3, and GBAR4 Ghost Beams

The ITM GBAR1, GBAR3, and GBAR4 Ghost Beams (see Figure 53) are collected by the PR and SR telescopes and will be caught in the scraper cavity beam dumps mounted to the HAM optical table in front of PR2, and SR2 mirrors as shown in Figure 4, and Figure 5.

Some of the ghost beam light will reflect from the cavity beam dumps and scatter from the IO and OUT tube walls, retracing their paths into the recycling cavity beam.

4.3.12.1 PR2/SR2 Cavity Beam Dump BRDF

The PR2/SR2 Cavity Beam Dump will be constructed of oxidized polished stainless steel with the first surface inclined at an incidence angle 56 deg and was measured to have a BRDF < 0.05 sr^{-1}. See T080064-00 Controlling Light Scatter in Advanced LIGO.

4.3.12.2 PR2/SR2Cavity Beam Dump Reflectivity

The light that is not absorbed by the PR2/SR2 Cavity Beam Dump will reflect from the beam dump surface onto the insides of the manifold. There, it will scatter from the wall, reflect again from the PR2/SR2 Cavity Beam Dump, and enter the recycling cavity mode.

The multi-bounce reflectivity of the PR2/SR2 Cavity Beam Dump is estimated to be 2.4E-5.

4.3.12.3 Scattered Light Displacement Noise of Ghost Beams

The scattered light displacement noise from the ITM AR ghost beams is shown in Figure 42.

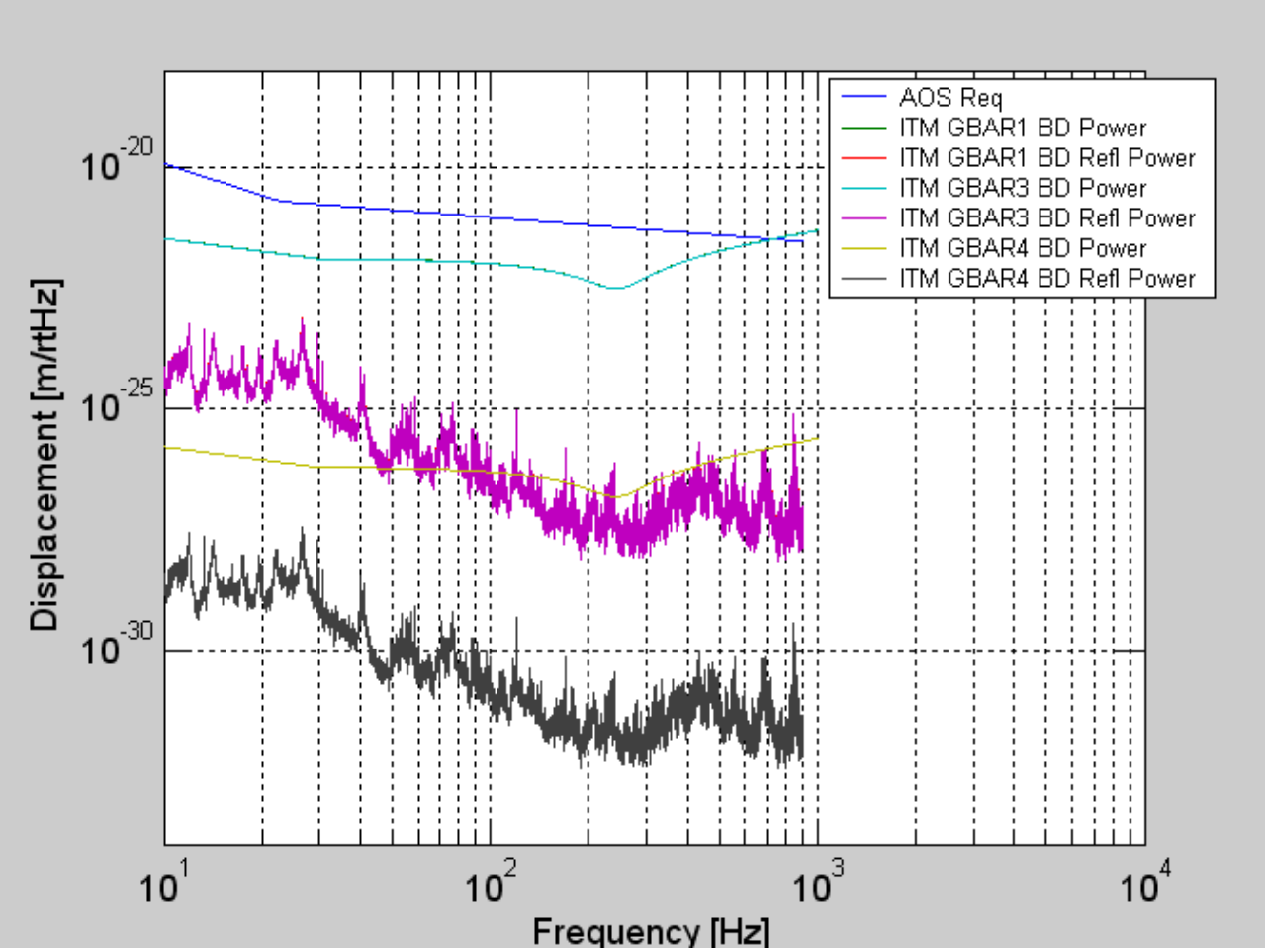

Figure 42: ITM GBAR1, GBAR3, and GBAR4 Beam Dump Scattered Light Displacement Noise

4.3.13 ITM HR, BS AR, AND BS HR Ghost Beams

The ITM HR3, ITM HR4, BS AR3X, BSAR4X, BSHR3X, AND BSHR4X Ghost Beams will pass through the Cryopump Baffle opening and hit the beam tube shark's-tooth baffles inside the arm.

4.3.13.1 Beam Tube Baffle BRDF and Reflectivity

The beam tube shark's-tooth baffles are made from oxidized, polished stainless steel with the first surface inclined at an incidence angle of 55 deg and was measured to have a BRDF < 0.05 sr^{-1}. See T080064-00 Controlling Light Scatter in Advanced LIGO. The multi-bounce reflectivity of the PRM Elliptical Baffle is estimated to be 2.4E-5.

4.3.13.2 Scattered Light Displacement Noise of Ghost Beams

The scattered light displacement noise from the ITM HR3 and ITM HR4 ghost beams is shown in Figure 43.

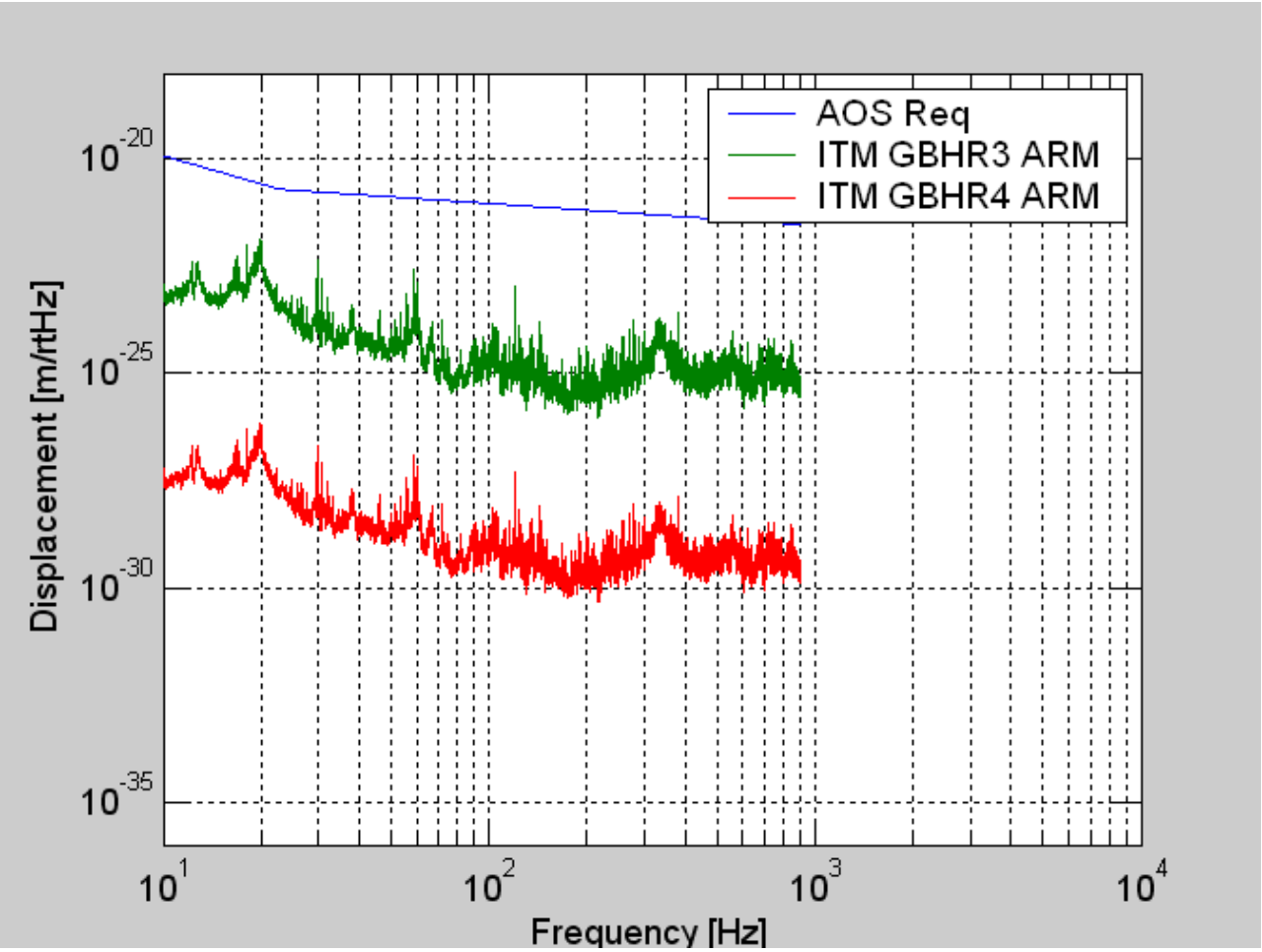

Figure 43: ITM GBHR Beam Dump Scattered Light Displacement Noise

The scattered light displacement noise from the BS AR3X, BSAR4X, BSHR3X, AND BSHR4X ghost beams is shown in Figure 44.

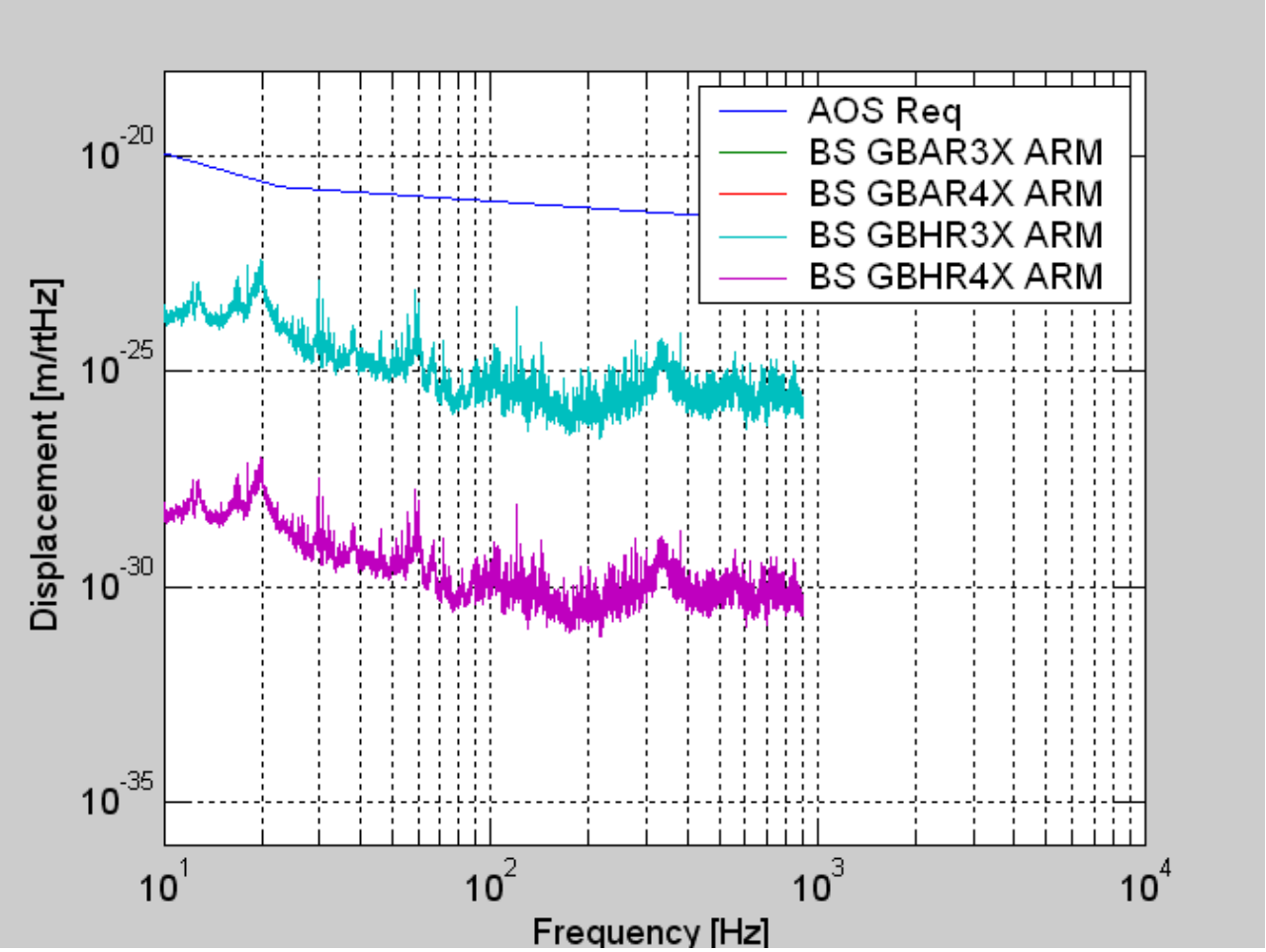

Figure 44: BS GBARX and GBHRX Scattered Light Displacement Noise

4.3.14 BS GBHR3P, BS GBHR

The BS AR3P and, BS HR3P (see Figure 54) are collected by the PR and SR telescopes and will be caught in the scraper cavity beam dumps mounted to the HAM optical table in front of PR2, and SR2 mirrors as shown in Figure 4, and Figure 5.

Some of the ghost beam light will reflect from the cavity beam dumps and scatter from the IO tube and OUT tube walls, retracing their paths into the recycling cavity beam.

4.3.14.1 Scattered Light Displacement Noise of Ghost Beams

The scattered light displacement noise from the BS AR3P and, BS HR3P ghost beams is shown in Figure 45.

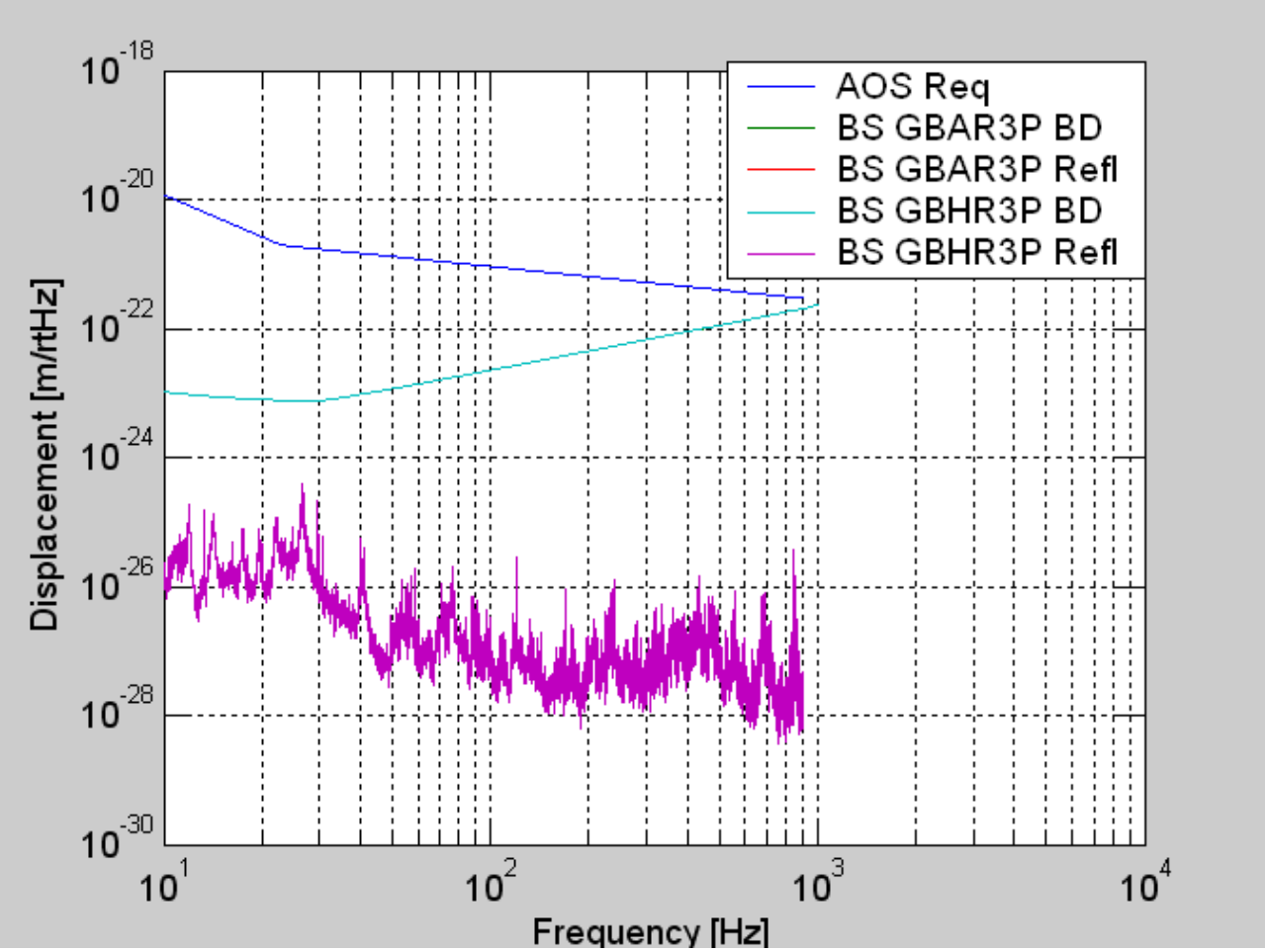

Figure 45: BS GBAR3P and BS GBHR3P Beam Dump Scattered Light Displacement Noise

4.3.15 ITMX PO Beam (BS GBAR1)

The ITMX PO beam (BS GBAR1) hits the center of the signal recycling telescope mirror SR3, then separates from the main beam and passes through a hole in the scraper beam dump in front of SR2 mirror and is picked off with a small steering mirror, as illustrated in the ZEMAX layout in Figure 41.

4.3.16 PRM Ghost Beams

4.3.16.1 PRM GBAR1

The PRM AR1 Ghost Beam is the reflection of the PSL beam from the AR surface of the PRM. This beam will scatter from the PRM AR Plate Beam Dump shown in Figure 6. A fraction of this scattered light will reflect from the AR surface and head toward the input Faraday isolator. This scattered light will be deflected by the Faraday isolator toward the REFL detection optics where some of it may reflect or scatter back and retrace its path back through the input Faraday isolator and inject noise into the input beam.

4.3.16.2 PRM GBAR3

The PRM AR3 Ghost Beam is the first internal reflection of the recycling cavity beam from the HR and AR surfaces that passes out through the AR surface. This beam will scatter from the PRM AR Plate Beam Dump shown in Figure 6. A fraction of this scattered light will retrace the path and inject noise directly into the recycling cavity.

4.3.16.3 PRM GBHR3

The PRM HR3 Ghost Beam is the first internal reflection of the recycling cavity beam from the AR surface that passes out through the HR surface. This beam will scatter from the PRM HR Plate Beam Dump shown in Figure 6. A fraction of this scattered light will retrace the path and inject noise directly into the recycling cavity.

4.3.16.4 PRM Plate Beam Dump Surface BRDF and Reflectivity

The PRM plate Beam Dump will be constructed of AR-coated black glass. The estimated BRDF is $< 0.05\ sr^{-1}$. See T080064-00 Controlling Light Scatter in Advanced LIGO.

The reflectivity of the PRM plate Beam Dump is estimated to be<0.025%.

4.3.16.5 Scattered Light Displacement Noise of Ghost Beams

The total scattered light displacement noise from the PRM ghost beams is shown in Figure 48.

4.3.17 PR2 Ghost Beams

4.3.17.1 PR2 GBAR0t

The PR2 AR0t Ghost Beam is the leakage through the HR side of the circulating recycling cavity beam from the PRM direction. This beam will scatter from the PR2 GBAR0t Cavity Beam Dump shown in Figure 46. A fraction of this scattered light will pass back through PR2 HR surface and inject noise directly into the recycling cavity.

4.3.17.2 PR2 GBAR0t Cavity Beam Dump Surface BRDF and Reflectivity

The PR2 GBAR0t Cavity Beam Dump will be constructed of oxidized polished stainless steel with the first surface inclined at an incidence angle 56 deg and was measured to have a BRDF $< 0.05\ sr^{-1}$. See T080064-00 Controlling Light Scatter in Advanced LIGO.

The reflectivity of the PR2 GBAR0t Beam Dump is estimated to be 2.4E-5.

4.3.17.3 RC PO Beam (PR2 GBARt)

The RC PO Beam (PR2 ARt Ghost Beam), shown in Figure 46, is the leakage through the HR side of the returning recycling cavity beam from the BS. This beam will be steered through a septum window onto the ISC detection bench on HAM1 and HAM7.

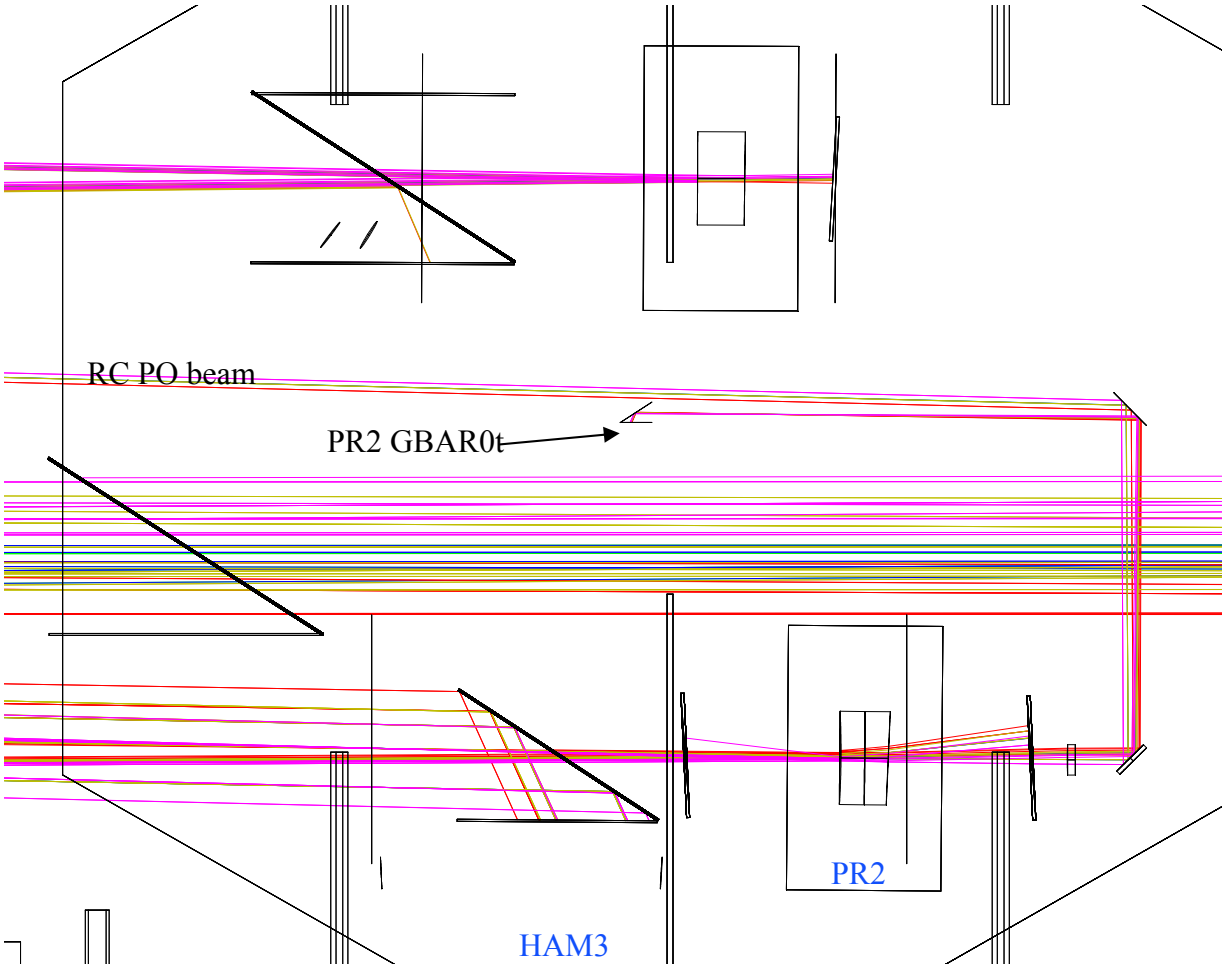

Figure 46: PR2 GBAR0t beam dump

4.3.17.4 PR2 GBAR3

The PR2 AR3 Ghost Beam is the first internal reflection from the HR and AR surfaces that passes out through the AR surface. This beam will scatter from the PR2 AR Plate Beam Dump shown in Figure 8. A fraction of this scattered light will retrace the path and inject noise directly into the recycling cavity.

The recycling cavity beam circulating in the opposite direction undergoes a similar scattering event and injects an additional equal amount of noise into the recycling cavity.

4.3.17.5 PR2 GBHR3

The PR2 HR3 Ghost Beam is the first internal reflection from the AR surface that passes out through the HR surface. This beam will scatter from the PR2 HR Plate Beam Dump shown in Figure 8. A fraction of this scattered light will retrace the path and inject noise directly into the recycling cavity.

The recycling cavity beam circulating in the opposite direction undergoes a similar scattering event and injects an additional equal amount of noise into the recycling cavity.

4.3.17.6 PR2 Plate Beam Dump Surface BRDF and Reflectivity

The PR2 plate Beam Dump will be constructed of AR-coated black glass. The estimated BRDF is $< 0.05\ sr^{-1}$. See T080064-00 Controlling Light Scatter in Advanced LIGO.

The reflectivity of the PR2 plate Beam Dump is estimated to be<0.025%.

4.3.17.7 Scattered Light Displacement Noise of Ghost Beams

The total scattered light displacement noise from the PR2 ghost beams is shown in Figure 48.

4.3.18 PR3 Ghost Beams

4.3.18.1 PR3 GBAR0t

The PR3 AR0t Ghost Beam is the transmission of the circulating recycling cavity beam from PR2 direction. This beam will scatter from the PR3 AR Plate Beam Dump shown in Figure 10. A fraction of this scattered light will pass back through PR3 HR surface and inject noise directly into the recycling cavity.

The recycling cavity beam circulating in the opposite direction undergoes a similar scattering event and injects an additional equal amount of noise into the recycling cavity.

4.3.18.2 PR3 GBAR3

The PR3 AR3 Ghost Beam is the first internal reflection from the HR and AR surfaces that passes out through the AR surface. This beam will scatter from the PR3 AR Plate Beam Dump shown in Figure 10. A fraction of this scattered light will retrace the path and inject noise directly into the recycling cavity.

The recycling cavity beam circulating in the opposite direction undergoes a similar scattering event and injects an additional equal amount of noise into the recycling cavity.

4.3.18.3 PR3 GBHR3

The PR3 HR3 Ghost Beam is the first internal reflection from the AR surface that passes out through the HR surface. This beam will be allowed to hit the IO beam tube wall. A fraction of this scattered light will retrace the path and inject noise directly into the recycling cavity.

The recycling cavity beam circulating in the opposite direction undergoes a similar scattering event and injects an additional equal amount of noise into the recycling cavity.

4.3.18.4 PR3 Plate Beam Dump Surface BRDF and Reflectivity

The PR3 plate Beam Dump will be constructed of AR-coated black glass. The measured BRDF $< 0.05\ sr^{-1}$. See T080064-00 Controlling Light Scatter in Advanced LIGO.

The reflectivity of the PR3 plate Beam Dump is estimated to be<0.025%.

4.3.18.5 Scattered Light Displacement Noise of PR3 Ghost Beams

The scattered light displacement noise from the PR3 AR and PR3 HR ghost beams are shown in Figure 48.

4.3.19 SRM Ghost Beams

4.3.19.1 SRM GBAR3

The SRM AR3 Ghost Beam is the first internal reflection from the HR and AR surfaces that passes out through the AR surface. This beam will scatter from the SRM AR Plate Beam Dump shown in Figure 7. A fraction of this scattered light will retrace the path and inject noise directly into the signal recycling cavity.

The signal recycling cavity beam circulating in the opposite direction undergoes a similar scattering event and injects an additional equal amount of noise into the recycling cavity.

4.3.19.2 SRM GBHR3

The SRM HR3 Ghost Beam is the first internal reflection from the AR surface that passes out through the HR surface. This beam will scatter from the SRM HR Plate Beam Dump shown in Figure 7. A fraction of this scattered light will reflect internally from the AR surface and inject noise directly into the recycling cavity.

The signal recycling cavity beam circulating in the opposite direction undergoes a similar scattering event and injects an additional equal amount of noise into the signal recycling cavity.

4.3.19.3 SRM Plate Beam Dump Surface BRDF and Reflectivity

The SRM plate Beam Dump will be constructed of AR-coated black glass. The measured BRDF < 0.05 sr^{-1}. See T080064-00 Controlling Light Scatter in Advanced LIGO.

The reflectivity of the SRM plate Beam Dump is estimated to be<0.025%.

4.3.19.4 Scattered Light Displacement Noise of Ghost Beams

The total scattered light displacement noise from the SRM ghost beams is shown in Figure 48.

4.3.20 SR2 Ghost Beams

4.3.20.1 SR2 GBAR0t

The SR2 AR0t Ghost Beam is the leakage through the HR side of the circulating signal recycling cavity beam from the SR3 direction. This beam will scatter from the SR2 GBAR0t Plate Beam Dump shown in Figure 47. A fraction of this scattered light will retrace the path and inject noise directly into the signal recycling cavity.

The signal recycling cavity beam circulating in the opposite direction undergoes a similar scattering event and injects an additional equal amount of noise into the recycling cavity.

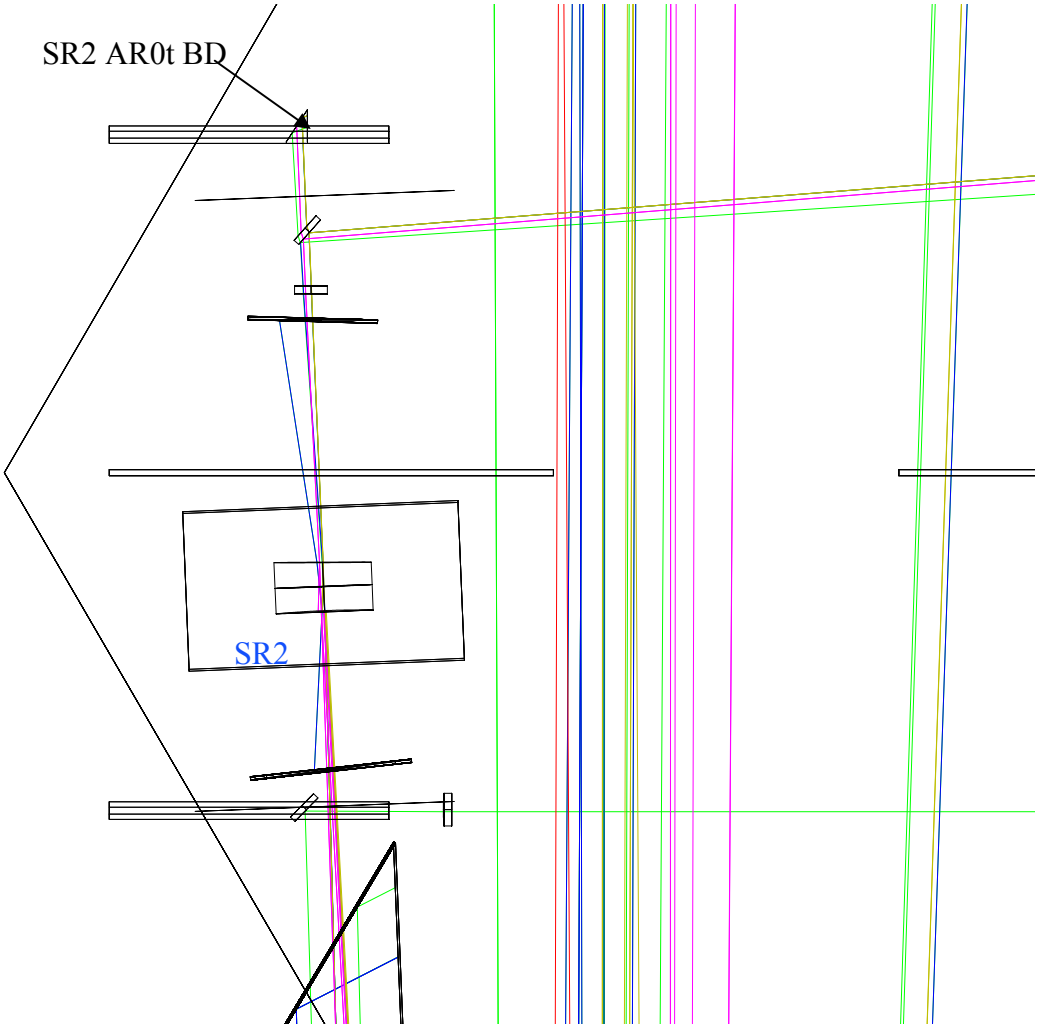

Figure 47: SR2 AR0t beam dump

4.3.20.2 SR2 GBAR3

The SR2 AR3 Ghost Beam is the first internal reflection from the HR and AR surfaces that passes out through the AR surface. This beam will scatter from the SR2 AR Plate Beam Dump shown in Figure 9. A fraction of this scattered light will retrace the path and inject noise directly into the recycling cavity.

The recycling cavity beam circulating in the opposite direction undergoes a similar scattering event and injects an additional equal amount of noise into the recycling cavity.

4.3.20.3 SR2 GBHR3

The SR2 HR3 Ghost Beam is the first internal reflection from the AR surface that passes out through the HR surface. This beam will scatter from the SR2 HR Plate Beam Dump shown in Figure 9. A fraction of this scattered light will retrace the path and inject noise directly into the recycling cavity.

The recycling cavity beam circulating in the opposite direction undergoes a similar scattering event and injects an additional equal amount of noise into the recycling cavity.

4.3.20.4 SR2 Plate Beam Dump Surface BRDF and Reflectivity

The SR2 plate Beam Dump will be constructed of AR-coated black glass. The measured BRDF < 0.05 sr^{-1}. See T080064-00 Controlling Light Scatter in Advanced LIGO.

The reflectivity of the SR2 plate beam dump is estimated to be<0.025%.

4.3.20.5 Scattered Light Displacement Noise of Ghost Beams

The total scattered light displacement noise from the SR2 ghost beams is shown in Figure 48.

4.3.21 SR3 Ghost Beams

4.3.21.1 SR3 GBAR0t

The SR3 AR0t Ghost Beam is the transmission of the circulating signal recycling cavity beam from the BS direction. This beam will scatter from the SR3 AR Plate Beam Dump shown in Figure 11. A fraction of this scattered light will retrace the path and inject noise directly into the recycling cavity.

The signal recycling cavity beam circulating in the opposite direction undergoes a similar scattering event and injects an additional equal amount of noise into the signal recycling cavity.

4.3.21.2 SR3 GBAR3

The SR3 AR3 Ghost Beam is the first internal reflection from the HR and AR surfaces that passes out through the AR surface. This beam will scatter from the SR3 AR Plate Beam Dump shown in Figure 11. A fraction of this scattered light will retrace the path and inject noise directly into the recycling cavity.

The signal recycling cavity beam circulating in the opposite direction undergoes a similar scattering event and injects an additional equal amount of noise into the signal recycling cavity

4.3.21.3 SR3 GBHR3

The SR3 HR3 Ghost Beam is the first internal reflection from the AR surface that passes out through the HR surface. This beam will be allowed to hit the OUT beam tube wall. A fraction of this scattered light will retrace the path and inject noise directly into the recycling cavity.

The recycling cavity beam circulating in the opposite direction undergoes a similar scattering event and injects an additional equal amount of noise into the recycling cavity.

4.3.21.4 SR3 Plate Beam Dump Surface BRDF and Reflectivity

The SR3 plate Beam Dump will be constructed of AR-coated black glass. The measured BRDF < 0.05 sr^{-1}. See T080064-00 Controlling Light Scatter in Advanced LIGO.

The reflectivity of the SR3 Beam Dump is estimated to be<0.025%.

4.3.21.5 Scattered Light Displacement Noise of SR3 Ghost Beams

The scattered light displacement noise from the SR3 AR and SR3 HR ghost beams are shown in Figure 48.

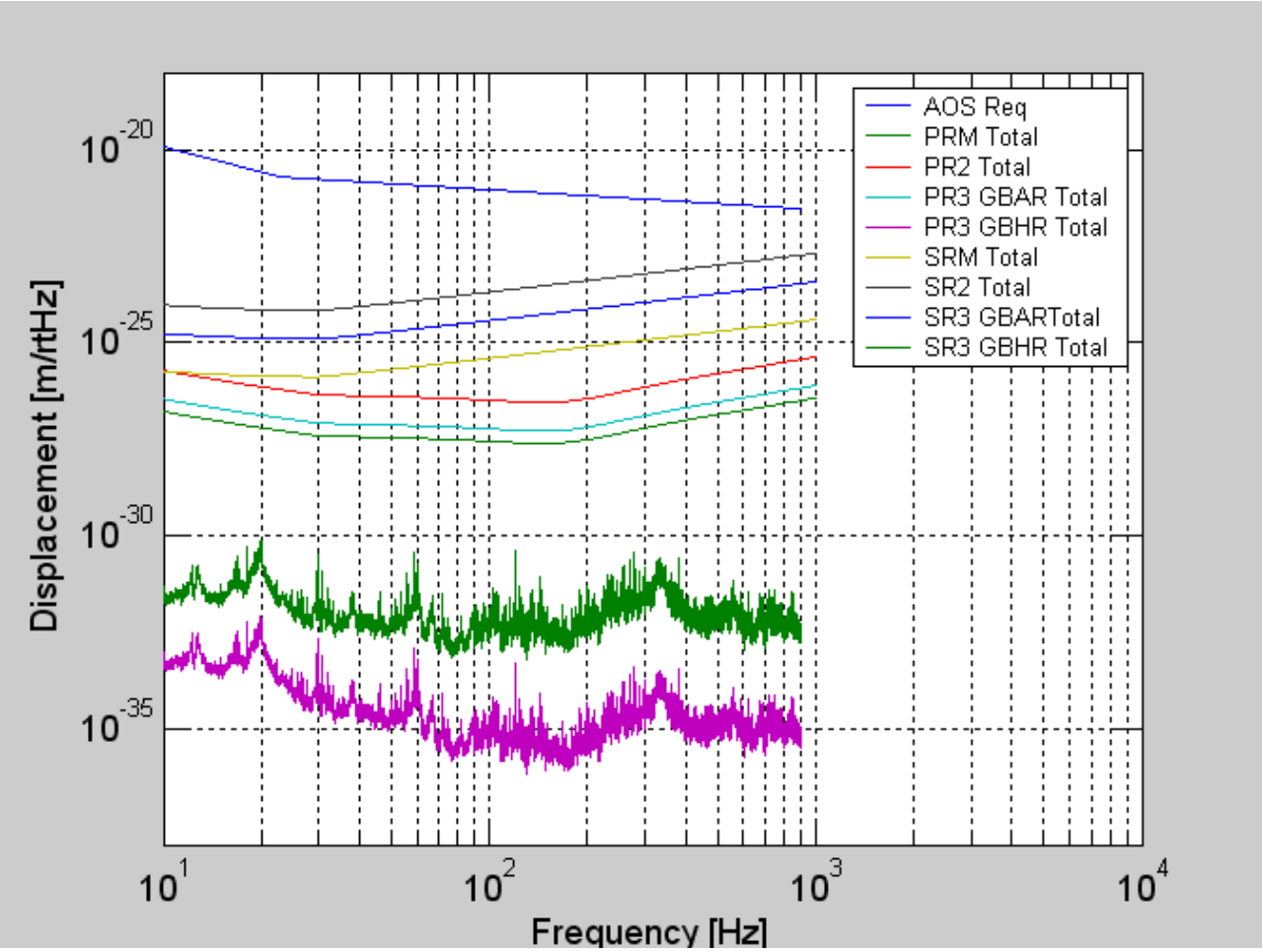

Figure 48: PRM, PR2, PR3, SRM, SR2, SR3, Scattered Light Displacement Noise

4.4 Stray Light Control Physical Characteristics

4.4.1 Faraday Isolator

Table 4: Faraday Isolator Characteristics

Parameter	**Value**
Configuration	Single Faraday isolator
Wavelength	1064 nm
Clear Aperture	20 mm
Rotator material	TGG crystal
Rotator crystal wedge angle front and back surface	1 deg
Total wavefront distortion	<1 λ @ 633 nm
Rotator transmissivity across clear aperture	>97 %
Input/output polarizer	Calcite, air-spaced Brewster's angle
Polarizer transmissivity per surface	>99.9 %
Half-wave rotation plate	Zero-order quartz

Table 5 : Faraday Isolator Suspension Characteristics

Parameter	**Value**
Frame	Modified LOS
Suspension	Four wire marionette
Amplitude response	See Figure 23
Damping	Eddy current
Height adjustment	manual
Yaw adjustment	manual
Pitch adjustment	Remote, Pico Motor

4.4.2 Arm Cavity Baffle

Table 6: Arm Cavity Baffle Characteristics

Parameter	**Value**
Aperture diameter	346 mm
Outer diameter blockage	>850 mm
Material	Oxidized polished stainless steel
BRDF	<0.05 sr^-1

Parameter	Value
Reflectivity	<0.05
Weight	TBD kg

Table 7: Arm Cavity Baffle Suspension

Parameter	Value
Frame	Aluminum frame
Suspension	Two wire, suspended from HEPI stage "0"
Amplitude response	See Figure 26
Damping	Q < 1000

4.4.3 Arm Cavity Baffle Cylinder

Table 8: Arm Cavity Baffle Cylinder Characteristics

Parameter	Value
diameter	1400 mm
Length	500 mm
Material	Oxidized polished stainless steel
BRDF	<0.05 sr^-1
Reflectivity	<0.05
Weight	TBD kg

Table 9: Arm Cavity Baffle Suspension

Parameter	Value
Frame	TBD
Suspension	Two wire, suspended from HEPI stage "0"
Amplitude response	See Figure 26
Damping	Q < 1000

4.4.4 Elliptical Baffle

4.4.4.1 ITM Elliptical Baffle

Table 10: ITM Elliptical Baffle Characteristics

Parameter	**Value**
Suspension	See Figure 26
Damping	Q < 1000
Aperture major diameter	259 mm
Aperture minor diameter	224 mm
Material	Oxidized polished stainless steel
BRDF	<0.05 sr^-1
Reflectivity	<3E-5
Weight	TBD kg

4.4.4.2 PRM Elliptical Baffle

Table 11: PRM Elliptical Baffle Characteristics

Parameter	**Value**
Suspension	Attached to HAM optics table
Damping	none
Aperture major diameter	259 mm
Aperture minor diameter	224 mm
Material	Oxidized polished stainless steel
BRDF	<0.05 sr^-1
Reflectivity	<3E-5
Weight	TBD kg

4.4.5 Manifold Baffle

Table 12: Manifold Baffle

Parameter	Value
Suspension	See Figure 31
Damping	none
Aperture	769 mm radius
Outer diameter	1860 mm
Material	Oxidized polished stainless steel
BRDF	<0.05 sr^-1
Reflectivity	<3E-5
Weight	TBD kg

4.4.6 Septum Window

Table 13: Septum Window Characteristics

Parameter	Value
Clear aperture diameter	60 mm @ 56 deg incidence
Wavefront distortion	<0.14 λ @ 633 nm
BRDF @ 56 deg incidence	< 5E-6 sr^-1
Reflectivity	<2.5E-3
Diameter of substrate	TBD
Thickness	TBD
Material	Grade A fused silica, super polished
Attachment to Flange	O-ring seal

4.4.7 PR2/SR2 Cavity Beam Dump

Table 14: Cavity Beam Dump Characteristics

Parameter	Value
Suspension	Direct to HAM table
Damping	none
Aperture	TBD
Material	Oxidized polished stainless steel

Parameter	Value
BRDF	<0.05 sr^-1
Reflectivity	<3E-5
Weight	TBD kg

4.4.8 Cryopump Baffle

Table 15: Cryopump Baffle Characteristics

Parameter	Value
Location	Corner Station-- x arm, y arm End Station-- x arm, y arm
Suspension	See Figure 31
Aperture diameter	769 mm
Outer diameter	conical
Material	Oxidized polished stainless steel
BRDF	<0.05 sr^-1
Reflectivity	<3E-5
Weight	TBD

4.5 Stray Light Control Interface Definitions

4.5.1 Interfaces to other LIGO detector subsystems

4.5.1.1 Mechanical Interfaces

The beam dumps will attach to the optical tables or be suspended from the HEPI stage “0” in the HAM and BSC chambers, without interfering with the COC mirror structures. Earthquake stops will attach to the chamber wall.

The ITM Elliptical Baffle will hang from the BSC optics table or from the HEPI stage “0” and will have earthquake stops attached to the chamber wall.

The PRM Elliptical Baffle will mount directly to the HAM optical table.

The Arm Cavity Baffles will hang from the ITM and ETM HEPI stage “0”and will have earthquake stops attached to the chamber wall.

The Cryopump Baffle will be suspended from a mounting ring that is held in position inside the manifold piece by means of compressive forces.

The Manifold Baffle will be held in position inside the manifold by means of compressive forces.

4.5.1.2 Electrical Interfaces

4.5.1.2.1 Suspended Baffles and Beam Dumps

All the suspended baffles and beam dumps are passively damped and will require no electrical interfaces.

4.5.1.2.2 Faraday Isolator

The Faraday Isolator will be suspended from a modified LOS, and appropriate electronic control signals to the Pico Motor will be used for pitch steering.

4.5.1.3 Optical Interfaces

The Cavity Beam Dumps will intercept the ghost beams while maintaining adequate clearance from the main recycling cavity beams.

The PRM elliptical baffle will vignette the main beam incident onto the BS from the PRM direction to an elliptical cross section as described in 4.3.6.2.5.

The ITM elliptical baffle will vignette the main beam incident onto the BS from the ITM direction to an elliptical cross section as described in 4.3.6.1.6.

4.5.1.4 Stay Clear Zone

4.5.1.4.1 Arm Cavity Baffle

The aperture of the Arm Cavity Baffle will be 346 mm, which is larger than the diameter of the ITM and ETM COC. The aperture will be concentric with the COC within 4 mm.

4.5.1.4.2 ITMX, ITMY, and BS Beam Dump

The Cavity Beam Dumps will have a stay clear zone of >25 mm from the elliptical edges of the main recycling cavity beam.

4.5.1.4.3 Cryopump Baffle

The Cryopump Baffle will be concentric to the spool piece diameter within 4 mm. The clearance between the 1 ppm edge of the main beam and the centered Cryopump Baffle aperture will be > 7 mm.

4.5.1.4.4 Elliptical Baffle

The Elliptical Baffles will be concentric with the centerline of the IFO main beam within 4 mm.

4.5.2 Interfaces external to LIGO detector subsystems

There are no interfaces external to the LIGO detector.

4.6 Stray Light Control Reliability

All Stray Light Control baffles and beam dumps are passive and are expected to have 100% availability. The MTBF is expected to be equal to the life of the IFO.

The Faraday Isolator will be suspended by a passive two-wire suspension with vertical blade springs. The reliability should be excellent.

4.7 Stray Light Control Maintainability

The following components are susceptible to failure:

1) Pico Motor. Both the Faraday Isolator suspension and the ETM Telescope suspension use Pico Motors for initial alignment.

If this component fails, the failure will be ignored until a major realignment of the beam path requires that the ETM Telescope and the Faraday Isolator be realigned. At which time, an incursion into the vacuum chamber will be required.

4.8 Stray Light Control Environmental Conditions

4.8.1.1.1.1 Natural Environment

4.8.1.1.1.1.1 Temperature and Humidity

The SLC assemblies are designed to operate in the high vacuum environment of the IFO and in the controlled LVEA environment during installation.

Table 16 Environmental Performance Characteristics

Operating	Non-operating (storage)	Transport
+20C to +25C, 20-70% RH, non- condensing	0C to +60C, 10-90% RH, non-condensing	0C to +60C, 10-90% RH, non- condensing

4.8.1.1.1.1.2 Atmospheric Pressure

The Brewster's window will function with a differential pressure of 1 atmosphere under normal atmospheric pressure conditions.

4.8.1.1.1.1.3 Seismic Disturbance

The suspended SLC assemblies and the assemblies mounted to the vacuum chambers will withstand ground seismic disturbances.

4.8.1.1.1.2 Induced Environment

4.8.1.1.1.2.1 Electromagnetic Radiation

NA

4.8.1.1.1.2.2 Acoustic

NA

4.8.1.1.1.2.3 Mechanical Vibration

NA

4.9 Stray Light Control Transportability

All items will be transportable by commercial carrier without degradation in performance. As necessary, provisions will be made for measuring and controlling environmental conditions (temperature and accelerations) during transport and handling. Special shipping containers, shipping and handling mechanical restraints, and shock isolation will be utilized to prevent damage. All containers will be movable for forklift. All items over 100 lbs. that must be moved into place within LIGO buildings will have appropriate lifting eyes and mechanical strength to be lifted by cranes.

5 Stray Light Control Design and Construction

The design and construction of the Stray Light Control subsystem allow adequate cleaning, either on site or at an appropriate outside vendor, and will fit inside the vacuum baking ovens on site.

5.1.1.1 Materials and Processes

The materials and processes used in the fabrication of the Stray Light Control subsystem will be compatible with the LIGO approved materials list.

Metal components will have quality finishes on all surfaces, suitable for vacuum finishes. Aluminum components used in the vacuum will not have anodized surfaces.

5.1.1.1.1 Materials

A list of currently approved materials for use inside the LIGO vacuum envelope can be found in LIGO Vacuum Compatible Materials List (LIGO-E960022). All fabricated metal components exposed to vacuum will be made from stainless steel, copper, or aluminum. Other metals are subject to LIGO approval. Pre-baked viton (or fluorel) may be used subject to LIGO approval. All materials used inside the vacuum chamber will comply with LIGO Vacuum Compatibility, Cleaning Methods and Procedures (LIGO-E960022-00-D).

The only lubricating films permitted within the vacuum are dry plating of vacuum compatible materials such as silver and gold.

5.1.1.1.2 Processes

5.1.1.1.2.1 Cleaning

All materials used inside the vacuum chambers will be cleaned in accordance LIGO-E960022-00-D or LIGO-E000007-00, and Specification Guidance for Seismic Component Cleaning, Baking, and Shipping Preparation (LIGO-L970061-00-D). To facilitate final cleaning procedures, parts will be cleaned after any processes that result in visible contamination from dust, sand or hydrocarbon films.

Materials will be joined in such a way as to facilitate cleaning and vacuum preparation procedures; i.e. internal volumes will be provided with adequate openings to allow for wetting, agitation and draining of cleaning fluids and for subsequent drying.

5.1.1.1.3 Component Naming

All components will be identified using the LIGO Naming Convention (LIGO-E950111-A-E). This will include identification (part or drawing number, revision number, serial number) physically stamped on all components, in all drawings and in all related documentation.

5.1.1.2 Stray Light Control Workmanship

All components will be manufactured according to good commercial practice.

5.1.1.3 Stray Light Control Interchangeability

Common elements with ordinary dimensional tolerances will be interchangeable.

5.1.1.4 Stray Light Control Safety

This item will meet all applicable NSF and other Federal safety regulations, plus those applicable State, Local and LIGO safety requirements. A hazard/risk analysis will be conducted in accordance with guidelines set forth in the LIGO Project System Safety Management Plan LIGO-M950046-F, section 3.3.2.

5.1.1.5 Stray Light Control Human Engineering

NA

5.1.2 Stray Light Control Assembly and Maintenance

Assembly fixtures and installation procedures will be developed in conjunction with the Stray Light Control hardware design. These will include (but not be limited to) fixtures and procedures for:

- installation and assembly of beam dumps and baffles into the vacuum
- assembly of the in vacuum components in a clean room (class 100) environment

5.1.3 Stray Light Control Documentation

The documentation will consist of working drawings, assembly drawings, and alignment procedures

5.1.3.1 Stray Light Control Specifications

Specifications for the purchase of specialized components and assemblies such as Faraday isolator, optical mirrors, windows, and lenses will be developed.

5.1.3.2 Stray Light Control Design Documents

The following documents will be produced:

- LIGO Stray Light Control Preliminary Design Document (including supporting technical design and analysis documentation)
- LIGO Stray Light Control Final Design Document (including supporting technical design and analysis documentation)
- LIGO Stray Light Control Installation Procedures

5.1.3.3 Stray Light Control Engineering Drawings and Associated Lists

A complete set of drawings suitable for fabrication will be provided along with Bill of Material (BOM) and drawing tree lists. The drawings will comply with LIGO standard formats and will be provided in electronic format. All documents will use the LIGO drawing numbering system, be drawn using LIGO Drawing Preparation Standards, etc.

5.1.3.4 Stray Light Control Technical Manuals and Procedures

5.1.3.4.1 Procedures

Procedures will be provided for the installation, and final alignment of the Stray Light Control elements.

5.1.3.5 Stray Light Control Documentation Numbering

All documents will be numbered and identified in accordance with the LIGO documentation control numbering system LIGO document TBD

5.1.3.6 Stray Light Control Test Plans and Procedures

All test plans and procedures will be developed in accordance with the LIGO Test Plan Guidelines, LIGO document TBD.

5.1.4 Stray Light Control Logistics

The design will include a list of all recommended spare parts and special test equipment required.

5.1.5 Stray Light Control Precedence

The relative importance of the positioning of the beam dumps and baffles will be as follows:

1) satisfy the stay clear requirements
2) align the baffles and beam dumps with the centers of the ghost beams

5.1.6 Stray Light Control Qualification

N/A

6 Quality Assurance Provisions

This section includes all of the examinations and tests to be performed in order to ascertain that the fabricated SLC elements conform to the requirements in section 3.

6.1 General

6.1.1 Responsibility for Tests

AOS will conduct tests to verify the as-delivered performance specifications of the sub-system.

6.1.2 Special Tests

6.1.2.1 Engineering Tests

6.1.2.1.1 Witness Sample Scattering Tests of Baffle and Beam Dump Material

6.1.2.1.2 ETM Telescope Performance Test

6.1.2.1.3 ETM Telescope Suspension Damping Test

6.1.2.1.4 Faraday Isolator Performance Test

6.1.2.1.5 Faraday Isolator Suspension Damping Test

6.1.2.1.6 TBD

6.1.2.2 Reliability Testing

No reliability testing is anticipated.

6.1.3 Configuration Management

Configuration control of specifications and designs will be in accordance with the LIGO Detector Implementation Plan.

6.2 Quality conformance inspections

Design and performance requirements identified in this specification and referenced specifications will be verified by inspection, analysis, demonstration, similarity, test or a combination thereof per the Verification Matrix, Appendix 1 (TBD). Verification method selection shall be specified by individual specifications, and documented by appropriate test and evaluation plans and procedures. Verification of compliance to the requirements of this and subsequent specifications will be accomplished by the following methods or combination of methods:

6.2.1 Inspections

Manufactured parts with LIGO identification numbers or marks will be inspected to determine conformity with the procurement specification.

Witness samples will be acceptable proof of the properties of HR and AR coatings applied to the optical surfaces.

6.2.2 Demonstration

The required attenuation and transmissivity characteristics of the assembled Faraday isolator will be demonstrated before installation.

The resonance and damping characteristics of the suspended beam dumps and baffles will be demonstrated before installation.

6.2.3 Test

Appropriate tests will be implemented to verify the specifications of the purchased components. TBD

7 Preparation for Delivery

Packaging and marking of equipment for delivery will be in accordance with the Packaging and Marking procedures specified herein.

7.1 Preparation

- Vacuum preparation procedures as outlined in E960022-B LIGO Vacuum Compatibility, Cleaning Methods and Qualification Procedures will be followed for all components intended for use in vacuum. After wrapping vacuum parts as specified in this document, an additional, protective outer wrapping and provisions for lifting shall be provided.
- Electronic components will be wrapped according to standard procedures for such parts.

7.2 Packaging

Procedures for packaging will ensure cleaning, drying, and preservation methods adequate to prevent deterioration, appropriate protective wrapping, adequate package cushioning, and proper containers. Proper protection will be provided for shipping loads and environmental stress during transportation, hauling and storage. The shipping crates used for large items will use for guidance military specification MIL-C-104B, Crates, Wood; Lumber and Plywood Sheathed, Nailed and Bolted. Passive shock witness gauges will accompany the crates during all transits.

For the viewports, the shipping preparation will include double bagging with Ameristat 1.5TM plastic film (heat sealed seams as practical, with the exception of the inner bag, or tied off, or taped with care taken to insure that the tape does not touch the cleaned part). The bag will be purged with dry nitrogen before sealing.

7.3 Marking

Appropriate identification of the product, both on packages and shipping containers; all markings necessary for delivery and for storage, if applicable; all markings required by regulations, statutes, and common carriers; and all markings necessary for safety and safe delivery will be provided.

Identification of the material will be maintained through all manufacturing processes. Each component will be uniquely identified. The identification will enable the complete history of each component to be maintained (in association with Documentation “travelers”). A record for the optical lever support structures will indicate all weld repairs and fabrication abnormalities.

The specification for marking will state that marking fluids, die stamps and/or electro-etching is not permitted. A vibratory tool with a minimum tip radius of 0.005" is acceptable for marking on surfaces that are not hidden from view. Engraving and stamping are also permitted.

8 Appendix A—Scattered Light Noise Theory

8.1 Scattered Light Requirement

A DARM signal is obtained when the differential arm length is modulated as a result of a gravity wave strain. The DARM signal was calculated in reference T060073-00 Transfer Functions of Injected Noise, and is defined by the following expression:

$$V_{signal} := DARM \cdot L \cdot h_{SRD} \cdot \sqrt{P_0}$$

Where L is the arm length, h_{SRD} is the minimum SRD gravity wave strain spectral density requirement, P_0 is the input laser power into the IFO, and DARM is the signal transfer function.

In a similar manner, an apparent signal (scattered light noise) occurs when a scattered light field with a phase shift is injected into the IFO at some particular location, e.g. through the back of the ETM mirror. The scattered light noise is defined by the following expression:

$$V_{noise} := SNXXX \cdot \delta_{SN} \cdot \sqrt{P_{SNi}}$$

P_{SNi} is the scattered light power injected into the IFO mode, δ_{SN} is the phase shift of the injected field, and SNXXX is the noise transfer function for that particular injection location.

The phase shift spectral density of the injected field due to the motion of the scattering surface is given by

$$\delta_{SNi} := \frac{4 \cdot \pi \cdot x_s}{\lambda}$$

where x_s is the spectral density of the longitudinal motion of the scattering surface.

In general, the different scattering sources are not coherent and must be added in quadrature. The requirement for total scattered light displacement noise can be stated with the following inequality:

$$\sqrt{\sum_{i=1}^{n} \left(\frac{SNXXX}{DARM} \cdot \frac{4 \cdot \pi \cdot x_s}{\lambda} \cdot \sqrt{\frac{P_{SNi}}{P_0}} \right)^2} < \frac{1}{10} \cdot L \cdot h_{SRD}$$

The SNXXX/DARM scattered light noise transfer functions for various injection locations within the IFO were calculated by Hiro (T060073-00 Transfer Functions of Injected Noise) and are shown in Figure 49: Scattered Light Noise Transfer Functions.

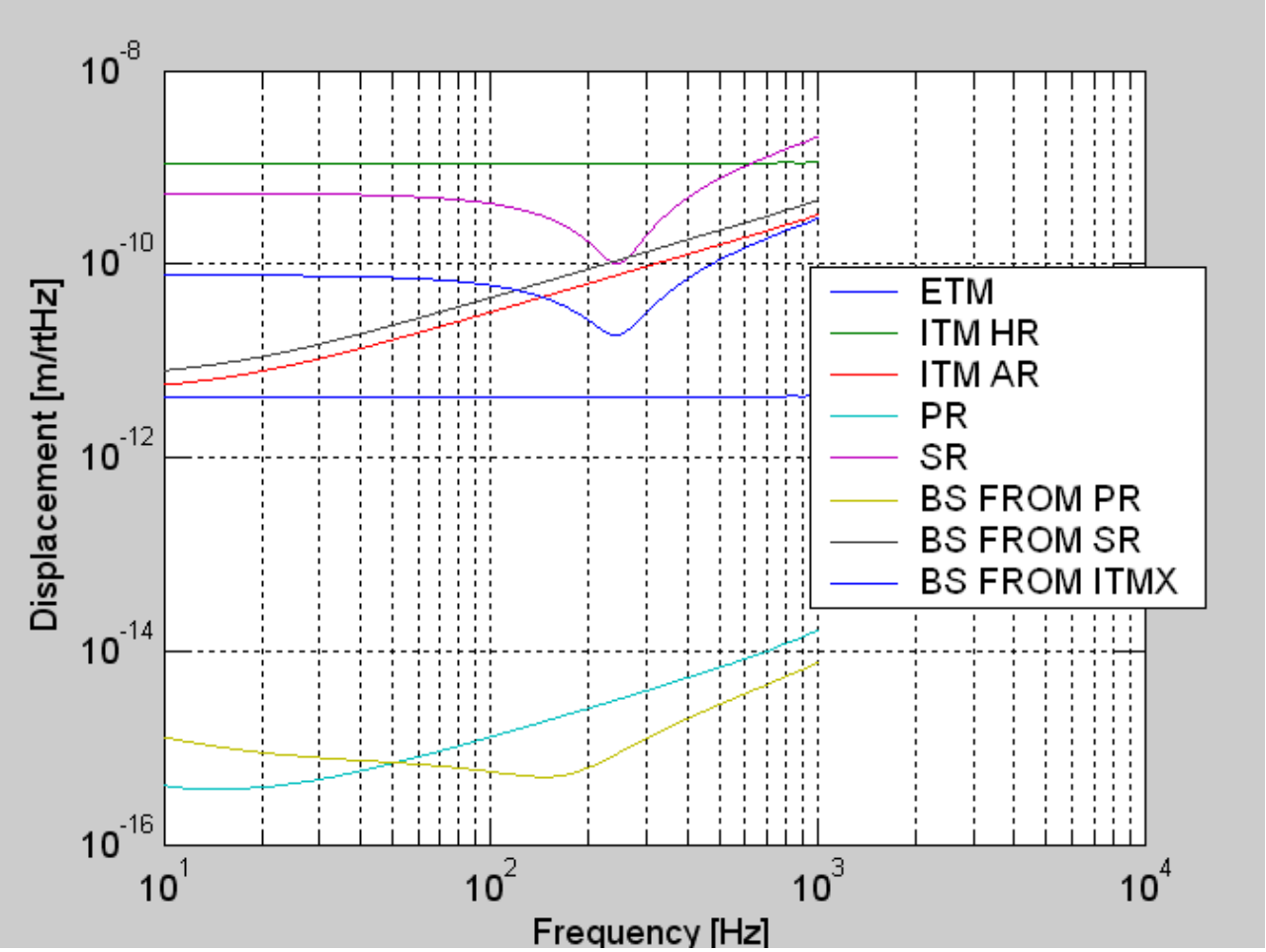

Figure 49: Scattered Light Noise Transfer Functions

8.2 Scattered Power into the IFO

The light power scattered into the interferometer from the ith source is calculated as follows:

$$P_{SNi} := P_{in} \cdot BRDF \cdot \Delta\Omega \cdot \frac{w_{IFO}^{2}}{w_{SN}^{2}} \cdot T$$

Where P_{in} is the power incident on the scattering surface, BRDF is the fraction of incident light that is scattered per unit solid angle, $\Delta\Omega$ is the solid angle subtended by the mode inside the IFO arm, w_{IFO} is the beam waist of the mode inside the arm, w_{SN} is the beam waist of the beam incident on the scattering surface, and T is the transmissivity of the path from the scattering surface to the injection point in the IFO.

The effective solid angle increases whenever the IFO beam waist has been transformed to a smaller waist by an AOS telescope or some other focusing element in the ISC detection system, because the product of solid angle and beam waist cross-sectional area is proportional to the total radiant

flux, which is an optical invariant. Therefore, as the area of the beam waist decreases the effective solid angle increases proportionally.

8.2.1 Output Faraday Isolator Scatter

The power incident on the Faraday isolator is given by

$$P_{FIin} := P_0 \cdot G_{AS}$$

G_{AS} is the dark port signal ratio.

The light power scattered into the IFO from the nine surfaces before the Faraday rotator magnet is given by

$$P_{FIs} := 9 \cdot P_{FIin} \cdot BRDF_{FI} \cdot \Delta\Omega_{IFO} \cdot \frac{w_0^2}{w_{FI}^2}$$

The scattering surface has the seismic motion of the HAM requirement, attenuated by the motion transfer function of the Faraday Isolator requirement.

The scattered light is injected into the SRM mirror, and the appropriate scattered light noise transfer function is 'SRM'. The displacement noise (m/rt Hz) is

$$DN_{faradsifo} := TF_{sr} \cdot \left(\frac{P_{farads}}{P_{psl}} \right)^{0.5} \cdot x_{ham} \cdot 2 \cdot k \cdot faradisolre$$

8.2.2 Arm Cavity Baffle Surface Scatter

The small angle scattered power from the far arm cavity mirror passes through the beam tube to the near arm cavity mirror. The power in the annulus between the cryopump baffle and the ITM (ETM) outside diameter will hit the Arm Cavity Baffle. See Figure 50.

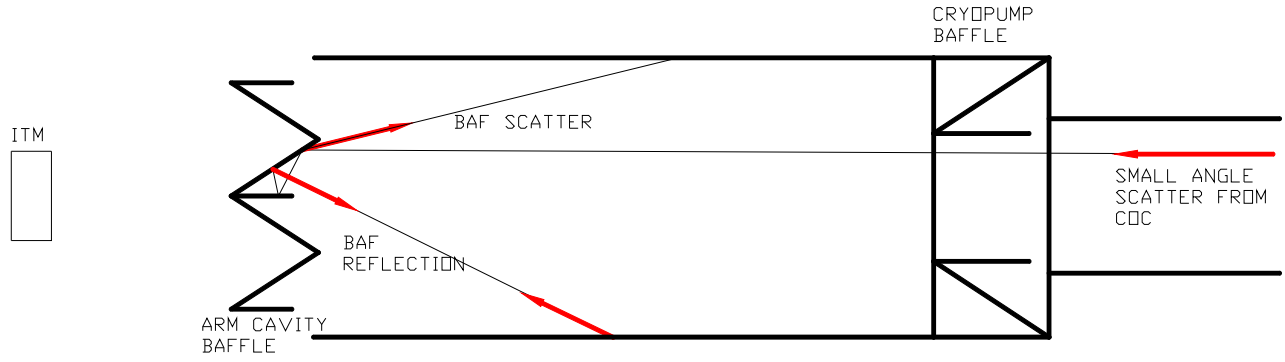

Figure 50: ARM CAVITY BAFFLE SCATTER

The offset between the arm cavity mirror and the beam tube axis will be ignored.

$$P_{acb} := P_a \cdot \int_{\theta_{ac}}^{\theta_{cp}} 2 \cdot \pi \cdot \theta \cdot BRDF_1(\theta)\, d\theta$$

The half-angle from the beam tube centerline to the AC baffle inner edge is

$$\theta_{ac} := \frac{R_{ac}}{L}$$

The half-angle from the beam tube centerline to the cryopump baffle outer edge is

$$\theta_{cp} := \frac{R_{cp}}{L}$$

P_a is the circulating power in each arm.

The light power scattered from four Arm Cavity Baffles into the mode cross section and re-scattered by the far COC into the IFO mode is given by

$$P_{acbafs} := \sqrt{4} \cdot P_{acb} \cdot BRDF_{bd} \cdot \frac{\pi \cdot w_{ifo}^2}{L^2} \cdot BRDF_1\left(30 \cdot 10^{-6}\right) \cdot \Delta_{ifc}$$

The scattering surface is suspended from the BSC HEPI ring and has the seismic motion of the HEPI requirement, attenuated by the motion transfer function of the Arm Cavity Baffle requirement.

The scattered light is injected into the arm cavity, and the appropriate scattered light noise transfer function is 'ITM_HR'. The displacement noise (m/rt Hz) is

$$DN_{acbaf} := TF_{itmhr} \left(\frac{P_{acbafs}}{P_{psl}} \right)^{0.5} \cdot x_{hepi} \cdot 2 \cdot k \cdot acbatter$$

8.2.3 Arm Cavity Baffle Reflected Light

The power reflected from the Arm Cavity Baffle and incident on the vacuum manifold wall is given by

$$P_{armbafrefl} := P_{acb} \cdot R_{bd}$$

where R_{bd} is the net reflectivity of the baffle.

This light will scatter from the wall, reflect again from the Arm Cavity Baffle toward the far COC, and finally scatter from the COC into the mode of the IFO. The scattered power is given by

$$P_{armbafrefls} := R_{bd} \cdot P_{armbafrefl} BRDF_{wall} \frac{\pi \cdot w_{ifo}^2}{L^2} \cdot BRDF_1\left(30 \cdot 10^{-6}\right) \cdot \Delta_{ifc}$$

The scattering surface has the seismic motion of the beam tube.

The scattered light is injected into the arm cavity, and the appropriate scattered light noise transfer function is 'ITM_HR'. The displacement noise (m/rt Hz) is

$$DN_{armbafrefls} := TF_{itmhr}\left(\frac{P_{armbafrefls}}{P_{psl}}\right)^{0.5} \cdot x_{beamtube} \cdot 2 \cdot k$$

8.2.4 ITM Elliptical Baffle Surface Scatter

See Figure 51. When the IFO arm cavity is on resonance, the power exiting the arm cavity into the recycling cavity through the ITM is exactly twice the power incident on the ITM from the recycling cavity side. The two counter-propagating beams are exactly 180 degrees out of phase and they interfere at the surface of the ITM. The resultant beam, with a power equal to the power recycling cavity arm power, appears to reflect from the ITM back into the power recycling cavity.

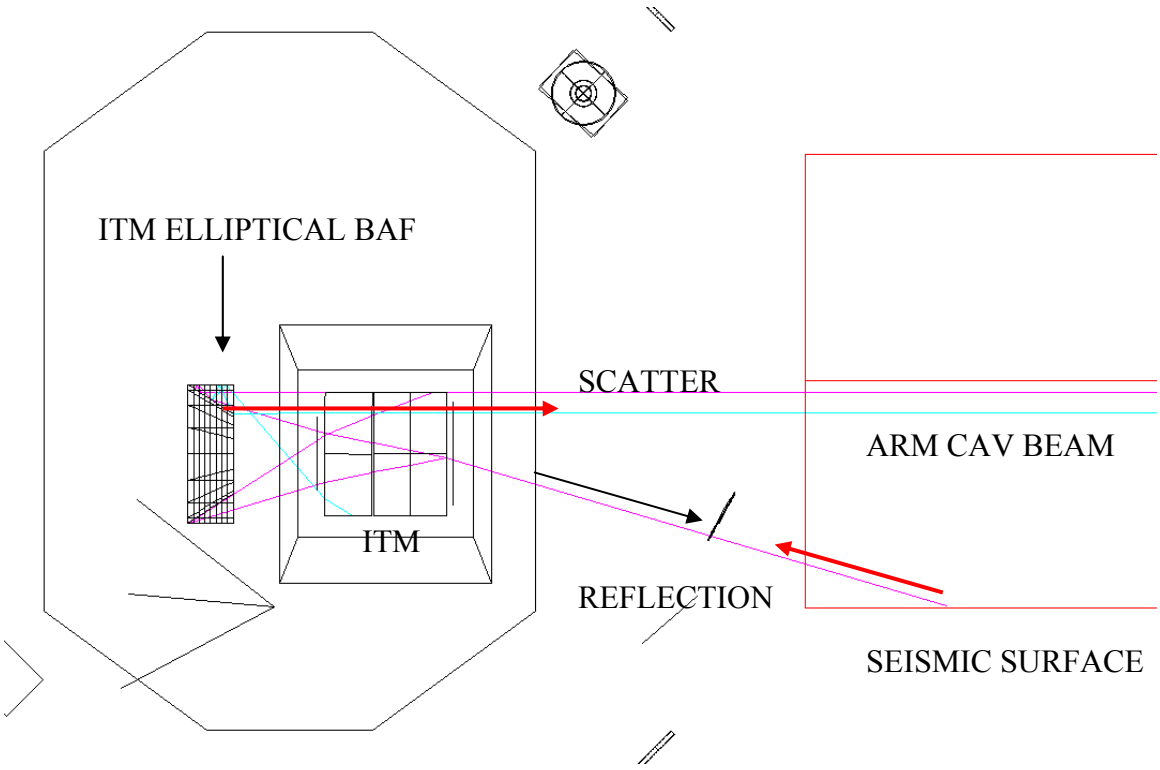

Figure 51: ITM ELLIPTICAL BAFFLE SCATTER AND REFLECTION

However, in the actual LIGO IFO the recycling cavity beam has a truncated Gaussian profile with an elliptical cross section. Beyond the edges of the sharp elliptical boundary, the Gaussian shaped

beam exiting from the arm cavity is not opposed with a Gaussian power recycling cavity beam and will strike the elliptical baffle with twice the irradiance of the power recycling cavity beam.

The Gaussian irradiance parameter, P_{0itm}, of the beam exiting the ITM is twice the irradiance parameter, P_{0rc}, of the recycling cavity beam.

$$P_{0itm} := 2 \cdot P_{0rc}$$

The exitance function from the ITM is given by

$$I_{ITM}(x,y) := 2 \cdot \frac{P_{0itm}}{\pi \cdot w^2} \cdot e^{-2 \cdot \left(\frac{x^2+y^2}{w^2} \right)}$$

and the irradiance function inside the power recycling cavity arm is given by

$$I_{rc}(x,y) := 2 \cdot \frac{P_{0rc}}{\pi \cdot w^2} \cdot e^{-2 \cdot \left(\frac{x^2+y^2}{w^2} \right)}$$

The total power exiting from the ITM is

$$P_{itm} := \int_0^R I_{itm}(r) \cdot 2 \cdot \pi \cdot r \, dr$$

$$P_{itm} = 2.1084 \times 10^3$$

The total power from the exiting ITM beam that passes through the elliptical baffle is

$$P_{ell} := 4 \cdot \int_0^b \int_0^{a \cdot \sqrt{1 - \frac{y^2}{b^2}}} I_{ITM}(x,y) \, dx \, dy$$

Then, the power that hits the elliptical baffle from the ITM side is the difference

$$P_{ellbaf} := P_{itm} - P_{ell}$$

The light power scattered from the two Elliptical Baffles and then re-scattered into the IFO mode at the far COC is given by

$$P_{itmellbafs} := \sqrt{2} \cdot T_{itmhr} \cdot P_{itmellbaf} \cdot BRDF_{ellbaf} \cdot \frac{\pi \cdot w_{ifo}^2}{L^2} \cdot BRDF_1\left(30 \cdot 10^{-6}\right) \cdot \Delta_{ifo}$$

where T_{itmhr} is the transmissivity of the ITM mirror, and the scattering BRDF from the far COC mirror is evaluated at the incidence angle 30E-6 rad.

The scattering surface is suspended from the BSC HEPI ring and has the seismic motion of the HEPI requirement, attenuated by the motion transfer function of the ITM Elliptical Baffle requirement.

The scattered light is injected into the arm cavity, and the appropriate scattered light noise transfer function is 'ITM_HR'. The displacement noise (m/rt Hz) is

$$DN_{itmellbaf} := TF_{itmhr} \cdot \left(\frac{P_{itmellbafs}}{P_{psl}}\right)^{0.5} \cdot x_{hepi} \cdot ellipbafatten \cdot 2 \cdot k$$

8.2.5 ITM Elliptical Baffle Reflected Light

The power reflected from the ITM Elliptical Baffle and incident on the vacuum manifold wall is given by

$$P_{ellbafRin} := P_{ellbaf} \cdot R_{ellbaf}$$

where R_{ellbaf} is the reflectivity of the baffle surface.

The light will scatter from the wall, reflect from the Elliptical Baffle, and transmit through the ITM into the mode of the IFO at the far COC. The scattered power is given by

$$P_{elleRs} := P_{ellbafRin} \cdot BRDF_{VAC} \cdot R_{ellbaf} \cdot T_{itm} \cdot \frac{\pi \cdot w_0^2}{L^2}$$

The scattering surface has the seismic motion of the BSC chamber wall.

The scattered light is injected into the arm cavity, and the appropriate scattered light noise transfer function is 'ITM_HR'. The displacement noise (m/rt Hz) is

$$DN_{itmellbafrefl} := TF_{itmhr} \cdot \left(\frac{P_{itmellbafrefls}}{P_{psl}}\right)^{0.5} \cdot x_{bscchamber} \cdot 2 \cdot k$$

8.2.6 PRM Elliptical Baffle

The prompt Gaussian beam that enters the power recycling cavity through the PRM HR surface is expanded by the PRM telescope (PR2 and PR3) and is vignetted into an elliptical cross section by the PRM Elliptical Baffle.

The expanded Gaussian irradiance functions at the PRM Elliptical Baffle, given in terms of radius and Cartesian coordinates, are

$$I_{psl}(r) := 2\cdot\frac{T_{prmhr}\cdot P_{psl}}{\pi\cdot w^2}\cdot e^{-2\cdot\left(\frac{r^2}{w^2}\right)}$$

$$I_{psl}(x,y) := 2\cdot\frac{T_{prmhr}\cdot P_{psl}}{\pi\cdot w^2}\cdot e^{-2\cdot\left(\frac{x^2+y^2}{w^2}\right)}$$

The total power passing through the PR3 mirror is

$$P_{pr3} := \int_0^{r_{pr3}} I_{psl}(r)\cdot 2\cdot\pi\cdot r\,dr$$

The total power passing through the PRM Elliptical Baffle is

$$P_{pr3rc} := 4\cdot\int_0^{b}\int_0^{a\cdot\sqrt{1-\frac{y^2}{b^2}}} I_{psl}(x,y)\,dx\,dy$$

The power hitting the baffle is the difference

$$P_{prmellbaf} := P_{pr3} - P_{pr3rc}$$

This power scatters back through the PRM telescope onto the PRM HR surface, where it re-scatters into the de-magnified mode volume of the recycling cavity. The scattering from the PRM will be evaluated at the maximum scattering angle at the surface of the PRM

$$\theta_{prmellbafs} := m\cdot\frac{w_{ifo}}{L}$$

where m is the magnification of the PRM telescope.

The scattered power into the IFO is given by

$$P_{prmellbafs} := P_{prmellbaf}\cdot BRDF_{ellbaf}\cdot\frac{\pi\cdot w_{rc}^2}{L_{prm2}^2}\cdot BRDF_1\left(\theta_{prmellbafs}\right)\cdot\frac{w_{ifo}^2}{w_{rc}^2}\cdot\Delta_{ifc}$$

where L_{prm2} is the distance from the recycling cavity beam waist (near PR2) and PRM, w_{rc} is the demagnified beam radius in the power recycling cavity.

The PRM Elliptical Baffle scattering surface is mounted to the HAM table and has the seismic motion of the HAM requirement.

The scattered light is injected into the BS from the PR side, and the appropriate scattered light noise transfer function is 'BS_from_PR'. The displacement noise (m/rt Hz) is

$$DN_{prmellbaf} := TF_{prbs} \cdot \left(\frac{P_{prmellbafs}}{P_{psl}} \right)^{0.5} \cdot x_{ham} \cdot 2 \cdot k$$

8.2.7 H2 Elliptical Scraper Mirror

The power that hits the H2 Elliptical Scraper Mirror is the same power that hits the elliptical baffle from the ITM side in the H1 interferometer.

$$P_{H2scrmir} := P_{itmellbaf}$$

The light power scattered from the two H2 Elliptical Scraper Mirror and then re-scattered into the IFO mode at the far COC is given by

$$P_{H2scrmirs} := \sqrt{2} \cdot T_{itmhr} \cdot P_{H2scrmir} \cdot BRDF_{H2scrmir} \cdot \frac{\pi \cdot w_{ifo}^{2}}{L^{2}} \cdot BRDF_1\left(30 \cdot 10^{-6}\right) \cdot \Delta_{ifo}$$

where T_{itmhr} is the transmissivity of the ITM mirror, and the scattering BRDF from the far COC mirror is evaluated at the incidence angle 30E-6 rad.

The scattering surface is suspended from the BSC optical table and has the seismic motion of the BSC requirement, attenuated by the motion transfer function of the H2 Elliptical Scraper Mirror suspension.

The scattered light is injected into the arm cavity, and the appropriate scattered light noise transfer function is 'ITM_HR'. The displacement noise (m/rt Hz) is

$$DN_{H2scrmirror} := TF_{itmhr} \cdot \left(\frac{P_{H2scrmirs}}{P_{psl}} \right)^{0.5} \cdot x_{bsc} \cdot H2scrmiratten \cdot 2 \cdot k$$

8.2.8 H2 Elliptical Scraper Mirror Beam Dump

The power that hits the H2 Elliptical Scraper Mirror Beam Dump is the power that reflects from the H2 Elliptical Scraper Mirror.

$$P_{h2scrmirbd} := P_{H2scrmir} \cdot R_{H2scrmi}$$

The light power scattered from the two H2 Elliptical Scraper Mirror Beam Dumps and then re-scattered into the IFO mode at the far COC is given by

$$P_{h2scrmirbds} := \sqrt{2} \cdot T_{itmhr} \cdot P_{h2scrmirbd} \cdot BRDF_{bd} \cdot \frac{\pi \cdot w_{ifo}^{2}}{L^{2}} \cdot BRDF_{1}\left(30 \cdot 10^{-6}\right) \cdot \Delta_{ifo}$$

where T_{itmhr} is the transmissivity of the ITM mirror, and the scattering BRDF from the far COC mirror is evaluated at the incidence angle 30E-6 rad.

The scattering surface is suspended from the BSC HEPI ring and has the seismic motion of the HEPI requirement, attenuated by the motion transfer function of the H2 Elliptical Scraper Mirror Beam Dump suspension.

The scattered light is injected into the arm cavity, and the appropriate scattered light noise transfer function is 'ITM_HR'. The displacement noise (m/rt Hz) is

$$DN_{H2scrmirror} := TF_{itmhr} \cdot \left(\frac{P_{H2scrmirs}}{P_{psl}} \right)^{0.5} \cdot x_{bsc} \cdot H2scrmiratten \cdot 2 \cdot k$$

8.2.9 H2 FM Beam Dump Surface Scatter

The power that hits the H2 FM Beam Dump is the leakage of the recycling cavity power in a single arm through the HR coating of the FM.

$$P_{FM} := P_{rca} \cdot \left(1 - R_{FMhr}\right)$$

The light power scattered from the four H2 FM Beam Dumps enters the arm cavity through the ITM and is re-scattered into the IFO mode at the far COC.

$$P_{FMbds} := \sqrt{4} \cdot T_{itmhr} \cdot P_{FM} \cdot BRDF_{ellbaf} \cdot \frac{\pi \cdot w_{ifo}^{2}}{L^{2}} \cdot BRDF_{1}\left(30 \cdot 10^{-6}\right) \cdot \Delta_{ifo}$$

where T_{itmhr} is the transmissivity of the ITM mirror, and the scattering BRDF from the far COC mirror is evaluated at the incidence angle 30E-6 rad.

The scattering surface is suspended from the BSC HEPI ring and has the seismic motion of the HEPI requirement, attenuated by the motion transfer function of the H2 FM Beam Dump suspension.

The scattered light is injected into the arm cavity, and the appropriate scattered light noise transfer function is 'ITM_HR'. The displacement noise (m/rt Hz) is

$$DN_{FMbd} := TF_{itmhr} \cdot \left(\frac{P_{FMbds}}{P_{psl}} \right)^{0.5} \cdot x_{hepi} \cdot FMbdatten \cdot 2 \cdot k$$

8.2.10 ITM (ETM) Wide-Angle Scatter

Point defects in the coatings and dust particles on the surface of the arm cavity mirrors will cause wide-angle scattered light. The scattering function appears to be Lambertian. See T070089-02 Wide-angle Scatter from LIGO Arm Cavities.

The wide-angle scattered light will predominately hit the back of the Arm Cavity Baffle and the Cylindrical Baffle between the mirror and the Arm Cavity Baffle. Some of the light will pass through the hole in the Arm Cavity Baffle and hit the manifold wall and the manifold baffle. Some of the light will hit the BSC chamber.

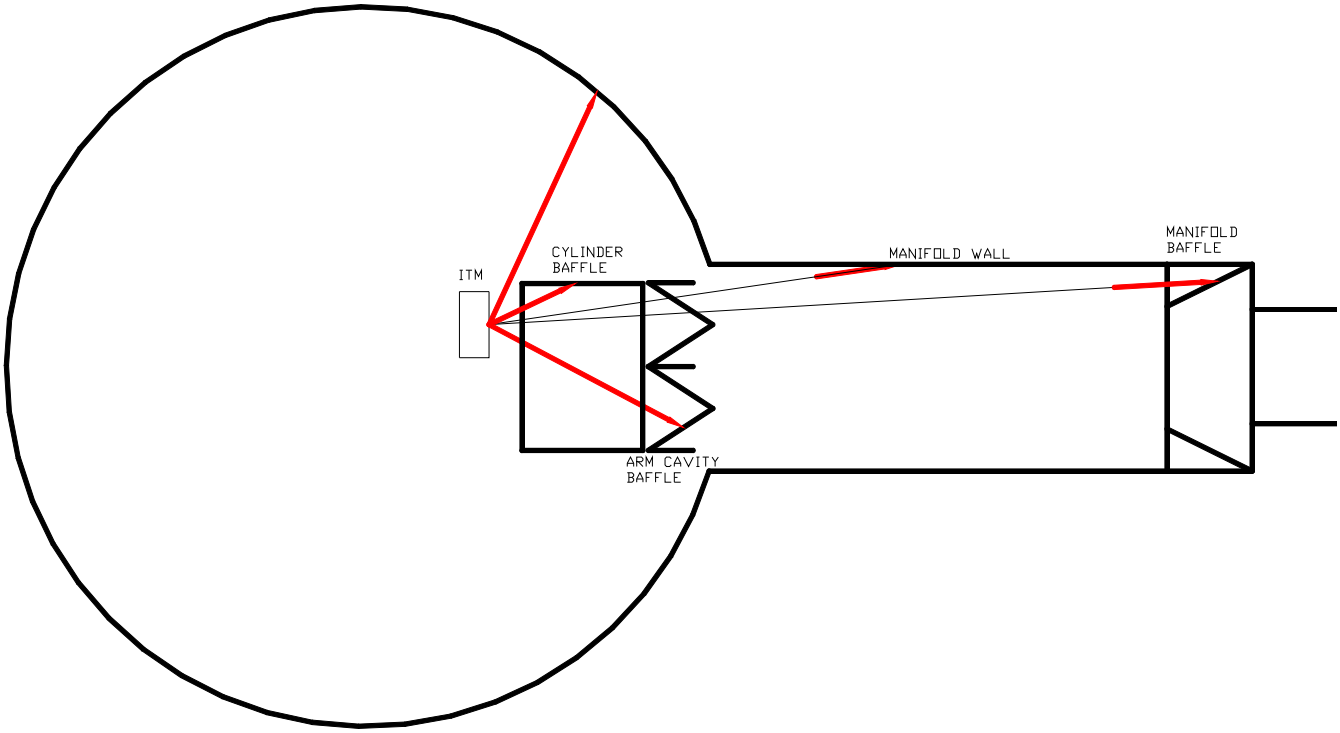

Figure 52: Wide-angle Scatter from ITM (ETM)

8.2.10.1 Scattering from the Back of Arm Cavity Baffle

In the following calculations, the offset of the ITM from the centerline of the arm cavity is ignored. The wide-angle scattered light hitting the back of the Arm Cavity Baffle is given by

$$P_{acbback}\left(L_{acb}, r_{acbo}\right) := P_a \cdot \int_{\theta_{acbi}\left(L_{acb}\right)}^{\theta_{acbo}\left(L_{acb}, r_{acbo}\right)} \frac{\alpha_{ws} \cdot \cos(\theta)}{\pi} \cdot 2 \cdot \pi \cdot \sin(\theta)\, d\theta$$

Where, the half-angle from the ITM centerline to the Arm Cavity Baffle outer edge is

$$\theta_{acbo}(L_{acb}, r_{acbo}) := \operatorname{atan}\left(\frac{r_{acbo}}{L_{acb}}\right)$$

The half-angle from the ITM centerline to the Arm Cavity Baffle inner edge is

$$\theta_{acbi}(L_{acb}) := \operatorname{atan}\left(\frac{r_{acbi}}{L_{acb}}\right)$$

and L_{acb} is the distance from the ITM to the Arm Cavity Baffle.

The power scattered onto the back of the Arm Cavity Baffle is

$$P_{acbbackifo}(L_{acb}, r_{acbo}) := \sqrt{4}\cdot P_a \cdot \left(C_2(L_{acb}, r_{acbo}) \cdot \alpha_{ws}^{\,2} \cdot \frac{\lambda^2}{L_{acb}^{\,2}} \cdot BRDF_{wall} \right)$$

Where the geometric function is

$$C_2(L_{acb}, r_{acbo}) := \frac{2}{\pi} \cdot \int_{\theta_{acbi}(L_{acb})}^{\theta_{acbo}(L_{acb}, r_{acbo})} \cos(\theta)^5 \cdot \sin(\theta)\, d\theta$$

8.2.10.2 Scattering from the COC Wide Angle Baffle

The wide-angle scattered light hitting the inside of the COC Wide Angle Baffle is

$$P_{accyl}(L_{acb}, r_{acbo}, L_{cyl}) := P_a \cdot \int_{\theta_{acbo}(L_{acb}, r_{acbo})}^{\theta_{accyl}(L_{acb}, r_{acbo}, L_{cyl})} \frac{\alpha_{ws} \cdot \cos(\theta)}{\pi} \cdot 2 \cdot \pi \cdot \sin(\theta)\, d\theta$$

Where the half-angle from the ITM centerline to the COC Wide Angle Baffle is

$$\theta_{accyl}(L_{acb}, r_{acbo}, L_{cyl}) := \operatorname{atan}\left(\frac{r_{acbo}}{L_{acb} - L_{cyl}}\right)$$

and L_{acb} is the length of the Arm Cavity Baffle, and L_{cyl} is the length of the COC Wide Angle Baffle.

The power scattered into the IFO mode is given by

$$P_{wsaccylifo}(L_{acb}, r_{acbo}, L_{cyl}) := \sqrt{4}\cdot P_a \cdot \left(C_4(L_{acb}, r_{acbo}, L_{cyl}) \cdot \alpha_{ws}^{\,2} \cdot \frac{\lambda^2}{r_{acbo}^{\,2}} \cdot BRDF_{cyl} \right)$$

Where the geometric function is

$$C_4\left(L_{acb}, r_{acbo}, L_{cyl}\right) := \frac{2}{\pi}\cdot\int_{\theta_{acbo}\left(L_{acb}, r_{acbo}\right)}^{\theta_{accyl}\left(L_{acb}, r_{acbo}, L_{cyl}\right)} \cos(\theta)^2\cdot\sin(\theta)^3\, d\theta$$

8.2.10.3 Total Scattered Light Displacement Noise from Arm Cavity Baffle and COC Wide Angle Baffle

The total scattered light from the Arm Cavity Baffle and the COC Wide Angle Baffle into the IFO is

$$P_{totalacbbackcy}\left(L_{acb}, r_{acbo}, L_{cyl}\right) := P_{acbbackifo}\left(L_{acb}, r_{acbo}\right) + P_{wsaccylifo}\left(L_{acb}, r_{acbo}, L_{cyl}\right)$$

The total scattered light displacement noise is

$$DN_{totalacbbackcyl} := TF_{itmhr}\left(\frac{P_{totalacbbackcy}\left(L_{acb}, r_{acbo}, L_{cyl}\right)}{P_{psl}}\right)^{0.5}\cdot x_{hepi}\cdot 2\cdot k\cdot acbatter$$

8.2.10.4 Scattering from the Manifold Baffle

The wide-angle scattered light hitting the Manifold Baffle is

$$P_{mb} := P_a\cdot\int_{\theta_{cp}}^{\theta_{mbo}} \frac{\alpha_{ws}\cdot\cos(\theta)}{\pi}\cdot 2\cdot\pi\cdot\sin(\theta)\, d\theta$$

Where the half-angle from the ITM centerline to the Manifold Baffle is

$$\theta_{mbo} := \operatorname{atan}\left(\frac{r_m}{L_m}\right)$$

and L_m is the distance from the ITM to the Manifold Baffle.

The power scattered into the IFO mode is given by

$$P_{wsmbifo} := \sqrt{4}\cdot P_a\cdot\left(C_1\cdot\alpha_{ws}^{\,2}\cdot\frac{\lambda^2}{r_m^{\,2}}\cdot BRDF_{bd}\right)$$

Where the geometric function is

$$C_1 := \frac{2}{\pi}\cdot\int_{\theta_{cp}}^{\theta_{mbo}} \cos(\theta)^2\cdot\sin(\theta)^3\, d\theta$$

8.2.10.5 Scatter from ITM Manifold Wall

The wide-angle scattered light hitting the Manifold wall is

$$P_{mw}(L_{acb}) := P_a\cdot\int_{\theta_{mbo}}^{\theta_{acbi}(L_{acb})} \frac{\alpha_{ws}\cdot\cos(\theta)}{\pi}\cdot 2\cdot\pi\cdot\sin(\theta)\, d\theta$$

The power scattered into the IFO mode is given by

$$P_{wsmbifo} := \sqrt{4}\cdot P_a\cdot\left(C_1\cdot\alpha_{ws}^2\cdot\frac{\lambda^2}{r_m^2}\cdot BRDF_{bd}\right)$$

Where the geometric function is

$$C_3(L_{acb}) := \frac{2}{\pi}\cdot\int_{\theta_{mbo}}^{\theta_{acbi}(L_{acb})} \cos(\theta)^2\cdot\sin(\theta)^3\, d\theta$$

8.2.10.6 Scattering from BSC Chamber Walls

The wide-angle scattered light hitting the BSC chamber wall is

$$P_{bsc}(L_{acb}, r_{acbo}, L_{cyl}) := P_a\cdot\int_{\theta_{accyl}(L_{acb}, r_{acbo}, L_{cyl})}^{\frac{\pi}{2}} \frac{\alpha_{ws}\cdot\cos(\theta)}{\pi}\cdot 2\cdot\pi\cdot\sin(\theta)\, d\theta$$

The power scattered into the IFO mode is given by

$$P_{wsbscifo}(L_{acb}, r_{acbo}, L_{cyl}) := \sqrt{4}\cdot P_a\cdot\left(C_5(L_{acb}, r_{acbo}, L_{cyl})\cdot\alpha_{ws}^2\cdot\frac{\lambda^2}{r_{bsc}^2}\cdot BRDF_{wall}\right)$$

where the geometric function is

$$C_5(L_{acb}, r_{acbo}, L_{cyl}) := \frac{2}{\pi} \cdot \int_{\theta_{accyl}(L_{acb}, r_{acbo}, L_{cyl})}^{\frac{\pi}{2}} \cos(\theta)^2 \cdot \sin(\theta)^3 \, d\theta$$

8.2.10.7 Total Wide-Angle Scattered Light Displacement Noise from BSC Chamber, Manifold Walls, and Manifold Baffle

The total scattered light from the BSC Chamber, Manifold Walls, and Manifold Baffle into the IFO is

$$P_{totalbscman}(L_{acb}, r_{acbo}, L_{cyl}) := P_{wsbscifo}(L_{acb}, r_{acbo}, L_{cyl}) + P_{wsmanifo}(L_{acb}) + P_{wsmbifo}$$

The scattered light is injected into the arm cavity, and the appropriate scattered light noise transfer function is 'ITM_HR'. The displacement noise (m/rt Hz) is

$$DN_{wsbscmanifo}(L_{acb}, r_{acbo}, L_{cyl}) := TF_{itmhr} \left(\frac{P_{totalbscman}(L_{acb}, r_{acbo}, L_{cyl})}{P_{psl}} \right)^{0.5} \cdot x_{manifold} \cdot 2 \cdot k$$

8.2.11 Septum Window Scatter

8.2.11.1 AS Output Window

The power incident on the AS output Window is given by

$$P_{assp} := P_{farad}$$

The light power scattered into the IFO mode from the two surfaces of the AS Output Window is given by

$$P_{assps} := N_{sp} \cdot P_{assp} \cdot BRDF_{sp} \cdot \frac{w_{ifo}^2}{w_{rc}^2} \cdot \Delta_{ifo} \cdot faradatter$$

The scattered light is injected through the SRM, and the appropriate scattered light noise transfer function is 'SRM'. The displacement noise (m/rt Hz) is

$$DN_{asspsifo} := TF_{sr} \cdot \left(\frac{P_{assps}}{P_{psl}} \right)^{0.5} \cdot x_{hamflange} \cdot 2 \cdot k$$

8.2.11.2 AS Output Window Reflection

The reflected power incident on the AS Output Window beam dump is given by

$$P_{asspbd} := R_{sp} \cdot P_{assp}$$

where R_{sp} is the Fresnel reflectivity of the window surfaces.

The light power scattered into the IFO mode from the AS Output Window beam dump is given by

$$P_{assprefls} := N_{sp} \cdot P_{asspbd} \cdot BRDF_{bd} \cdot \frac{w_{ifo}^2}{w_{rc}^2} \cdot \Delta_{ifo} \cdot R_{sp} \cdot faradatte$$

The total scattered light displacement noise is

$$DN_{asspreflsifo} := TF_{sr} \cdot \left(\frac{P_{assprefls}}{P_{psl}} \right)^{0.5} \cdot x_{ham} \cdot 2 \cdot k$$

8.2.11.3 ITMX PO Septum Window

The power incident on the ITMX PO Septum Window is given by

$$P_{itmxposp} := R_{bsar} \cdot P_{rca}$$

The light power scattered into the IFO mode from the two surfaces of the ITMX PO Septum Window is given by

$$P_{itmxposps} := N_{sp} \cdot P_{itmxposp} \cdot BRDF_{sp} \cdot \frac{w_{ifo}^2}{w_{rc}^2} \cdot \Delta_{ifo} \cdot R_{bsar}$$

The scattered light is injected into the ITM AR, and the appropriate scattered light noise transfer function is ‘ITM_AR. The displacement noise (m/rt Hz) is

$$DN_{itmxpospsifo} := TF_{itmar} \cdot \left(\frac{P_{itmxposps}}{P_{psl}} \right)^{0.5} \cdot x_{hamflange} \cdot 2 \cdot k$$

8.2.11.4 ITMX PO Septum Window Reflection

The reflected power incident on the ITMX PO Septum Window beam dump is given by

$$P_{itmxpospbd} := R_{sp} \cdot P_{itmxpos}$$

The light power scattered into the IFO mode from the ITMX PO Septum Window beam dump is given by

$$P_{itmxpospreflsifo} := N_{sp} \cdot P_{itmxpospbd} BRDF_{bd} \cdot \frac{w_{ifo}^2}{w_{rc}^2} \cdot \Delta_{ifo} \cdot R_{sp} \cdot R_{bsar}$$

The total scattered light displacement noise is

$$DN_{itmxpospreflsifo} := TF_{itmar} \cdot \left(\frac{P_{itmxpospreflsifo}}{P_{psl}} \right)^{0.5} \cdot x_{ham} \cdot 2 \cdot k$$

8.2.11.5 RC PO Septum Window

The power incident on the RC PO Septum Window is given by

$$P_{rcposp} := G_{refl} P_{psl} \cdot \left(1 - R_{pr2hr}\right) \cdot \left(1 - R_{pr2ar}\right)$$

where R_{pr2hr} and R_{pr2ar} are the Fresnel reflectivity of the HR and AR surfaces of the PR2 mirror, and G_{refl} is the reflected port signal ratio.

The light power scattered into the IFO mode from the two surfaces of the RC PO Septum Window is given by

$$P_{rcposps} := N_{sp} \cdot P_{rcposp} \cdot BRDF_{sp} \cdot \frac{w_{ifo}^2}{w_{rc}^2} \cdot \Delta_{ifo} \cdot \left(1 - R_{pr2hr}\right) \cdot \left(1 - R_{pr2ar}\right)$$

The scattered light is injected into the RC from the PRM direction, and the appropriate scattered light noise transfer function is ‘BS_FROM_PRM’. The displacement noise (m/rt Hz) is

$$DN_{rcpospsifo} := TF_{prbs} \cdot \left(\frac{P_{rcposps}}{P_{psl}} \right)^{0.5} \cdot x_{hamflange} \cdot 2 \cdot k$$

8.2.11.6 RC PO Septum Window Reflection

The reflected power incident on the RC PO Septum Window beam dump is given by

$$P_{rcpospbd} := R_{sp} \cdot P_{rcposp}$$

The light power scattered into the IFO mode from the RC PO Septum Window beam dump is given by

$$P_{rcpospreflsifo} := N_{sp} \cdot P_{rcpospbd} \cdot BRDF_{bd} \cdot \frac{w_{ifo}^2}{w_{rc}^2} \cdot \Delta_{ifo} \cdot R_{sp} \cdot \left[\left(1 - R_{pr2hr}\right) \cdot \left(1 - R_{pr2ar}\right) \right]$$

The total scattered light displacement noise is

$$DN_{rcpospreflsifo} := TF_{prbs} \cdot \left(\frac{P_{rcpospreflsifo}}{P_{psl}} \right)^{0.5} \cdot x_{ham} \cdot 2 \cdot k$$

8.2.12 ITMY Hartmann Viewport

The power transmitted through the SR2 HR surface is

$$P_{hartytransbd} := G_{as} \cdot P_{psl} \cdot \left(1 - R_{sr2hr}\right) \cdot \left(1 - R_{sr2ar}\right)$$

The power incident on the Hartmann viewport is

$$P_{hartyvp} := P_{hartytransbd} \cdot R_{hartybs}$$

where $R_{hartybs}$ is the reflectivity of the Hartmann beam splitter.

The light power scattered into the IFO mode from the Hartmann viewport is given by

$$P_{hartyvps} := N_{sp} \cdot P_{hartyvp} \cdot BRDF_{sp} \cdot \frac{w_{ifo}^2}{w_{rc}^2} \cdot \Delta_{ifo} \cdot R_{hartybs} \cdot \left[\left(1 - R_{sr2hr}\right) \cdot \left(1 - R_{sr2ar}\right)\right]$$

The scattered light is injected into the BS from the SRM direction, and the appropriate scattered light noise transfer function is 'BS_FROM_SRM'. The displacement noise (m/rt Hz) is

$$DN_{hartyvpsifo} := TF_{srbs} \cdot \left(\frac{P_{hartyvps}}{P_{psl}}\right)^{0.5} \cdot x_{hamflange} \cdot 2 \cdot k$$

8.2.13 ITMX Hartmann Viewport

The power incident on the Hartmann viewport is

$$P_{hartxvp} := P_{itmxposp} \cdot T_{hartxbs}$$

where $T_{hartxbs}$ is the transmissivity of the Hartmann beam splitter.

The light power scattered into the IFO mode from the Hartmann viewport is given by

$$P_{hartxvps} := N_{sp} \cdot P_{hartxvp} \cdot BRDF_{sp} \cdot \frac{w_{ifo}^2}{w_{rc}^2} \cdot \Delta_{ifo} \cdot T_{hartxbs}$$

The total scattered light displacement noise is

$$DN_{hartxvpsifo} := TF_{itmar} \cdot \left(\frac{P_{hartxvps}}{P_{psl}}\right)^{0.5} \cdot x_{hamflange} \cdot 2 \cdot k$$

8.2.14 Ghost Beams

8.2.14.1 Ghost Beam Naming Convention

The ghost beam naming conventions for the COC mirrors and the beam splitter are shown in the following figures.

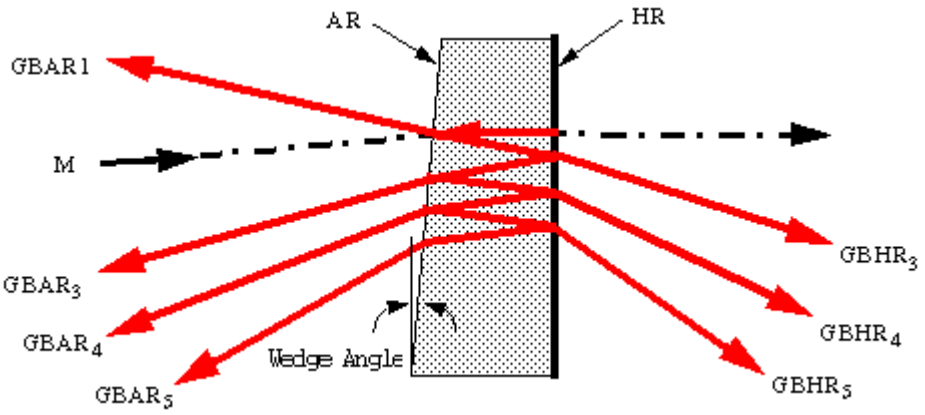

Figure 53: PRM, SRM, ITM, and ETM ghost beam naming convention

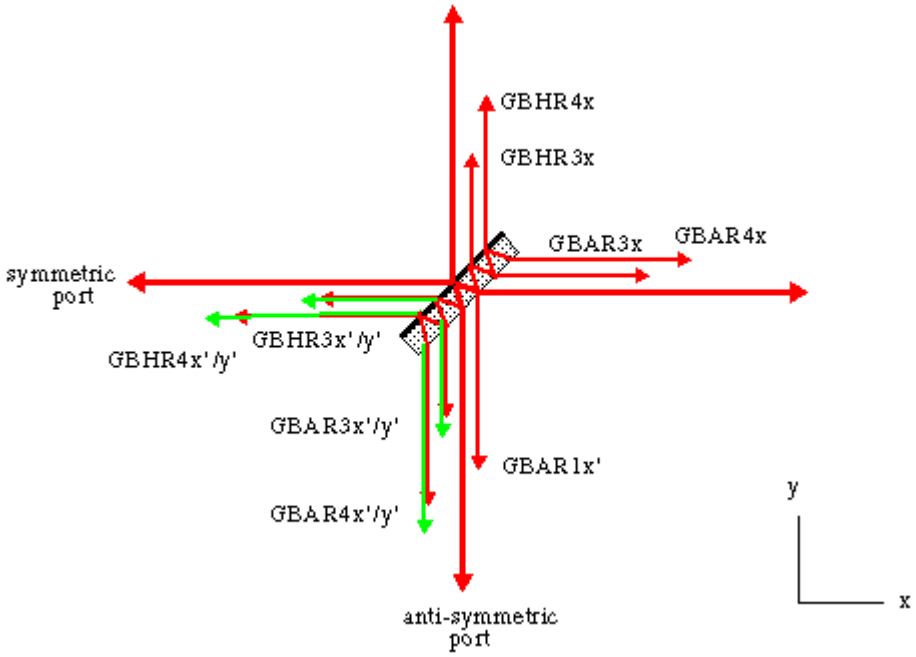

Figure 54: BS ghost beam naming convention

The GBAR3x'/y' are superimposed, and are renamed GBAR3P. Likewise, the other superimposed pairs are renamed GBAR4P, GBHR3P, and GBAR4P.

8.2.14.2 ITMAR1

The ITMAR1 ghost beam is collected by the PRM and SRM telescopes and hits the beam dumps in front of PR2 and SR2. The power incident on ITMAR1 Beam Dumps is given by

$$P_{itmar1bd} := P_{rca} \cdot R_{itma}$$

where R_{itmar} is the reflectivity of the AR surface of the ITM.

The light power scattered into the IFO from the ITM Beam Dump is given by

$$P_{itmar1bds} := \sqrt{2} \cdot P_{itmar1bd} \cdot BRDF_{bd} \cdot \frac{w_{ifo}^2}{w_{rc}^2} \cdot \Delta_{ifo} \cdot R_{itma}$$

The scattered light displacement noise is

$$DN_{itmar1bd} := TF_{itmbs} \left(\frac{P_{itmar1bds}}{P_{psl}} \right)^{0.5} \cdot x_{ham} \cdot 2 \cdot k$$

8.2.14.3 ITMAR1 REFL

The power reflected from the ITMAR1 Beam Dump and incident on the IO tube wall is given by

$$P_{itmar1bdrefl} := P_{itmar1bd} \cdot R_{bd}$$

The light power scattered into the IFO from the wall is given by

$$P_{itmar1bdrefls} := \sqrt{2} \cdot R_{bd} \cdot P_{itmar1bdrefl} \cdot BRDF_{wall} \frac{w_{ifo}^2}{w_{rc}^2} \cdot \Delta_{ifo} \cdot R_{itma}$$

The scattered light displacement noise is

$$DN_{itmar1bdrefl} := TF_{itmbs} \left(\frac{P_{itmar1bdrefls}}{P_{psl}} \right)^{0.5} \cdot x_{hamflange} \cdot 2 \cdot k$$

8.2.14.4 ITMAR3

The ITMAR3 ghost beam is collected by the PRM and SRM telescopes and hits the beam dumps in front of PR2 and SR2. The power incident on ITMAR3 Beam Dumps is given by

$$P_{itmar3bd} := P_{rca} \cdot R_{itmhr}^2 \cdot R_{itmar} \left(1 - R_{itmar} \right)^2$$

where R_{itmhr} is the reflectivity of the HR surface of the ITM.

The light power scattered into the IFO from the ITM Beam Dump is given by

$$P_{itmar3bds} := \sqrt{2} \cdot P_{itmar3bd} \cdot BRDF_{bd} \cdot \frac{w_{ifo}^2}{w_{rc}^2} \cdot \Delta_{ifo} \cdot R_{itmhr}^2 \cdot R_{itmar} \cdot \left(1 - R_{itmar}\right)^2$$

The scattered light displacement noise is

$$DN_{itmar3bd} := TF_{itmbs} \cdot \left(\frac{P_{itmar3bds}}{P_{psl}}\right)^{0.5} \cdot x_{ham} \cdot 2 \cdot k$$

8.2.14.5 ITMAR3 REFL

The power reflected from the ITMAR3 Beam Dump and incident on the IO tube wall is given by

$$P_{itmar3bdrefl} := P_{itmar3bd} \cdot R_{bd}$$

The light power scattered into the IFO from the wall is given by

$$P_{itmar3bdrefls} := \sqrt{2} \cdot R_{bd} \cdot P_{itmar3bdrefl} \cdot BRDF_{wall} \cdot \frac{w_{ifo}^2}{w_{rc}^2} \cdot \Delta_{ifo} \cdot R_{itmhr}^2 \cdot R_{itmar} \cdot \left(1 - R_{itmar}\right)^2$$

The scattered light displacement noise is

$$DN_{itmar3bdrefl} := TF_{itmbs} \cdot \left(\frac{P_{itmar3bdrefls}}{P_{psl}}\right)^{0.5} \cdot x_{hamflange} \cdot 2 \cdot k$$

8.2.14.6 ITMHR3

The ITMHR3 ghost beam passes into the arm beam tube and hits the beam tube baffle. The ITMHR3 ghost beam power incident on Beam Tube Baffle in the arm is given by

$$P_{itmhr3btbaf} := P_{rca} \cdot \left(1 - R_{itmar}\right) \cdot R_{itmhr} \cdot R_{itmar} \cdot T_{itmh}$$

where T_{itmhr} is the transmissivity of the HR surface of the ITM.

The light power scattered into the recycling cavity through the ITM from the Beam Tube Baffle is given by

$$P_{itmhr3btbafs} := \sqrt{2} \cdot P_{itmhr3btbaf} \cdot BRDF_{bd} \cdot \Delta_{ifo} \cdot \left[\left(1 - R_{itmar}\right) \cdot R_{itmhr} \cdot R_{itmar} \cdot T_{itmhr}\right]$$

The scattered light displacement noise is

$$DN_{itmhr3btbaf} := TF_{itmbs} \cdot \left(\frac{P_{itmhr3btbafs}}{P_{psl}}\right)^{0.5} \cdot x_{beamtube} \cdot 2 \cdot k$$

8.2.14.7 BSAR3

The BSAR3 ghost beam passes into the arm beam tube and hits the beam tube baffle. The BSAR3 ghost beam power incident on Beam Tube Baffle in the arm is given by

$$P_{bsar3btbaf} := 2 \cdot P_{rca} \cdot \left(1 - R_{bshr}\right) \cdot R_{bsar} \cdot R_{bshr} \cdot \left(1 - R_{bsar}\right) \cdot \left(1 - R_{itmhr}\right)$$

where R_{bshr} is the reflectivity of the HR surface of the BS and R_{bsar} is the reflectivity of the AR surface of the BS.

The light power scattered into the IFO from the Beam Tube Baffle is given by

$$P_{bsar3btbafs} := P_{bsar3btbaf} \cdot BRDF_{bd} \cdot \Delta_{ifo} \cdot \left[\left(1 - R_{bshr}\right) \cdot R_{bsar} \cdot R_{bshr} \cdot \left(1 - R_{bsar}\right) \cdot \left(1 - R_{itmhr}\right)\right]$$

The scattered light displacement noise is

$$DN_{bsar3btbaf} := TF_{itmbs} \cdot \left(\frac{P_{bsar3btbafs}}{P_{psl}}\right)^{0.5} \cdot x_{beamtube} \cdot 2 \cdot k$$

8.2.14.8 BSHR3

The BSHR3 ghost beam passes into the arm beam tube and hits the beam tube baffle. The power incident on Beam Tube Baffle is given by

$$P_{bshr3btbaf} := 2 \cdot P_{rca} \cdot \left(1 - R_{bshr}\right) \cdot R_{bsar} \cdot \left(1 - R_{bshr}\right) \cdot \left(1 - R_{itmhr}\right)$$

The light power scattered into the IFO from the Beam Tube Baffle is given by

$$P_{bshr3btbafs} := P_{bshr3btbaf} \cdot BRDF_{bd} \cdot \Delta_{ifo} \cdot \left(1 - R_{bshr}\right) \cdot R_{bsar} \cdot \left(1 - R_{bshr}\right) \cdot \left(1 - R_{itmhr}\right)$$

The scattered light displacement noise is

$$DN_{bshr3btbaf} := TF_{itmbs} \cdot \left(\frac{P_{bshr3btbafs}}{P_{psl}}\right)^{0.5} \cdot x_{beamtube} \cdot 2 \cdot k$$

8.2.14.9 BSAR3P

The BSAR3P ghost beam is collected by the SRM telescope and hits the beam dump in front of SR2. The power incident on the BSAR3P beam dump from the two collinear beams is given by

$$P_{bsar3pbd} := 2 \cdot P_{rca} \cdot \left[\left(1 - R_{bsar}\right)^2 \cdot R_{bshr}^2 \cdot R_{bsar} + \left(1 - R_{bshr}\right) \cdot R_{bsar} \cdot R_{bshr} \cdot \left(1 - R_{bsar}\right)\right]$$

The light power scattered into the IFO from the BSAR3P beam dump is given by

$$P_{bsar3pbds} := P_{bsar3pbd} \cdot BRDF_{bd} \cdot \frac{w_{ifo}^2}{w_{rc}^2} \cdot \Delta_{ifo} \cdot \left[\left(1 - R_{bsar}\right)^2 \cdot R_{bshr}^2 \cdot R_{bsar} + \left(1 - R_{bshr}\right) \cdot R_{bsar} \cdot R_{bshr} \cdot \left(1 - R_{bsar}\right)\right]$$

The scattered light displacement noise is

$$DN_{bsar3pbd} := TF_{itmar}\cdot\left(\frac{P_{bsar3pbds}}{P_{psl}}\right)^{0.5}\cdot x_{ham}\cdot 2\cdot k$$

8.2.14.10 BSAR3P REFL

The power reflected from the BSAR3P Beam Dump and incident on the OUT tube wall is given by

$$P_{bsar3pbdrefl} := P_{bsar3pbd}\cdot R_{bd}$$

The light power scattered into the IFO from the wall is given by

$$P_{bsar3pbdrefls} := R_{bd}\cdot P_{bsar3pbdrefl}\cdot BRDF_{wall}\cdot\frac{w_{ifo}^{2}}{w_{rc}^{2}}\cdot\Delta_{ifo}\cdot\left[\left(1-R_{bsar}\right)^{2}\cdot R_{bshr}^{2}\cdot R_{bsar}+\left(1-R_{bshr}\right)\cdot R_{bsar}\cdot R_{bshr}\cdot\left(1-R_{bsar}\right)\right]$$

The scattered light displacement noise is

$$DN_{bsar3pbdrefl} := TF_{itmar}\cdot\left(\frac{P_{bsar3pbdrefls}}{P_{psl}}\right)^{0.5}\cdot x_{hamflange}\cdot 2\cdot k$$

8.2.14.11 BSHR3P

The BSHR3P ghost beam is collected by the PRM telescope and hits the beam dump in front of PR2. The power incident on the BSHR3P beam dump from the two collinear beams is given by

$$P_{bshr3pbd} := 2\cdot P_{rca}\cdot\left[\left(1-R_{bsar}\right)\cdot R_{bshr}\cdot R_{bsar}\cdot\left(1-R_{bshr}\right)+\left(1-R_{bshr}\right)^{2}\cdot R_{bsar}\right]$$

The light power scattered into the IFO from the BSHR3P beam dump is given by

$$P_{bshr3pbds} := P_{bshr3pbd}\cdot BRDF_{bd}\cdot\frac{w_{ifo}^{2}}{w_{rc}^{2}}\cdot\Delta_{ifo}\cdot\left[\left(1-R_{bsar}\right)\cdot R_{bshr}\cdot R_{bsar}\cdot\left(1-R_{bshr}\right)+\left(1-R_{bshr}\right)^{2}\cdot R_{bsar}\right]$$

The scattered light displacement noise is

$$DN_{bshr3pbds} := TF_{itmar}\cdot\left(\frac{P_{bshr3pbds}}{P_{psl}}\right)^{0.5}\cdot x_{ham}\cdot 2\cdot k$$

8.2.14.12 BSHR3P REFL

The power reflected from the BSHR3P Beam Dump and incident on the IO tube wall is given by

$$P_{bshr3pbdrefl} := P_{bshr3pbd}\cdot R_{bd}$$

The light power scattered into the IFO from the wall is given by

$$P_{bshr3pbdrefls} := R_{bd} \cdot P_{bshr3pbdrefl} BRDF_{wall} \frac{w_{ifo}^2}{w_{rc}^2} \cdot \Delta_{ifo} \cdot \left[\left(1 - R_{bsar}\right) \cdot R_{bshr} \cdot R_{bsar} \cdot \left(1 - R_{bshr}\right) + \left(1 - R_{bshr}\right)^2 \cdot R_{bsar} \right]$$

The scattered light displacement noise is

$$DN_{bshr3pbdrefls} := TF_{itmar} \left(\frac{P_{bshr3pbdrefls}}{P_{psl}} \right)^{0.5} \cdot x_{hamflange} \cdot 2 \cdot k$$

8.2.15 PRM

8.2.15.1 PRMAR1

The power incident on the PRMAR1 beam dump is given by

$$P_{prmar1bd} := P_{psl} \cdot R_{prmar}$$

The light power scattered into the IFO from the PRMAR1 beam dump is given by

$$P_{prmar1bds} := P_{prmar1bd} \cdot BRDF_{platebd} \cdot \frac{w_{ifo}^2}{w_{rc}^2} \cdot \Delta_{ifo} \cdot R_{prmar} \cdot faradatten \cdot T_{prmar} \cdot T_{prmhr}$$

8.2.15.2 PRMAR3

The power incident on the PRMAR3 beam dump is given by

$$P_{prmar3bd} := P_{rct} \cdot T_{prmhr} \cdot R_{prmar} \cdot R_{prmhr} \cdot T_{prmar}$$

The light power scattered into the IFO from the PRMAR3 beam dump is given by

$$P_{prmar3bds} := P_{prmar3bd} \cdot BRDF_{platebd} \cdot \frac{w_{ifo}^2}{w_{rc}^2} \cdot \Delta_{ifo} \cdot \left(T_{prmhr} \cdot R_{prmar} \cdot R_{prmhr} \cdot T_{prmar} \right)$$

8.2.15.3 PRMHR3

The power incident on the PRMHR3 beam dump is given by

$$P_{prmhr3bd} := P_{rct} \cdot T_{prmhr}^2 \cdot R_{prmar}$$

The light power scattered into the IFO from the PRMHR3 beam dump is given by

$$P_{prmhr3bds} := P_{prmhr3bd} \cdot BRDF_{platebd} \cdot \frac{w_{ifo}^2}{w_{rc}^2} \cdot \Delta_{ifo} \cdot \left(T_{prmhr}^2 \cdot R_{prmar} \right)$$

8.2.15.4 Total Displacement Noise from PRM

The total light power scattered into the IFO from the PRM beam dumps is given by

$$P_{prmtotals} := P_{prmar1bds} + 2 \cdot \left(P_{prmar3bds} + P_{prmhr3bds} \right)$$

The scattered light displacement noise is

$$DN_{prmsifo} := TF_{prbs} \cdot \left(\frac{P_{prmtotals}}{P_{psl}} \right)^{0.5} \cdot x_{ham} \cdot 2 \cdot k$$

8.2.16 PRM2

8.2.16.1 PR2AR0t

The circulating power in the recycling cavity that transmits through the PR2 mirror from the PRM mirror and is incident on the PR2AR0t beam dump is given by

$$P_{pr20tbd} := P_{rct} \cdot T_{pr2hr} \cdot T_{pr2ar}$$

The light power scattered into the IFO from the PR2AR0t beam dump is given by

$$P_{pr20tbds} := P_{pr20tbd} \cdot BRDF_{bd} \cdot \frac{w_{ifo}^2}{w_{rc}^2} \cdot \Delta_{ifo} \cdot \left(T_{pr2hr} \cdot T_{pr2ar} \right)$$

8.2.16.2 PR2AR3

The power incident on the PR2AR3 beam dump is given by

$$P_{pr2ar3bd} := P_{rct} \cdot T_{pr2hr} \cdot R_{pr2ar} \cdot R_{pr2hr} \cdot T_{pr2ar}$$

The light power scattered into the IFO from the PR2AR3 beam dump is given by

$$P_{pr2ar3bds} := P_{pr2ar3bd} \cdot BRDF_{platebd} \cdot \frac{w_{ifo}^2}{w_{rc}^2} \cdot \Delta_{ifo} \cdot \left(T_{pr2hr} \cdot R_{pr2ar} \cdot R_{pr2hr} \cdot T_{pr2ar} \right)$$

8.2.16.3 PR2HR3

The power incident on the PR2HR3 beam dump is given by

$$P_{pr2hr3bd} := P_{rct} \cdot T_{pr2hr}^{2} \cdot R_{pr2ar}$$

The light power scattered into the IFO from the PR2HR3 beam dump is given by

$$P_{pr2hr3bds} := P_{pr2hr3bd} \cdot BRDF_{platebd} \cdot \frac{w_{ifo}^{2}}{w_{rc}^{2}} \cdot \Delta_{ifo} \cdot \left(T_{pr2hr}^{2} \cdot R_{pr2ar} \right)$$

8.2.16.4 Total Displacement Noise from PR2

The total light power scattered into the IFO from the PR2 beam dumps is given by

$$P_{pr2totals} := 2 \cdot \left(P_{pr20tbds} + P_{pr2ar3bds} + P_{pr2hr3bds} \right)$$

The scattered light displacement noise is

$$DN_{pr2sifo} := TF_{prbs} \cdot \left(\frac{P_{pr2totals}}{P_{psl}} \right)^{0.5} \cdot x_{ham} \cdot 2 \cdot k$$

8.2.17 PRM3

8.2.17.1 PR3AR0t

The circulating power in the recycling cavity that transmits through the PR3 mirror from the PR2 mirror and is incident on the PR3AR0t beam dump is given by

$$P_{pr30tbd} := P_{rct} \cdot T_{pr3hr} \cdot T_{pr3ar}$$

The light power scattered into the IFO from the PR3AR0t beam dump is given by

$$P_{pr30tbds} := P_{pr30tbd} \cdot BRDF_{platebd} \cdot \Delta_{ifo} \cdot \left(T_{pr3hr} \cdot T_{pr3ar} \right)$$

8.2.17.2 PR3AR3

The power incident on the PR3AR3 beam dump is given by

$$P_{pr3ar3bd} := P_{rct} \cdot T_{pr3hr} \cdot R_{pr3ar} \cdot R_{pr3hr} \cdot T_{pr3ar}$$

The light power scattered into the IFO from the PR3AR3 beam dump is given by

$$P_{pr3ar3bds} := P_{pr3ar3bd} \cdot BRDF_{platebd} \cdot \Delta_{ifo} \cdot \left(T_{pr3hr} \cdot R_{pr3ar} \cdot R_{pr3hr} \cdot T_{pr3ar} \right)$$

8.2.17.3 PR3HR3

The power incident on the PR3HR3 beam dump is given by

$$P_{pr3hr3bd} := P_{rct} \cdot T_{pr3hr}^{2} \cdot R_{pr3ar}$$

The light power scattered into the IFO from the PR3HR3 beam dump is given by

$$P_{pr3hr3bds} := P_{pr3hr3bd} \cdot BRDF_{wall} \cdot \Delta_{ifo} \cdot \left(T_{pr3hr}^{2} \cdot R_{pr3ar} \right)$$

8.2.17.4 Total Displacement Noise from PR3

The total light power scattered into the IFO from the PR3 beam dumps is given by

$$P_{pr3ars} := 2 \cdot \left(P_{pr30tbds} + P_{pr3ar3bds} \right)$$

The scattered light displacement noise is

$$DN_{pr3arsifo} := TF_{prbs} \cdot \left(\frac{P_{pr3ars}}{P_{psl}} \right)^{0.5} \cdot x_{ham} \cdot 2 \cdot k$$

8.2.18 SRM

8.2.18.1 SRMAR3

The power incident on the SRMAR3 beam dump is given by

$$P_{srmar3bd} := P_{sc} \cdot T_{srmhr} \cdot R_{srmar} \cdot R_{srmhr} \cdot T_{srmar}$$

The light power scattered into the IFO from the SRMAR3 beam dump is given by

$$P_{srmar3bds} := P_{srmar3bd} \cdot BRDF_{platebd} \cdot \frac{w_{ifo}^{2}}{w_{rc}^{2}} \cdot \Delta_{ifo} \cdot \left(T_{srmhr} \cdot R_{srmar} \cdot R_{srmhr} \cdot T_{srmar} \right)$$

8.2.18.2 SRMHR3

The power incident on the SRMHR3 beam dump is given by

$$P_{srmhr3bd} := P_{sc} \cdot T_{srmhr}^{2} \cdot R_{srmar}$$

The light power scattered into the IFO from the PRMAR1 beam dump is given by

$$P_{srmhr3bds} := P_{srmhr3bd} \cdot BRDF_{platebd} \cdot \frac{w_{ifo}^2}{w_{rc}^2} \cdot \Delta_{ifo} \cdot \left(T_{srmhr}^2 \cdot R_{srmar} \right)$$

8.2.18.3 Total Displacement Noise from SRM

The total light power scattered into the IFO from the SRM beam dumps is given by

$$P_{srmtotals} := 2 \cdot \left(P_{srmar3bds} + P_{srmhr3bds} \right)$$

The scattered light displacement noise is

$$DN_{srmsifo} := TF_{srbs} \cdot \left(\frac{P_{srmtotals}}{P_{psl}} \right)^{0.5} \cdot x_{ham} \cdot 2 \cdot k$$

8.2.19 SRM2

8.2.19.1 SR2AR0t

The circulating power in the signal recycling cavity that transmits through the SR2 mirror from the SRM mirror and is incident on the SR2AR0t beam dump is given by

$$P_{sr20tbd} := P_{sc} \cdot T_{sr2hr} \cdot T_{sr2ar}$$

The light power scattered into the IFO from the SR2AR0t beam dump is given by

$$P_{sr20tbds} := P_{sr20tbd} \cdot BRDF_{bd} \cdot \frac{w_{ifo}^2}{w_{rc}^2} \cdot \Delta_{ifo} \cdot \left(T_{sr2hr} \cdot T_{sr2ar} \right)$$

8.2.19.2 SR2AR3

The power incident on the SRMAR3 beam dump is given by

$$P_{sr2ar3bd} := P_{sc} \cdot T_{sr2hr} \cdot R_{sr2ar} \cdot R_{sr2hr} \cdot T_{sr2ar}$$

The light power scattered into the IFO from the SRMAR3 beam dump is given by

$$P_{sr2ar3bds} := P_{sr2ar3bd} \cdot BRDF_{platebd} \cdot \frac{w_{ifo}^2}{w_{rc}^2} \cdot \Delta_{ifo} \cdot \left(T_{sr2hr} \cdot R_{sr2ar} \cdot R_{sr2hr} \cdot T_{sr2ar} \right)$$

8.2.19.3 SR2HR3

The power incident on the SRMHR3 beam dump is given by

$$P_{sr2hr3bd} := P_{sc} \cdot T_{sr2hr}^{2} \cdot R_{sr2ar}$$

The light power scattered into the IFO from the SRMHR3 beam dump is given by

$$P_{sr2hr3bds} := P_{sr2hr3bd} \cdot BRDF_{platebd} \cdot \frac{w_{ifo}^{2}}{w_{rc}^{2}} \cdot \Delta_{ifo} \cdot \left(T_{sr2hr}^{2} \cdot R_{sr2ar} \right)$$

8.2.19.4 Total Displacement Noise from SR2

The total light power scattered into the IFO from the SR2 beam dumps is given by

$$P_{sr2totals} := 2 \cdot \left(P_{sr20tbds} + P_{sr2ar3bds} + P_{sr2hr3bds} \right)$$

The scattered light displacement noise is

$$DN_{sr2sifo} := TF_{srbs} \cdot \left(\frac{P_{sr2totals}}{P_{psl}} \right)^{0.5} \cdot x_{ham} \cdot 2 \cdot k$$

8.2.20 SRM3

8.2.20.1 SR3AR0t

The circulating power in the signal recycling cavity that transmits through the SR3 mirror from the SR2 mirror and is incident on the SR3AR0t beam dump is given by

$$P_{sr30tbd} := P_{sc} \cdot T_{sr3hr} \cdot T_{sr3ar}$$

The light power scattered into the IFO from the SR3AR0t beam dump is given by

$$P_{sr30tbds} := P_{sr30tbd} \cdot BRDF_{platebd} \cdot \Delta_{ifo} \cdot \left(T_{sr3hr} \cdot T_{sr3ar} \right)$$

8.2.20.2 SR3AR3

The power incident on the SR3AR3 beam dump is given by

$$P_{sr3ar3bd} := P_{sc} \cdot T_{sr3hr} \cdot R_{sr3ar} \cdot R_{sr3hr} \cdot T_{sr3ar}$$

The light power scattered into the IFO from the SR3AR3 beam dump is given by

$$P_{sr3ar3bds} := P_{sr3ar3bd} \cdot BRDF_{platebd} \cdot \Delta_{ifo} \cdot \left(T_{sr3hr} \cdot R_{sr3ar} \cdot R_{sr3hr} \cdot T_{sr3ar} \right)$$

8.2.20.3 SR3H3

The power incident on the SR3HR3 beam dump is given by

$$P_{sr3hr3bd} := P_{sc} \cdot T_{sr3hr}^{2} \cdot R_{sr3ar}$$

The light power scattered into the IFO from the SR3HR3 beam dump is given by

$$P_{sr3hr3bds} := P_{sr3hr3bd} \cdot BRDF_{wall} \cdot \Delta_{ifo} \cdot \left(T_{sr3hr}^{2} \cdot R_{sr3ar} \right)$$

8.2.20.4 Total Displacement Noise from SR3AR

The total light power scattered into the IFO from the SR3 beam dumps is given by

$$P_{sr3ars} := 2 \cdot \left(P_{sr30tbds} + P_{sr3ar3bds} \right)$$

The scattered light displacement noise is

$$DN_{sr3arsifo} := TF_{srbs} \cdot \left(\frac{P_{sr3ars}}{P_{psl}} \right)^{0.5} \cdot x_{ham} \cdot 2 \cdot k$$

8.2.21 Cryopump Baffle Scatter

The power incident on the Cryopump Baffle is given by

$$P_{cp} := P_{a} \cdot \int_{\theta_{cp}}^{\theta_{bt}} 2 \cdot \pi \cdot \theta \cdot BRDF_{1}(\theta) \, d\theta$$

The half-angle from the beam tube centerline to the arm beam tube baffle inner edge is

$$\theta_{bt} := \frac{R_{bt}}{L}$$

The light power scattered into the IFO from the Cryopump Baffle is given by

$$P_{cps} := \sqrt{4} \cdot P_{cp} \cdot BRDF_{cp} \cdot \frac{\pi \cdot w_{ifo}^{2}}{L^{2}} \cdot BRDF_{1}\left(30 \cdot 10^{-6} \right) \cdot \Delta_{ifc}$$

The scattered light is injected into the arm cavity, and the appropriate scattered light noise transfer function is ‘ITM_HR’. The displacement noise (m/rt Hz) is

$$DN_{cpbaf} := TF_{itmhr}\left(\frac{P_{cps}}{P_{psl}}\right)^{0.5} \cdot x_{beamtube} \cdot 2 \cdot k \cdot cpatter$$

8.2.22 Cryopump Baffle Reflected Scatter

The power reflected by the Cryopump Baffle and incident on the wall is given by

$$P_{cpr} := R_{cpb} \cdot P_{cp}$$

where R_{cpb} is the reflectivity of the Cryopump Baffle.

The light power scattered into the IFO from the wall is given by

$$P_{cprs} := \sqrt{4} \cdot P_{cpr} \cdot BRDF_{wall} R_{cpb} \cdot \frac{\pi \cdot w_{ifo}^{2}}{L^{2}} \cdot BRDF_{1}\left(30 \cdot 10^{-6}\right) \cdot \Delta_{ifc}$$

The displacement noise (m/rt Hz) is

$$DN_{cpbafrefl} := TF_{itmhr}\left(\frac{P_{cprs}}{P_{psl}}\right)^{0.5} \cdot x_{beamtube} \cdot 2 \cdot k$$

$$DN_{etmbafrefl} := TF_{etm}\left(\frac{P_{etmbafrefls}}{P_{psl}}\right)^{0.5} \cdot x_{beamtube} \cdot 2 \cdot k$$

8.2.23 Fringe-Wrapping

In the small phase-shift approximation the temporal DARM signal (noise) due to light scattered into the IFO mode is

$$S_{SN}(t) := SNXXX \cdot E_{SN} \cdot \frac{4 \cdot \pi}{\lambda} \cdot x_g \cdot A_{SEIi} \cdot \sin\left(2 \cdot \pi \cdot f_0 \cdot t\right)$$

The motion of the scattering surface is written as the underlying ground seismic motion, x_g, times the motion amplitude transfer function of the scattering surface, A_{SEIi}.

The amplitude displacement spectral density is given by the following expression with the transfer coefficient calculated by Hiro (T060073-00 Transfer Functions of Injected Noise)

$$S_{SN}\left(f_0\right) := SNXXX \cdot E_{SN} \cdot \frac{4 \cdot \pi}{\lambda} \cdot x_g\left(f_0\right) \cdot A_{SEIi}$$

When the horizontal displacement of the scattering surface exceeds approximately λ/8, the amplitude of the noise no longer increases at the frequency of the scattering surface motion, but

becomes non-sinusoidal and is up-converted to noise at odd harmonics of the scattering surface motion frequency. This phenomenon is called fringe-wrapping.

$$S_{SN}(t) := SNXXX \cdot E_{SN} \cdot \sin\left(\frac{4\cdot\pi}{\lambda} \cdot x_g \cdot A_{SEIi} \cdot \sin\left(2\cdot\pi\cdot f_0 \cdot t\right)\right)$$

We will assume that the transfer functions SNXXX are valid for large phase-shift signals.

This time function is represented exactly by the Bessel series expansion in odd harmonics of the scattering surface frequency, f_0, with amplitudes given by the Bessel functions of integral order m_n and argument θ.

$$S_{SN}(t) := S_B(\theta, t)$$

$$S_B(\theta, t) := 2 \cdot \sum_n \left(Jn(m_n, \theta) \cdot \sin\left(2\cdot\pi\cdot m_n \cdot f_0 \cdot t\right)\right)$$

$$\theta := \frac{4\cdot\pi}{\lambda} \cdot x_g \cdot A_{SEI}$$

$$m_n := 2\cdot n - 1$$

At the onset of fringe-wrapping, a significant distortion of the noise temporal waveform has already occurred, as shown in

Figure 55, with the generation of up-converted noise at odd harmonics of the surface motion. The actual time signal and the Bessel function representation of the time signal are both plotted in the figure and agree exactly.

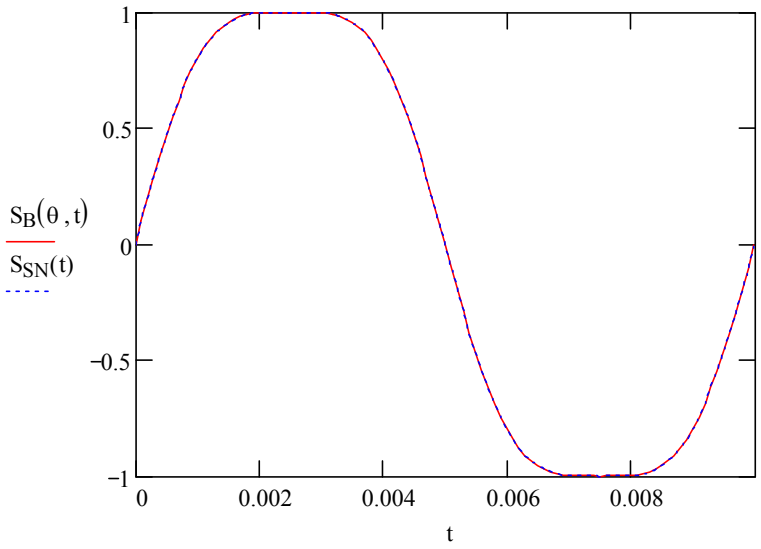

Figure 55: Noise Waveform at the Onset of Fringe-Wrapping, λ/8

If the displacement of the scattering surface is increased to λ/4, the fringe-wrapping becomes clearly visible, as shown in Figure 56. The fundamental and the third harmonic contribute most of the noise, as seen by the coefficients of the Bessel functions in the adjacent table.

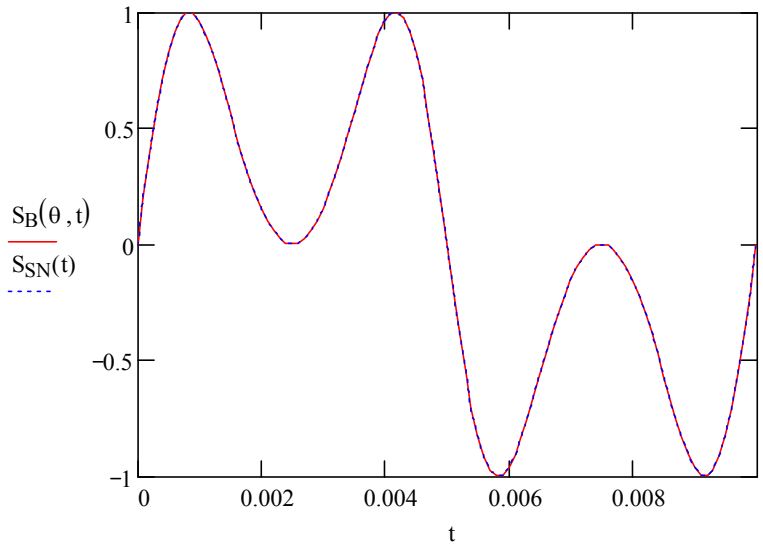

m =

	0
0	0
1	1
2	3
3	5
4	7
5	9
6	11
7	13
8	15
9	17
10	19
11	21

$Jn(m_n, \theta) =$

0.285
0.333
0.052
$3.42 \cdot 10^{-3}$
$1.25 \cdot 10^{-4}$
$2.925 \cdot 10^{-6}$
$4.767 \cdot 10^{-8}$
$5.728 \cdot 10^{-10}$
$5.287 \cdot 10^{-12}$
$3.868 \cdot 10^{-14}$
0

Figure 56: Displacement Noise waveform with Fringe-wrapping, λ/4

The displacement spectral density, m/rt Hz, of the fringe-wrapped signal (noise) at an up-converted frequency is given by the Bessel function series

$$S_{SNsum}(f) := E_{SN} \cdot SNXXX \cdot 2 \cdot \sum_n \left| Jn\left(m_n, \theta\left(\frac{f}{m_n}\right)\right)\right|$$

Note that the Bessel function phase is evaluated by using the motion of the surface at the lower frequency that corresponds to an odd multiple of the up-converted frequency.

8.2.23.1.1.1 Damped Pendulum Example

Assume that the scattering surface is suspended from a damped, simple pendulum with resonant frequency = 1 Hz, Q = 1000; and the displacement spectral density of the suspension point x_g is 1E-7 m/ rt Hz.

The amplitude response of the pendulum is given by

$$A_{SEI}(f) := \left| \frac{1}{1 + i \cdot \frac{f}{Q \cdot f_0} - \left(\frac{f}{f_0}\right)^2} \right|$$

The calculated noise displacement spectral density is shown in Figure 57. The total displacement noise, shown in cyan, has peaks at the fringe-wrapped harmonics of the fundamental surface

motion. The displacement noise of the fundamental disturbance is shown in red, shifted upwards slightly in the graph for clarity. Additional displacement noise caused by fringe-wrapping is evident at the 3rd and 5th harmonics of the fundamental disturbance.

Even, with such a large motion of the suspension point, the fringe wrap noise of the suspended surface is negligible at frequencies an order of magnitude higher than the fundamental pendulum frequency.

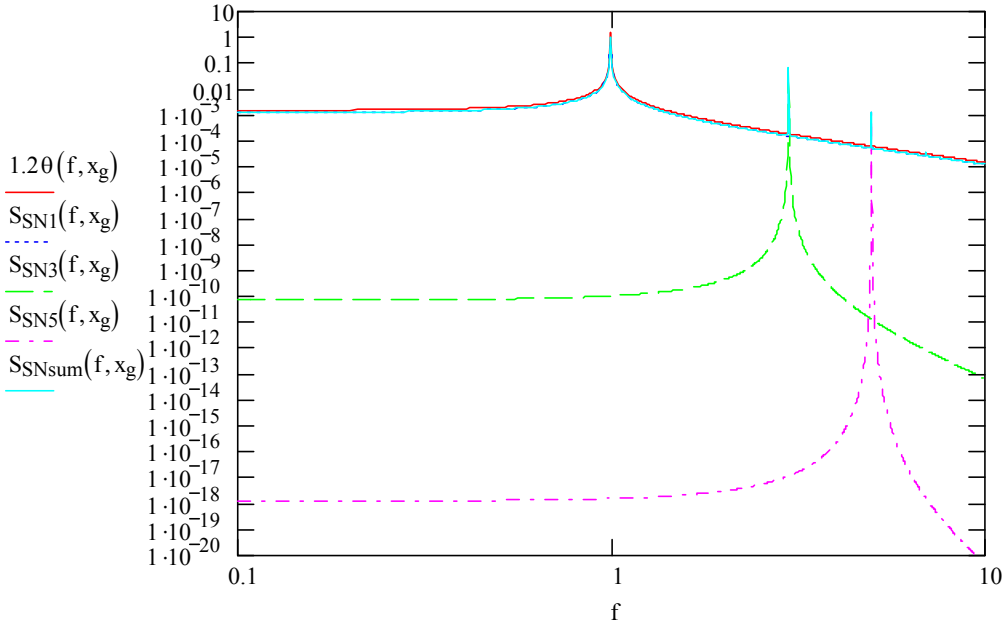

Figure 57: Scattered Light Displacement Noise Caused by Fringe-wrapping